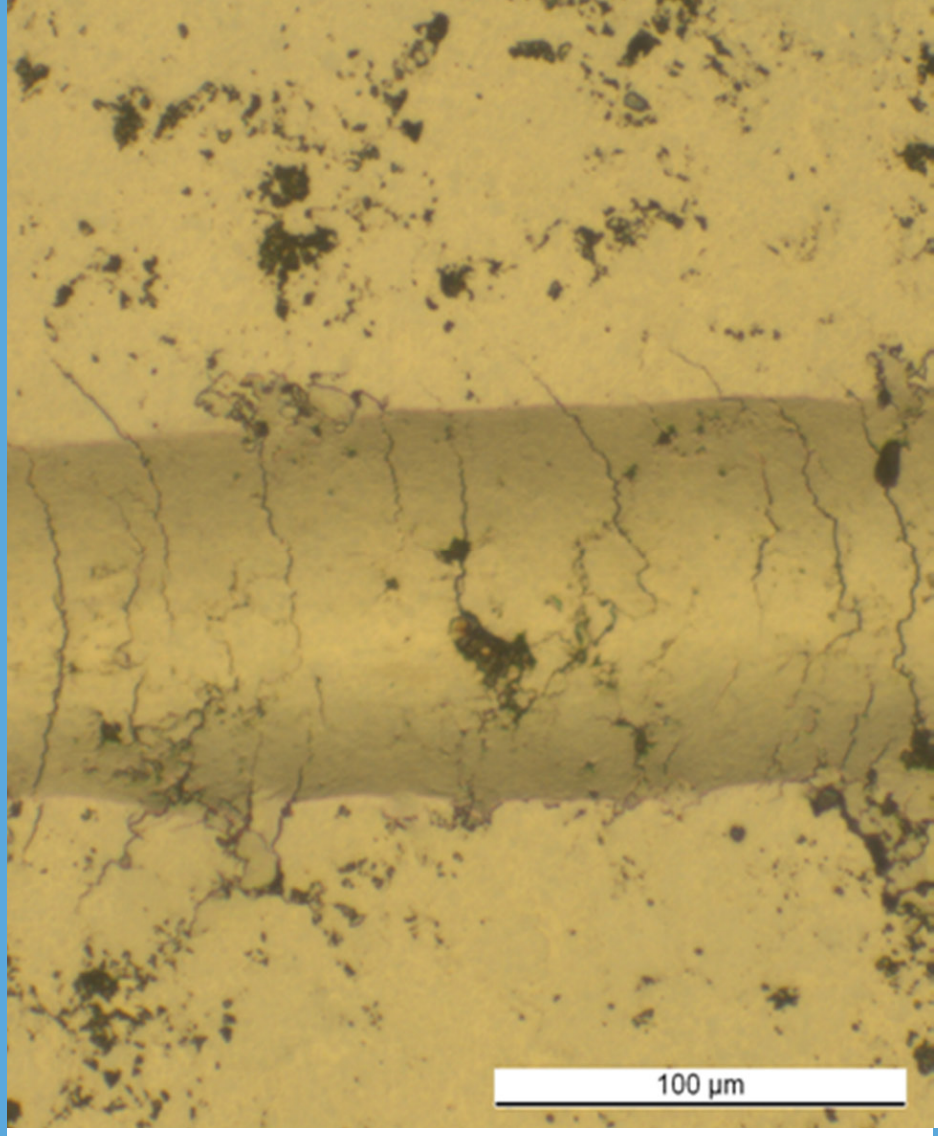

SCIENCE • TECHNOLOGY • RESEARCH HIGHLIGHTS • VISIONS •

Dissertation
29

Wear Resistant Carbide-Based Thermal Sprayed Coatings: Process, Properties, Mechanical Degradation and Wear

Arash Ghabchi

VTT

VTT SCIENCE 29

Wear Resistant Carbide-Based Thermal Sprayed Coatings: Process, Properties, Mechanical Degradation and Wear

Arash Ghabchi

A Dissertation Presented by Arash Ghabchi to The Graduate School in Partial Fulfilment of the Requirements for the Degree of Doctor of Philosophy in Materials Science and Engineering, Stony Brook University, Long Island, New York, USA, September 2011.

ISBN 978-951-38-7960-0 (Soft back ed.)
ISBN 978-951-38-7961-7 (URL: http://www.vtt.fi/publications/index.jsp)

VTT Science 29

ISSN-L 2242-119X
ISSN 2242-119X (Print)
ISSN 2242-1203 (Online)

JULKAISIJA – UTGIVARE – PUBLISHER

VTT
PL 1000 (Tekniikantie 4 A, Espoo)
02044 VTT
Puh. 020 722 111, faksi 020 722 7001

VTT
PB 1000 (Teknikvägen 4 A, Esbo)
FI-02044 VTT
Tfn. +358 20 722 111, telefax +358 20 722 7001

VTT Technical Research Centre of Finland
P.O. Box 1000 (Tekniikantie 4 A, Espoo)
FI-02044 VTT, Finland
Tel. +358 20 722 111, fax + 358 20 722 7001

Kopijyvä Oy, Kuopio 2013

Wear Resistant Carbide-based Thermal Sprayed Coatings: Process, Properties, Mechanical Degradation and Wear

Arash Ghabchi. Espoo 2013. VTT Science 29. 136 p.

Abstract

Thermally sprayed ceramic-metallic composite (CerMet) materials consist of ceramic particles mainly in form of carbides reinforced by metallic binder exhibit unique microstructural and mechanical characteristics. Such structure brings in a novel combination of hardness and toughness enabling application of this class of material in wear resistant surfaces. Final deposit microstructure that defines the mechanical properties and wear performance of material depends on process parameters and starting material characteristics. Complex interaction of in-flight particles with supersonic flame, formation of complex defective deposit structure comprising of pores, cracks and splat boundaries make comprehending of interrelation of process, microstructure, properties and performance a difficult task. Additional challenge is development of systematic understanding on mechanical degradation, damage and wear mechanisms of cermet coatings due to their complex structure.

This dissertation attempts to address these issues first by taking a systematic step by step approach, process map, to establish a correlation between process, particle state, microstructure and properties. Different strategies were proposed and examined to control the high velocity thermal spray process. This strategy assessment enabled a better control over in-flight particles state in high velocity thermal spray process and provided better understanding on interaction of in-flight particles with the flame.

Further, possible advantages of reducing the carbide particle size from micron to nano in terms of mechanical properties and different wear performance were explored. It was suggested that poor wear performance of nano-structured coating is due to presence of brittle phases and less available binder promotes the excessive stress detrimental to load carrying capability of material. Material damage and wear mechanisms of coating under different tribological conditions were examined. The results suggest a correlation between relative abrasive particle size/carbide particle size and observed wear mechanism. Additionally effect of surface open porosities was highlighted. A surface damage mechanisms map was developed for coatings under increasing tangential force. This work has significant implications in improved material and process design of composite wear resistant structures and systems as it provides comprehensive qualitative insight to the wear mechanism of complex composite thermally sprayed structures under different tribological contact conditions. Additionally, this work provides an establishment between process, microstructure, properties and performance for this class of materials.

Keywords wear, thermal spray, coating

Dedication

I dedicate this dissertation to my family:

To my wife, Sahar, who has unconditionally supported me with her love and has sacrificed many things in her life for me to get this far. She always encouraged me all of these years standing next to me and patiently listened to my boring daily research stories pretending to be exciting.

To my father, the world's greatest teacher, who thought me the value of science and education and handed me a powerful tool called "vision". I had the chance to sit in his geometry class for two years.

To my mother, who raised me and tought me to love by giving her unconditional love and care.

Acknowledgment

I would like sincerely to thank professor Sanjay Sampath, director of Center for Thermal Spray Research, for his endless supports during these years. He not only was supportive in my research also made it possible for me to overcome my personal life obstacles that without his help was impossible. He opened the door to the world of possibilities and exciting challenges in science and engineering for me. Thank you for giving me the opportunity to be part of CTSR.

I also thank Dr. Erja Turunen, Vice President of advanced materials, who supported my research during my stay at VTT Technical Research Center of Finland.

I also would like to thank professor Kenneth Holmberg for his guidance and sharing with me his insights in field of surface engineering and tribology. It was a great pleasure to work with him at VTT.

I thank my colleague Mr. Tommi Varis for our fruitful discussions on different topics of thermal spray.

I thank all my friends and colleagues for their support in CTSR, Stony Brook University, VTT, Helsinki University of Technology and Tampere University of Technology.

Academic dissertation

Stony Brook University –The Graduate School

Arash Ghabchi

We, the dissertation committee for the above candidate for the Doctor of Philosophy degree, hereby recommend Acceptance of this dissertation:

Supervisor Prof. Sanjay Sampath
Distinguished Professor, Materials Science and Engineering Department, Stony Brook University

Prof. T.A. Venkatesh
Assistant Professor, Materials Science and Engineering Department, Stony Brook University

Dr. Erja Turunen
Adjunct Professor, Materials Science and Engineering Department, Stony Brook University

Prof. Kenneth Holmberg
Professor, VTT Technical Research Center of Finland

This dissertation is accepted by the Graduate School.

Lawrence Martin
Dean of the Graduate School

Contents

List of Figures

List of Tables

1. Thermal spray processes and application of thermal sprayed cermet coatings in wear resistant surfaces

1.1 Thermal spray processes

The term “thermal spray” (TS) is referred to array of coating processes used to apply metallic, ceramic, composite and polymeric coatings on different substrate materials. Thermal spraying consists of introducing the raw materials in form of wire, rod or powder to the energy source to heat up the materials. Fully or partially-molten particles are accelerated towards the substrate by gases and projected on the substrate. Upon impact, particles are flattened and solidified to form a disk shape structure called “splat”. With overlapping the splats and adhering to each other continuous layer of coating is formed. Due to the nature of deposition process (individual particles), deposits will exhibit lamellar structure. Based on different variables such as sprayed materials, spray parameters and substrate characteristics (material, temperature, roughness) splats might be observed in different shapes. Unique lamellar structure of thermal sprayed coatings provides new possibilities to design material with desired properties and performance. However, such a deposit structure (lamellar structure) and variations in final splat shape and formation mechanisms yield a complex system that makes the understanding of deposit formation, structure, properties and performance an intricate task. The complexity of thermal spray deposits have been recognized and appreciated and efforts to address and understand such complexities are still undergoing.

Depending on energy source, thermal spray processes are categorized to; flame spray, electric arc spray, and plasma arc spray. Similar to other deposition techniques this technique also has advantages and disadvantages. As advantages; it is possible to apply wide range of materials and deposit coatings without significant heat input. The latter advantage (no significant heat input) makes it a desirable technique to be used as dimensional repair technique without changing properties and dimensions of parent part. As disadvantages employing this technique it is only possible to coat what the torch can see which makes it difficult or impossible to coat small and deep cavities [1]. Advances in material development, process and monitoring systems as well as adequate knowledge of coating formation and evaluation techniques have moved TS as a reliable tech-

nique to improve functionality of surfaces rather than to be used only as an additive layer for dimensional repair purposes.

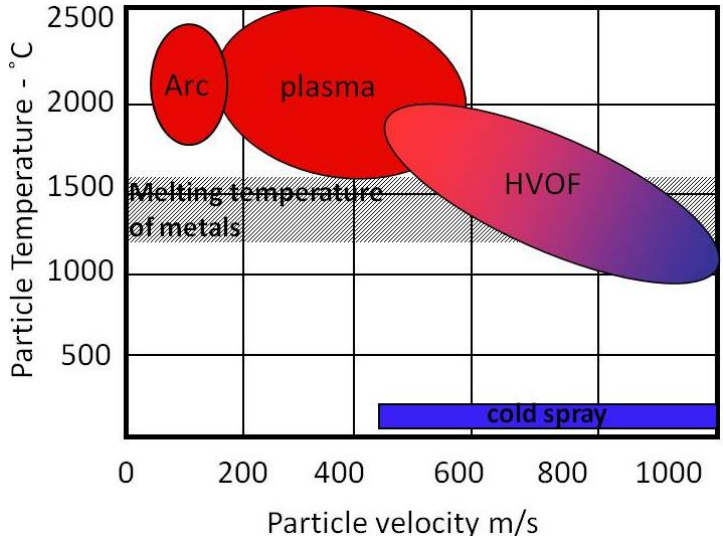

Figure 1.1. Particle temperature and velocity in different thermal spray techniques.

Due to such advances, productivity and reliability of TS technique has been promoted and it has gained great industrial interests in wear and corrosion resistant, thermal and electrical protection/conduction applications.

1.2 High Velocity Oxy-fuel (HVOF) technique

In High Velocity Oxy-Fuel (HVOF) technique fuel (hydrogen, propane, propylene, kerosene and acetylene) and oxygen are used to create combustion with temperature up to 2500–3000 °C. In this technique gases are accelerated to about 2200 m/s. The feedstock materials are injected axially or radially into the nozzle or combustion chamber,. Employing HVOF technique enables to produce denser coating with low oxidation and low decomposition mainly owing to higher gas velocities and lower flame temperature in comparison to plasma or arc spray technique. The schematic of average operating in-flight particles temperature and velocity in different TS systems is shown in Figure 1.1. These two features (low heat input and high kinetic energy) in HVOF systems enable to have more control over thermally activated transformations. There are three generations of HVOF torch systems developed. In 1st and 2nd generation, combustion takes place at 3–5 bars pressure and powder is axially injected to the combustion chamber. The straight nozzle is used in these two generations. In 3rd generation design, combustion takes place at 6–10 bars pressure, powder can be injected radial or axial

to the combustion chamber or to the nozzle directly. The nozzle used in this design is converging/diverging (De Laval). Employing 3rd generation design it is possible to obtain 30% to 50% higher particle velocity. This design enables a better control over heating of particles. Improved velocity and efficient particle heat input might be beneficial in terms of deposition efficiency. Figure 1.2 is a schematic of three generations of HVOF torches. There are number of gas fuel HVOF torches available such as Diamond Jet (DJ-HVOF) from Sulzer Metco, HV-2000 from TAFA Praxair, Detonation Gun from Praxair Inc and JetKote, from Deloro Stellite. Additionally, there are number of HVOF systems available that use liquid fuel such as; JP-5000-8000 from TAFA Praxair and CJS from thermico.

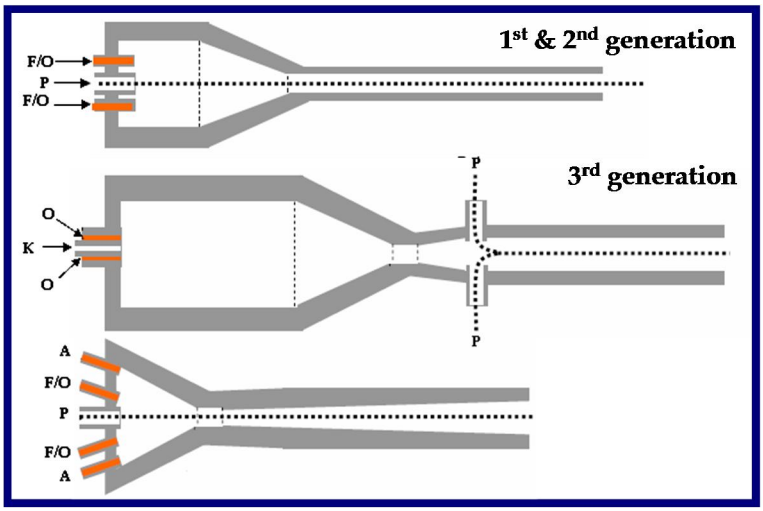

Figure 1.2. Schematic of different designs of HVOF torches. A – Compressed air, F – Fuel gas, O – Oxygen, K – Kerosene, P – Powder.

To reduce the oxidization and decomposition of material in HVOF process, another HV technique emerged which is called high velocity air fuel (HVAF) that uses the air instead of oxygen as an oxidizer. HVAF technique provides a flame with slightly higher gas velocities and lower temperature. It is noted that by this technique it is possible to deposit coatings that are less affected by oxidization and decomposition.

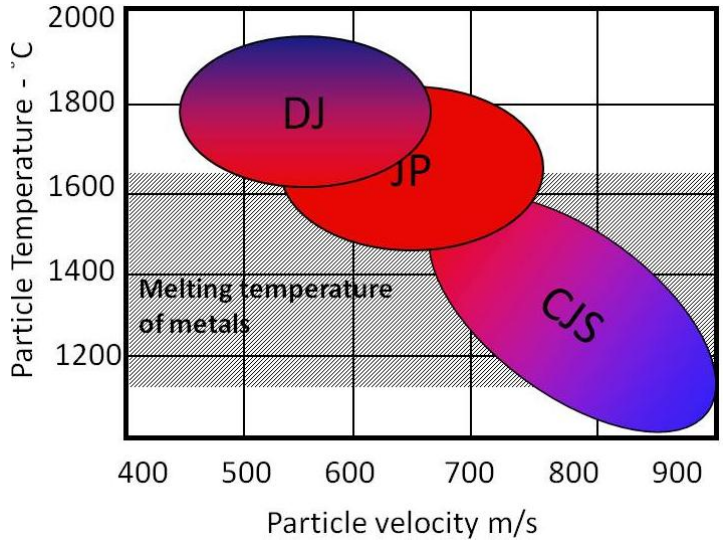

Figure 1.3. Particle temperature and velocity of carbide based coatings applied by different commercially available HVOF systems.

In most recent years another HV technique is developed by Thermico, Germany, this system is operated with hydrogen-stabilized kerosene-oxygen combustion. The combustion process takes place in two steps in order to realize improved control of the level of thermal energy introduced into the process. The hydrogen is burned with excessive oxygen in a short subsonic high pressure combustion chamber. Because of its lower reactivity, the injected liquid fuel is only burned in the supersonic section of the nozzle downstream of the throat. In this technique the jet temperature is controlled by a kerosene-oxygen system and the jet velocity is controlled by hydrogen-oxygen system. In fact in this setting, temperature and velocity control system is decoupled. This unique design provides control on temperature that enables to process very fine powder fractions without overheating the particles. This technique provides even denser coatings compared to other gas or liquid fuel HVOF technique with negligible oxidation or decarburization. Figure 1.3 shows the general trends of temperature and velocity in different developed HVOF torches. Development trend in HVOF torches over the time in recent years is towards the higher velocity and lower particle temperature. Table 1.1 shows the characteristics of each HVOF torch that are commercially available.

Table 1.1. Characteristics of commercially available HVOF torches.

	Fuel	Nozzle system	Gas velocity (m/s)	Combustion pressure (bar)	Powder feeding
Diamond Jet (DJ-2600, DJ-2700)	Hydrogen, Methane, Ethylene, Propylene, Propane	De laval	2140	7	Axially
JetKote	Hydrogen, Propylene, Ethylene, Propane, Methane	Straight	2500	4.5–7.5	Axially
HV2000	Hydrogen, Propylene, Propane	Straight	-	-	Axially
JP-5000	Kerosene	Straight	2200	5–10	Radially
CJS	Kerosene+hydrogen	Straight	-	6–20	Radially

1.3 Interactions at different levels: A multi disciplinary approach to deposit formation

1.3.1 Interaction of gases (Flame formation)

Starting from powder feeding to the thermal spray torch up to coating formation stage, different levels of interactions can be considered as interaction of gases for flame formation, interaction of flame stream with particles and interaction of in-flight particles with substrate The flame formation is result of interaction of different gases with each other or interaction of liquids and gases. This stage defines the chemistry and energy state (thermal and kinetic) of the flame. By controlling the chemistry and energy state of the flame it is possible to directly control and/or manipulate the state of the in-flight particles. For example by controlling the fuel to oxygen ratio, it is possible to control the flame chemistry ranging from oxidizing to reducing and obtained flame temperature. Furthermore by controlling the combustion chamber pressure that is related to the total flow of processing gases, different states of kinetic energy for the flame can be achieved.

1.3.2 Interaction of flame stream with particles

Second stage of interaction involves the interaction of feedstock materials with the flame and the environmental gases. As soon as feedstock material enters the flame stream, heat transfer takes place from the flame to the particle surface by convection and it continues from the surface of the particle towards the center by conduction. Particle/gas heat transfer coefficient and thermal conductivity of parti-

cles play important role at this stage. The kinetic energy of flame transfers to the particles and causes dragging and accelerating of particles. At this stage depending on flame chemistry during the flight of particles within the flame towards the substrate, particles might undergo oxidation (in oxidizing flame conditions) or retain their original phases (in reducing conditions). Reducing flames help to shield the particles from oxidation by consuming the oxygen around the flying particles. In some flame spray processes with smaller flames there is possibility that in-flight particles get exposed to ambient gases. The same criteria can be considered in processing of carbide-based composites to control the decomposition of material. However, most important consideration in processing the carbide based materials is controlling the heat input during their flight within the flame which can be controlled by temperature and dwell time of particles (depends on velocity and stand off distance).

The level of interaction of feedstock particles with the flame also highly depends on the particles characteristics. The main particle characteristics are; particle material, particle size, density and morphology of particles. Heat transfer properties of flame and particles define that during particles flight how well the particles absorb the heat from the flame and transfer it to the core. During the interaction of particles with the flame smaller particles heat up and accelerate quickly compared to the bigger particles. Difference in particle size causes presence of particles at different melting states within the flame as the smaller particles can be fully molten but bigger ones are still in their partially molten or solid state. In sever situations there is possibility of evaporation of small particles. Presence of solid particles in flame stream might cause reduction in deposition efficiency as un-molten particles bounce back from the surface leaving the craters and do not get deposited. In addition to fluctuation in melting state due to different particle size the kinetic energy (velocity) of particles will be different as well. The effect of heat input to the particles employing air plasma and HVOF techniques are shown in Figure 1.4 by capturing the splats on the substrate. As it is shown in Figure 1.4a particles undergone melting and carbides are dissolved into the binder. This means higher melting state of particles that is due to higher temperature and lower velocity experienced by particles in this process. Figure 1.4b shows the CrC-NiCr particles processed by HVOF technique, carbide particles are retained in the microstructure. However, lower melting state (lower temperature and higher velocity) results in particles with higher unmolten fraction that makes the adhering of particles more difficult. The craters observed on the substrate are due to impact of high velocity solid particles which bounced back from the surface.

Effect of particle density is considered to be similar as the particle size. Particles density is highly dependant on employed manufacturing techniques. For instance, powders manufactured by agglomeration and sintering show lower density compared to agglomerated, sintered and plasma densified powders.

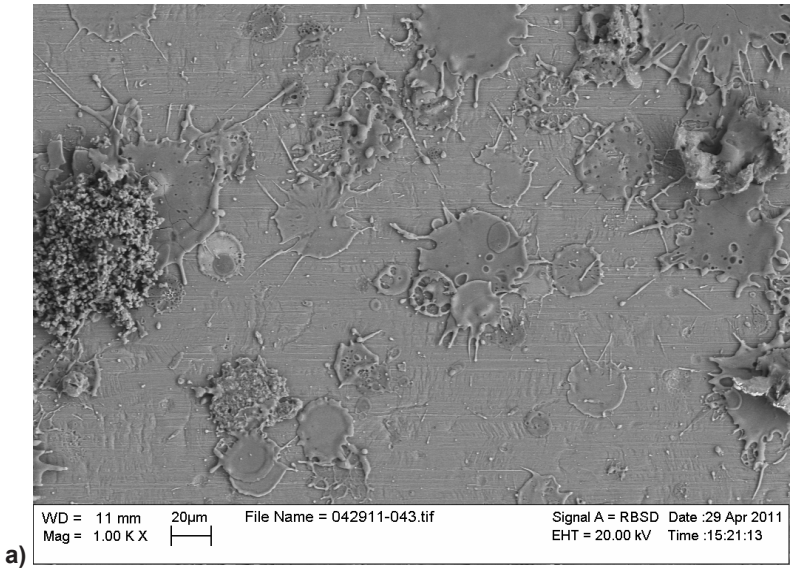

Figure 1.4. (a) CrC-NiCr splats sprayed by APS (high heat input) that shows full decomposition, and (b) HVOF (low heat input) that shows retaining the CrC. In (b) low melting of particles leave the particles in their solid state and cause crater trace on the substrate surface. (Courtesy of Dr. Yikai Chen).

Lower powder density means higher surface-to-volume fraction that is translated to higher heat absorption. In some cases excessive heat input might be detrimental to

particle structure. For example in processing of carbide based composites excessive heat input intensifies the decomposition of carbides.

Particle morphology has main effect on how the particles are flying within the flame. In fact the particle morphology plays a role on how the kinetic energy of the flame is transferred to the particles. Another parameter which has practical importance is the flowability of the particles that is directly correlated to particle size as well as morphology. Problem with flowability of particles might cause the clogging in the spray torch or the feeding system.

1.3.3 Interaction of in-flight particles with substrate

Interaction of in-flight particles with substrate yields to coating formation by following consecutive steps:

- *Successful impingement of in-flight particles:* Not all of the in-flight particles will contribute to the coating formation as some fractions of those will only hit the substrate and bounce back. It usually happens in processing of particles with higher fraction of un-molten material.
- *Flattening, solidification and bonding of particles on the substrate surface to form splats (first layer formation):* Splat formation depends on in-flight particles state before impingement, particles characteristics and the substrate characteristics. If the particle contains higher amount of molten material the spreading will be easier. Another factor defining the spreading of particle is velocity (kinetic energy) of impinging particles. Higher velocity yields to better spreading and formation of splats with bigger surface area. Changing the thermal conductivity, surface roughness and the temperature of substrate will also have effect on dynamics of splat formation. At each splat certain amount of stresses will be developed due to severity of quenching that is in away related to how well the splat is in touch with substrate. Sometimes high amount of quenching stress at single splats might cause fracture and cracking of splats.
- *Continuous coating build up by splat formation over the previous layer of material:* The dynamics of formation of second layer and so on will be different as the materials are being deposited on previously deposited layer rather than the original surface of substrate. In this case the thermal conductivity and solidification dynamics will be different than the first layer. During the coating build up the stresses will be developed as well. Different stresses have been called peening\quenching stress, deposition stress and thermal stresses that are ranging from first layer to whole coating/substrate system. Stresses in thermal sprayed coatings play important role on performance of coating/substrate system as it might be one of the limiting factors in its wear and fatigue performance. Other important factors that are results of coating build up can be considered as porosities, splat/substrate adhesion and splat/splat cohesion.

1.4 Application of cermet (Ceramic-metallic) coatings in wear resistant surfaces

A combination of different performance characteristics such as abrasion, erosion and corrosion resistant make the cermets in form of coatings as a widely used material in industrial and engineering components. Cermets (with general formula of Carbide or oxide-Metal) are composite materials that contain hard carbide or oxide particles dispersed within tough metallic matrix. Such combination provides hardness owing to hard ceramic particles and toughness owing to metallic binder. Among different cermets, WC-Co has been well studied and has gained industrial interests due to its satisfactory and in some cases, superior erosion and abrasion performance. It has been shown by addition of chromium to the cobalt binder, erosion and corrosion resistance of the coating are improved several times [2, 3]. Recently the Hard Chrome Alternative Team, HCAT, validated the use of WC-CoCr coatings as a replacement to chrome plating for commercial and military airplanes landing gears. Successful replacement of chrome plating by WC-CoCr is owing to materials superior performance and the thermal spraying environmental friendly nature.

Many works have been done on evaluation of different properties and performance of thermally sprayed cermet coatings. Most of these studies are around WC-Co coatings produced by different thermal spray techniques. The main performance related properties studied in this class of materials has been wear of materials and in some cases corrosion performance. In general to have a mature understanding on processing, microstructure, properties and performance of cermet thermal sprayed coatings, following questions need to be answered:

- What is the effect of processing technique on microstructure, mechanical properties and wear performance of carbide based coatings?
- How the microstructure, mechanical properties and wear performance of carbide based coatings are affected by starting powder characteristics?
- How does carbide particle size affect the mechanical properties and wear performance?
- What are the main wear mechanisms encountered in wear process of carbide based coatings?
- How is wear performance affected by wear process parameter? (abrasive particle size and hardness, normal applied load, stress level.)

Following is a brief review of published works around carbide-based coatings.

1.4.1 Effects of process techniques, parametrs and starting material characteristics on microstructure, mechanical properties and wear performance of cermet coatings

Different thermal spraying techniques have been employed to process CerMet materials and their effects on wear performance of resultant coatings have been studied. Mainly this class of materials have been processed by air and vacuum plasma spray (APS, VPS), high power plasma spray (HPPS), low pressure plasma spray (LPPS), gas fuel and liquid fuel HVOF, HVAF and detonation spray [4–12]. Additionally, effects of different spraying conditions on wear performance of coatings were studied [9, 13–16].

As it is explained previously main difference between variable spraying techniques and processing parameters are obtained flame condition and chemistry that define temperature and velocity of flame. Different flame temperature and velocity result in different in-flight particle state. Air plasma spray technique (APS) applies temperature around 12000 °C. In this technique particle velocity is relatively low. Due to ambient atmosphere and longer dwell time (Low velocity), powders experience high level of oxidation and decomposition (decarburization). In vacuum plasma spray (VPS) technique the temperature is same as APS but the velocity slightly increased and due to vacuum there is no oxidation involved. In low pressure plasma spray, (LPPS) the temperature is same as APS and VPS but due to lower oxygen partial pressure, particles undergo small amount of oxidation. HVOF technique, applies higher velocity with lower flame temperature that results coatings with higher density. This is mainly due to higher kinetic energy of sprayed particles.

Liao et al. [5] showed presence of nanocrystalline and amorphous phases as well as secondary phases for both WC-Co coatings made by HVOF and APS. Nevertheless, he did not report extensive decarburization or presence of nanocrystalline and amorphous phases in coatings produced by VPS. The loss of Co in processing of WC-Co by plasma system is also reported and attributed to the evaporation of binder. Such loss was not observed in HVOF system [17, 18]. It is shown that in processing of WC-Co and WC-CoCr by HVOF system partial decarburization of WC to W_2C happens [6, 12, 19–21]. In processing of CrC-NiCr decarburization of carbides in form of Cr_7C_3 takes palce [5, 22]. Presence of nanocrystalline $Cr_{23}C_6$ was reported as a dispersed phase within NiCr metallic matrix [15]. However, severity of decarburization and oxidation of carbide-based materials depend mainly on flame chemistry and processing conditions. Additionally, phases and compositions that are present in starting powder also define coating final structure. It is shown by Li et al. [23] that the powder with WC particles aggregated with Co_3W_3C instead of metallic cobalt is more preferable for WC to decompose to W_2C. Sudaprasert et al. [8] showed that WC-Co coating processed by HVOGF system shows higher level of decarburization compared to HVOLF system. This is attributed to higher velocity (less dwell time) and lower temperature achieved by HVOLF system. A similar study was done by Jacobs et al. [11] to address the effects of HVOF and HVAF processing techniques on microstructure

of WC-CoCr and WC-Co coatings. They reported 10% carbon loss in processing the WC-CoCr by HVOF while there was no carbon loss for the coating processed by HVAF system. No oxidation and decarburization was observed in processing both WC-Co and WC-CoCr by HVAF system. Oxidation and decarburization was reported for coatings processed by HVOF system.

As decarburization plays an imperative role in microstructure, mechanical properties and performance of carbide-based thermal sprayed coatings, it will be discussed thoroughly later on.

Comparing hardness, residual stresses and porosity values it is noted coating made by HVOF technique gives highest hardness and lowest porosity values that is due to higher kinetic energy of particles upon impact [5, 7, 9, 12]. Coatings produced with VPS show the highest compressive stresses that might be advantageous for situations in which the coating is subjected to tensile stresses. However in this comparison no results of HVOF high kinetic energy torches (JP-5000 and CJS) were considered as they enable to produce dense coatings with even higher compressive stresses [5, 6]. Qiao et al. [14] cited that higher hardness values reached for WC-Co coatings processed at higher temperatures. Although they attributed the low hardness values to presence of weak bonding between WC and binder, nanometer pores and low adhesion between splats. Among carbide based coatings, WC coatings processed by HVOF technique with 12Co, 14CoCr and 17Co as binder in general have higher hardness than CrC-NiCr coatings. Further addition of metallic binder such as Ni or Ni-Cr-Fe-S-B lowers the hardness further [24].

Most of the authors pointed that coatings produced by HVOF technique, demonstrate better wear performance [5, 25–27]. The better performance of HVOF processed coating over APS, VPS and LPPS coatings attributed to lower porosity, better splat bonding, higher hardness and improved fracture toughness. Above mentioned improvements in HVOF processed coatings are due to higher kinetic energy and lower heat input of particles achieved in this process. Comparing HVOF with HVAF process an improvement of wear performance for HVAF processed coatings were observed that is also attributed to even denser coatings with less thermal affected structure [11]. However, it is noted that not always higher velocity yields better coating in terms of performance. For example, despite the higher velocity in HVOLF compared to HVOGF due to less heat absorbtion the core of particles remains un-molten and upon impact the particles suffer extensive mechanical damage that causes carbide fracture and deficient carbide-matrix bonding. Such structure yields to poor wear performance [8]. As the processing techniques, available materials and wear performance testing apparatus are different comparing the wear performance extracted from different references is a difficult and in some cases impossible task. However, published results within an identical report make it possible to draw the general picture for different comparative purposes. It is noted that in general abrasion wear performance of WC-CoCr is better than CrC-NiCr. It is hypothesized that wear improvement is result of higher hardness of WC particles over CrC particles [6]. In other studies it was reported that WC-CoCr exhibits improved erosion performance over WC-12Co [2, 24]. The better erosion performance is considered to be due to improvement of the bonding

between carbides and binder in CoCr binder over Co binder. CrC-NiCr shows better erosion-corrosion resistance over WC-Ni [13].

1.4.2 Decarburization in carbide based cermets

The first step to obtain a cermet coating applicable to wear situations is to satisfy two factors; well dispersed fine oxide or carbide particles within the metallic matrix and good cohesion between composite materials, hard particles and tough metallic binder [28, 29]. These are factors affecting the wear performance within one lamella. Most of the microstructures obtained by different TS techniques exhibit such features. Beside these two primary factors the overall coating microstructure and splat/splat bonding quality are important factors contributing to wear performance of coatings as well. Coatings microstructure and splat/splat bonding quality are greatly affected by feedstock material and processing conditions [12, 30]. Accordingly, understanding the microstructural evolution in cermet coatings is a crucial step towards providing in depth knowledge regarding to wear performance.

One phenomenon that directly affects the interfacial nature (carbide/matrix and splat/splat) and quality of sprayed WC-based coatings is decarburization and formation of W_2C phase. In WC-17%Co coatings in addition to WC and Co (f.c.c), presence of W_2C, W and amorphous/nanocrystalline Co based phases was reported [23, 31, 32]. Similar finding was also reported for WC-12Co [27, 33, 34] and WC-15Co [35, 36]. Due to partial decarburization of WC particles within the coating rounding of carbides were reported compared to carbide in starting feedstock material. W_2C was surrounded by nanocrystallin/amorphous Co rich binder and was located around the original WC particles [19, 21, 31, 32, 37].

Vinayo et al. [18] and Tu et al. [38] showed that WC in presence of oxygen transforms to W_2C and this phase transforms to a metallic W when high temperature and oxygen rich condition is obtained. Reactions taking place in thermal spraying of WC-Co are as follow:

1) $2WC + O_2 <=> W_2C + CO_2$
2) $W_2C + 1/2\ O_2 <=> W_2\ (CO)$
3) $W_2\ (CO) <=> 2W + CO.$

Further Fincke et al. [39] hypothesized that during thermal spraying carbon diffuses from the WC into the metallic matrix and that cobalt diffuses from the matrix into the carbide:

4) $4Co + 4WC + O_2 <=> 2Co_2W_4C + 2CO$
5) $3Co + 3WC + O_2 <=> Co_3W_3C + 2CO$
6) $12Co + 12WC + 5O_2 <=> 2Co_6W_6C + 10CO.$

He also showed the first three reactions can only happen on the surface of WC particles, and reactions 4–6 happen when there is sufficient WC dissolved into the liquid phase. In general, regarding to the published works following mechanisms can be considered to explain the formation of W_2C:

Direct oxidation of WC, [20] the thermal decomposition of WC to W_2C, preferential dissolution of C and transformation to W_2C with C diffusing away in the liquid Co [20]. It is hypothesized that W_2C precipitates from the melt after impingement of particles to the substrate. This is supported by absence of dislocations within the W_2C structure and presence of dislocations within the WC structure. Observed dislocations within WC are most probably formed due to the strike of WC particles to the substrate [20, 31].

Based on Stewart et al. [20] work a model for microstructural features observed in WC-Co coatings has been proposed. Based on this model the microstructure consists of melting of cobalt during spraying, dissolution of WC into the molten cobalt, loss of carbon from the periphery of the particles by oxidation, quenching and solidification of the particles upon impact that cause formation of amorphous binder phase and precipitation of W_2C and W.

There is still lack of information on thermodynamics and kinetics of decarburization in WC-CoCr cermet coatings as well as understanding the effect of decarburization on the interface quality. Thus, we need to have clear idea about influence of solidification rate and oxygen content in formation of nano-crystalline/amorphous phases and secondary phases formed due to decarburization.

1.4.3 Effect of carbide grain size on microstructure, properties and wear performance of cermet coatings

One of the most crucial parameters that affects mechanical properties and wear performance of carbide-based cermet coatings is carbide grain size. For sintered carbide-based cermets, researchers have shown obtaining superior mechanical properties and a gain in wear performance by reducing the carbide size [40–42]. The driving force for reducing the carbide grain size comes from the fact that as the carbide size becomes smaller, the binder mean free path is decreased, resulting in higher resistance against deformation and material loss. Many researchers [14, 21, 30, 35, 43–49] have pursued such a hypothesis to improve the wear performance of HVOF WC-Co by reducing the WC grain size to the nanoscale. Nevertheless, for thermal spray coatings, different researchers have shown sometimes contradictory wear performance results for the effect of reducing carbide size from conventional to nano.

It is shown that decarburization is more pronounced in processing the finer WC materials compared to the coarser one as the surface-to-volume ratio increase with decreasing the carbide size [14, 21, 30, 35, 43–49]. Qiao et al. [14] reported that higher temperature increases the bonding quality between WC and binder. He concluded that wear resistance decreases with increasing decarburization in sliding wear situation. Dent et al. [21] reported that nano-structured materials have lower abrasion resistance compared to the conventional one and they attributed the deficiency in wear to excessive decarburization of nano-structured WC materials. Similar to Dent et al. [21], Stewart et al. [35] reported lower wear resistance in all conditions for nano-composite coating compared to conventional coating. In another

study Bartuli et al. [43] showed gain using nano-structured composite material over conventional one regarding to its hardness, fracture toughness and wear resistance with reduced friction coefficient. However, they systematically optimized the processing parameters for deposition of nanostructured materials. Guilemany et al. [44] reported improvement in mechanical properties of nano-structured material. Nonetheless, they did not gain significant improvement in wear resistance of nano-structured coatings. Marple et al. [46] reported nano-structured coating containing micro-size WC particles (multimodal) shows improved hardness over conventional coating but there was a little or no improvement in wear resistance of this coating. However, they consider potential benefit and improvement using multimodal material as they observed improved deposition efficiency and larger processing window. Deposition efficiency improvement in this case might not be necessarily related to the carbide size reduction and it is most likely due to the particle size and morphology. Shipway et al. [47] reported that sliding wear resistance of nanostructured coating was even lower than conventional or sintered WC-Co. Yang et al. [48] reported a gain in dry sliding wear by using finer carbides. However, it needs to be considered that in this case finest carbide size that was employed had an average size of 0.8 μm which is much bigger compared to other reports (around 20 ~ 200nm). Guilemany et al. [50] showed that nanostructured coating exhibits higher hardness compared to bimodal or conventional but the best sliding and abrasion wear resistance belongs to bimodal coating.

1.4.4 Effect of tribo-medium characteristics on wear performance

Most important tribo-medium characteristics that have major impact on wear process are hardness and toughness of abrasive, erosive particles, particle size and shape, velocity and impact angel of particles in erosion tests.

Hardness is defined as resistance of a material to penetration by a hard indenter. Hardness of both counter faces has direct effect on penetration depth of abrasive particle on the material surface. However, hardness itself fails to predict the wear performance of some materials. As it is shown by Gahr [51] higher hardness does not however guarantee the better wear performance. For example cold work will increase the hardness significantly but will not improve wear resistance of metallic bulk materials. Debility in prediction of wear performance by hardness is due to the fact that hardness itself can not characterize dynamic interaction between abrasive particles and wearing material surfaces effectively. It is reported that wear rate of WC-Co increases employing the harder abrasive particles [52]. To consider two mating surfaces (abrasives and material) in relative motion as a system understanding the wear rate results are more plausible if the hardness is reported as a relative value of hardness of abrasive to hardness of material. One of the important factors in abrasion wear situations is penetration depth of abrasive particles into the material surface. The penetration depth of abrasive particles in abrasion wear test mainly depends on relative mechanical properties of material and the abrasive medium (hardness), applied load and shape of abrasive parti-

cles. Generally, spherical abrasive particles cause smaller amount of wear loss than angular particles in a given average particle size and hardness. Nevertheless, the effect of particle shape is smaller in three body abrasion as loose particles can reorient themselves during sliding and rolling contact compared with two body abrasion [51]. Figure 1.5 shows penetration depth of abrasive particle as a function of material surface hardness for two different particle shape (Sharp and spherical). It is assumed no crushing of particles happens and applied load on each individual abrasive particle is 5 Kg. Hardness of abrasive particle (2500 HV) is much higher than the hardness of material surface. As it is shown in Figure 1.5 the penetration depth of sharp particles always will be higher compared to spherical ones and pillowing of material for sharp particles will be more effective that results in higher wear.

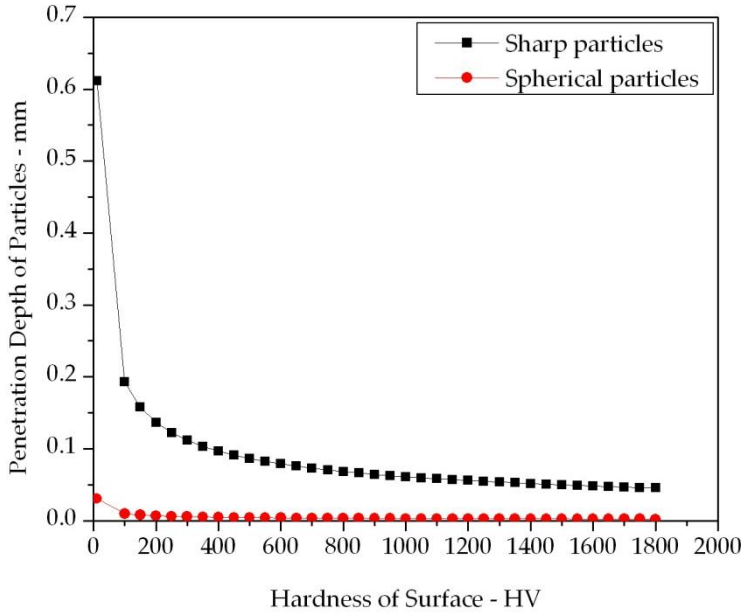

Figure 1.5. Penetration depth of sharp and spherical abrasive particles versus hardness of surface.

It is reported by Stewart et al. [35] that by increasing the abrasive particle size regardless of its hardness the wear rate will be increased. During erosive wear, the dependence of wear loss on the impact angle is influenced by the size of the impinging particles, the impact velocity and the target material. A trend has been observed that the wear loss increases, at a given impact angle, with increasing size and velocity of the impinging particles [51].

To our knowledge there is no particular understanding in effect of abrasive particle shape on mechanism of abrasive wear.

1.5 Conclusion

Definition of thermal spray process was given and complex physical and chemical phenomena involved from powder injection to coating formation was explained by recourse to a multidisciplinary approach that addresses different interactions at different levels of flame formation, particle impingement and coating build up. It was noted that melting state and kinetic energy of in-flight particles are crucial parameters in understanding and controlling the deposit formation. As processing and characterization of wear resistant carbide based coatings will be of primary interest of current study, a brief review of published works was provided. It was concluded that material decompositions, secondary carbide phase formation, porosities, splat/splat and carbide/binder bonding quality, purity of phases in starting feedstock material, binder material and content, reinforced carbide particle size as well as residual stresses are important factors controlling the wear. Advantage of reducing the carbide size down to 0.8 μm in terms of wear performance was reported. However, there is no confirmed evidence available demonstrating the advantage in wear by reducing the carbide size to nano-scale.

Decarburization and formation of secondary carbides within the microstructure has been considered to have a detrimental effect on wear performance. It can be concluded that there is a need to further understand the flame formation mechanism and interaction of in-flight particles with the flame to be able to optimize the process for improved wear performance. It was also noted that Because of different modifications applied to different wear test instruments in different laboratories comparing the results with each other is more difficult. Additionally each researcher has chosen a different way to report the results that makes the comparison more complicated. Part of the problem seems to be raised from different definitions considered for wear and variable classification considered for encountered wear situation.

References

1. Davis, J.R. Handbook of thermal spray technology. 2004: ASM international.

2. Karimi, A., et al. Slurry erosion behaviour of thermally sprayed WC-M coatings. Wear, 1995. 186–187(Part 2): p. 480–486.

3. Perry, J., T. Hodgkiess, and A. Neville. A. comparison of the corrosion behavior of WC-Co-Cr and WC-Co HVOF thermally sprayed coatings by in situ atomic force microscopy (AFM). Journal of Thermal Spray Technology, 2002. 11(4): p. 536–541.

4. Sugiyama, K., et al. Slurry wear and cavitation erosion of thermal-sprayed cermets. Wear, 2005. 258(5–6): p. 768–775.

5. Liao, H., B. Normand, and C. Coddet. Influence of coating microstructure on the abrasive wear resistance of WC/Co cermet coatings. Surface and Coatings Technology, 2000. 124(2–3): p. 235–242.

6. Murthy, J.K.N. and B. Venkataraman. Abrasive wear behaviour of WC-CoCr and Cr3C2-20(NiCr) deposited by HVOF and detonation spray processes. Surface and Coatings Technology, 2006. 200(8): p. 2642–2652.

7. Mann, B.S. and V. Arya. Abrasive and erosive wear characteristics of plasma nitriding and HVOF coatings: their application in hydro turbines. Wear, 2001. 249(5–6): p. 354–360.

8. Sudaprasert, T., P.H. Shipway, and D.G. McCartney. Sliding wear behaviour of HVOF sprayed WC-Co coatings deposited with both gas-fuelled and liquid-fuelled systems. Wear. 255(7–12): p. 943–949.

9. Qiao, Y., Y. Liu, and T. Fischer. Sliding and abrasive wear resistance of thermal-sprayed WC-CO coatings. Journal of Thermal Spray Technology, 2001. 10(1): p. 118–125.

10. Voyer, J. and B.R. Marple. Sliding wear behavior of high velocity oxy-fuel and high power plasma spray-processed tungsten carbide-based cermet coatings. Wear, 1999. 225–229(Part 1): p. 135–145.

11. Jacobs, L., M. Hyland, and M. De Bonte. Comparative study of WC-cermet coatings sprayed via the HVOF and the HVAF Process. Journal of Thermal Spray Technology, 1998. 7(2): p. 213–218.

12. Wayne, S. and S. Sampath. Structure/property relationships in sintered and thermally sprayed WC-Co. Journal of Thermal Spray Technology, 1992. 1(4): p. 307–315.

13. Espallargas, N., et al. Cr3C2-NiCr and WC-Ni thermal spray coatings as alternatives to hard chromium for erosion-corrosion resistance. Surface and Coatings Technology, 2008. 202(8): p. 1405–1417.

14. Qiao, Y., T.E. Fischer, and A. Dent. The effects of fuel chemistry and feedstock powder structure on the mechanical and tribological properties of HVOF thermal-sprayed WC-Co coatings with very fine structures. Surface and Coatings Technology, 2003. 172(1): p. 24–41.

15. Ji, G.-C., et al. Microstructural characterization and abrasive wear performance of HVOF sprayed Cr3C2-NiCr coating. Surface and Coatings Technology, 2006. 200(24): p. 6749–6757.

16. Zhao, L., et al. Influence of spray parameters on the particle in-flight properties and the properties of HVOF coating of WC-CoCr. Wear, 2004. 257(1–2): p. 41–46.

17. Varcalle, D.J. Jr., Smolik, G.C. Wilson, G. Iron and J.A. Walter. An evaluation of tungsten carbide-cobalt coatings fabricated with the plasma spray process. In Protective Coatings: Processing and Characterization. 1990. Hoboken, NJ.

18. Vinayo, M.E., et al. Plasma sprayed WC-Co coatings: Influence of spray conditions (atmospheric and low pressure plasma spraying) on the crystal structure, porosity, and hardness. Journal of Vacuum Science & Technology A: Vacuum, Surfaces, and Films, 1985. 3(6): p. 2483–2489.

19. Karimi, A. and C. Verdon. Hydroabrasive wear behaviour of high velocity oxyfuel thermally sprayed WC-M coatings. Surface and Coatings Technology, 1993. 62(1–3): p. 493–498.

20. Stewart, D.A., P.H. Shipway, and D.G. McCartney. Microstructural evolution in thermally sprayed WC-Co coatings: comparison between nanocomposite and conventional starting powders. Acta Materialia, 2000. 48(7): p. 1593–1604.

21. Dent, A., S. DePalo, and S. Sampath. Examination of the wear properties of HVOF sprayed nanostructured and conventional WC-Co cermets with different binder phase contents. Journal of Thermal Spray Technology, 2002. 11(4): p. 551–558.

22. Vuoristo, P., K.N., A. Mäkelä and T. Mäntylä. In 7th National Thermal Spray Conference. 1994. Boston.

23. Li, C.J., A. Ohmori, and Y. Harada. Effect of powder structure on the structure of hermally sprayed WC-Co coatings. Journal of Materials Science, 1996. 31(3): p. 785–794.

24. Hawthorne, H.M., et al. Comparison of slurry and dry erosion behaviour of some HVOF thermal sprayed coatings. Wear, 1999. 225–229(Part 2): p. 825–834.

25. Dorfman, M.R., B.A.K., J. Nerz, and A.J. Rotolico. A Technical Assessment of High-Velocity Oxygen-Fuel Versus High-Energy Plasma Tungsten Carbide-Cobalt Coatingsfor Wear Resistance. in 12th International Thermal Spray Conference. 1989. London: The Welding Institute.

26. Niemi, K., P.V., T. Mäntylä, G. Barbezat, A.R. Nocolle. Abrasion Wear Resistance of Carbide Coatings Deposited by Plasma and High Velocity Combustion Processes. in Thermal Spray: International Advances in Coating Technology. 1992. Materials Park, OH, USA: ASM International.

27. Nerz, J., B.K., A. Rotolico. Effects of Deposition Methods on the Physical Properties of Tungsten Carbide 12 wt.% cobalt Thermal Spray Coating. in Protective Coatings: Processing and Characterization. 1990. Warrendale, PA, USA: The Minerals, Metals and Materials Society.

28. Nerz, J., B. Kushner, and A. Rotolico. Microstructural evaluation of tungsten carbide-cobalt coatings. Journal of Thermal Spray Technology, 1992. 1(2): p. 147–152.

29. Hutchings, I.M. Tribological properties of metal matrix composites. Materials Science and Technology, 1994. 10: p. 513–517.

30. Usmani, S., et al. Effect of carbide grain size on the sliding and abrasive wear behaviour of thermally sprayed WC-Co coatings. Tribology Transactions, 1997. 40(3): p. 470–478.

31. Verdon, C., A. Karimi, and J.L. Martin. A study of high velocity oxy-fuel thermally sprayed tungsten carbide based coatings. Part 1: Microstructures. Materials Science and Engineering A, 1998. 246(1–2): p. 11–24.

32. Stewart, D.A., P.H. Shipway, and D.G. McCartney. Influence of heat treatment on the abrasive wear behaviour of HVOF sprayed WC-Co coatings. Surface and Coatings Technology, 1998. 105(1–2): p. 13–24.

33. Kim, H., Y. Kweon, and R. Chang. Wear and erosion behavior of plasma-sprayed WC-Co coatings. Journal of Thermal Spray Technology, 1994. 3(2): p. 169–178.

34. Barbezat, G., A.R. Nicol, and A. Sickinger. Abrasion, erosion and scuffing resistance of carbide and oxide ceramic thermal sprayed coatings for different applications. Wear, 1993. 162–164(Part 1): p. 529–537.

35. Stewart, D.A., P.H. Shipway, and D.G. McCartney. Abrasive wear behaviour of conventional and nanocomposite HVOF-sprayed WC-Co coatings. Wear, 1999. 225–229(Part 2): p. 789–798.

36. Usmani, S., S. Sampath, and H. Herman. Thermal spray processing of nanoscale materials ——A Conference Report with Extended Abstracts, in Journal of Thermal Spray Technology, C.C. Berndt, Editor. 1998, Springer Boston. p. 429–431.

37. Grimberg, I., et al. Tungsten carbide coatings deposited by high-velocity oxyfuel spraying on a metallized polymeric substrate. Surface and Coatings Technology, 1997. 90(1–2): p. 82–90.

38. Tu, D., et al. Tungsten carbide phase transformation during the plasma spray process. Journal of Vacuum Science & Technology A: Vacuum, Surfaces, and Films, 1985. 3(6): p. 2479–2482.

39. Fincke, J.R., W.D. Swank, and D.C. Haggard. Comparison of the Characteristics of HVOF and Plasma Thermal Spray, in Thermal Spray Industrial Applications, C.C.B.r.a.S. Sampath, Editor. 1994, ASM International. p. 325–330.

40. Jia, K. and T.E. Fischer. Abrasion resistance of nanostructured and conventional cemented carbides. Wear, 1996. 200(1–2): p. 206–214.

41. McCandlish, L.E., B.H. Kear, and B.K. Kim. Chemical Processing of Nanophase WC-Co Composite Powders. Materials Science and Technology, 1990. 6: p. 953–960.

42. McCandlish, L.E., B.H. Kear, and B.K. Kim. Processing and properties of nanostructured WC-Co. Nanostructured Materials, 1992. 1(2): p. 119–124.

43. Bartuli, C., et al. Parametric study of an HVOF process for the deposition of nanostructured WC-Co coatings. Journal of Thermal Spray Technology, 2005. 14(2): p. 187–195.

44. Guilemany, J.M., S. Dosta, J. Nin, and J.R. Miguel. Study of the Properties of WC-Co Nanostructured Coatings Sprayed by High-Velocity Oxyfuel. Journal of Thermal Spray Technology, 2005. 14(3): p. 405–413.

45. He, J. and J.M. Schoenung. A review on nanostructured WC-Co coatings. Surface and Coatings Technology, 2002. 157(1): p. 72–79.

46. Marple, B. and R. Lima. Process temperature/velocity-hardness-wear relationships for high-velocity oxyfuel sprayed nanostructured and conventional

cermet coatings. Journal of Thermal Spray Technology, 2005. 14(1): p. 67–76.

47. Shipway, P.H., D.G. McCartney, and T. Sudaprasert. Sliding wear behaviour of conventional and nanostructured HVOF sprayed WC-Co coatings. Wear, 2005. 259(7–12): p. 820–827.

48. Yang, Q., T. Senda, and A. Ohmori. Effect of carbide grain size on microstructure and sliding wear behavior of HVOF-sprayed WC-12% Co coatings. Wear, 2003. 254(1–2): p. 23–34.

49. Liu, Y., et al. Near-nanostructured WC-18 pct Co coatings with low amounts of non-WC carbide phase: Part II. Hardness and resistance to sliding and abrasive wear. Metallurgical and Materials Transactions A, 2002. 33(1): p. 159–164.

50. Guilemany, J.M., S. Dosta, and J.R. Miguel. The enhancement of the properties of WC-Co HVOF coatings through the use of nanostructured and microstructured feedstock powders. Surface and Coatings Technology, 2006. 201(3–4): p. 1180–1190.

51. Gahr, K.H.Z. Wear by hard particles. Tribology International, 1998. 31(10): p. 587–596.

52. Shipway, P.H. and J.J. Hogg. Dependence of microscale abrasion mechanisms of WC- Co hardmetals on abrasive type. Wear. 259(1–6): p. 44–51.

2. Tribology and wear: a comprehensive approach towards wear classification

2.1 Tribology

Based on merriam-webster online dictionary [1] tribology is defined as “a study that deals with the design, friction, wear and lubrication of interacting surfaces in relative motion (as in bearings or gears)”. Technically speaking, Jost in his report [2] calls tribology as “the science and technology of interacting surfaces in relative motion and of the practices related thereto”. The term, tribology, has gained more usage and became common in different engineering fields during the last 50 years. In early classical tribology books, it was considered as a “new term, which is not yet in common usage” [3].

Tribology covers many diverse disciplines including but not limited to physics, chemistry, mechanical engineering and material science and is of extreme technological importance. Similar to interdisciplinary nature of tribology it also deals with different size scales ranging from interacting atoms in contact to industrial machinery.

Beside the complexity of the multi-scale multi-disciplinary nature of tribological problems, still one of the main obstacles and challenges in this field seems to be choosing proper strategy and appropriate approach to understand the encountered contact conditions and resultant wear mechanisms. To overcome this problem there is an essential need to define a universal system consisting of all crucial variables involved in tribological problem of interest.

In this chapter different aspects and definitions of tribology and wear will be presented and limitations and applications of each definition will bee discussed. A tribo-system will be proposed as a primary tool to provide and identify most important variables of tribological problems. Finally a comprehensive approach for wear classification will be provided.

2.1.1 Tribo-system

In this framework a tribo-system is considered as set of body or bodies of interest in contact, tribological medium and tribological environment.

Bodies: In each tribo-system two primary solid bodies are considered and named as *first body* and *second body*. The first body is considered as the one

which its wear and friction is in main concern. The second body's wear and friction is not of primary concern. The contact conditions between first and second body mainly depend on presence or absence of *tribo-medium*.

A tribo-medium consists of fluids (lubricants or other gases) that might be mixed with particles. The presence of particles can be intentionally or be introduced during the tribological contact as detachments from the surfaces.

A tribo-environment is defined as the surrounding of the body or bodies in contact and tribo-medium. Figure 2.1 illustrates two different possible tribo-systems with each of its elements and their characteristics that have effect on system response and are needed to be considered in any tribological problems.

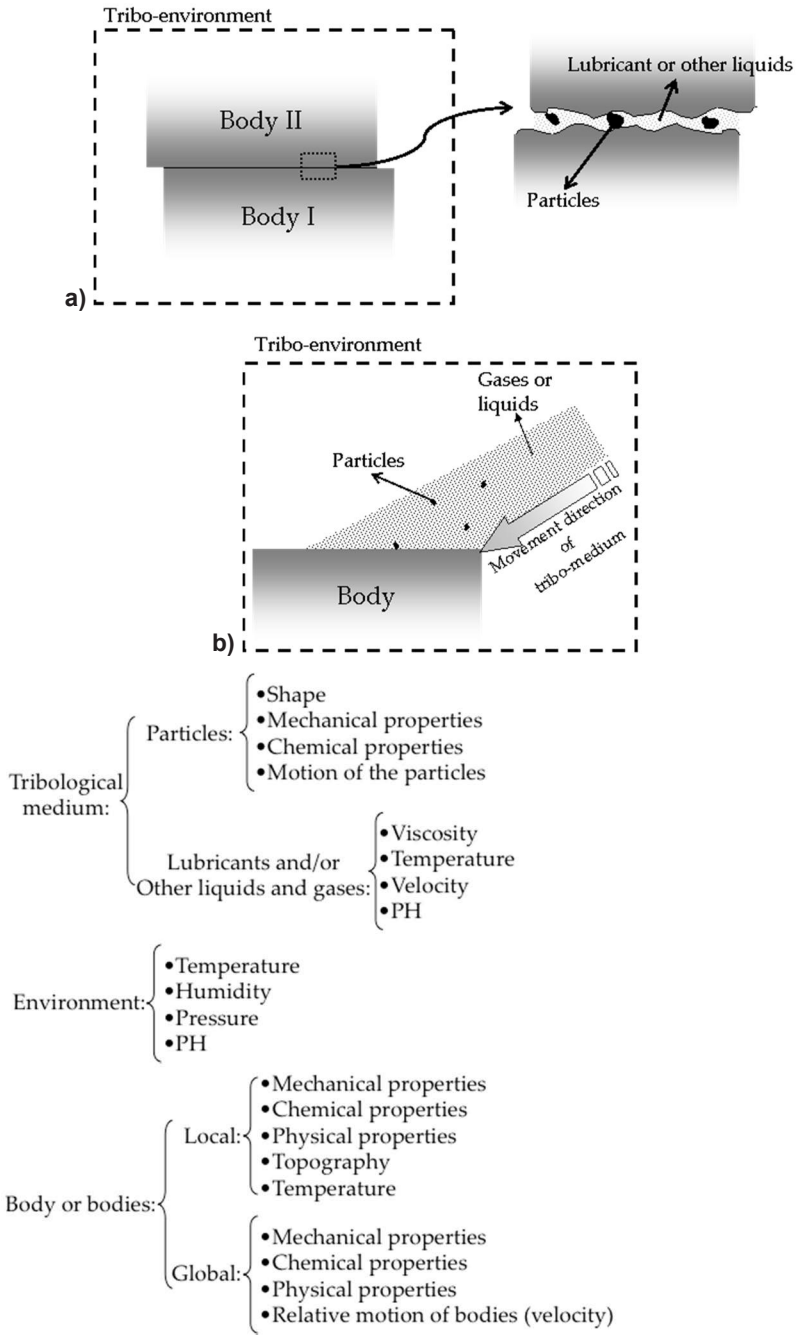

Figure 2.1. Two possible tribo-systems and related crucial parameters in each element of tribo-system.

2.2 Surface damages

Before moving to wear definition and explaining different wear mechanisms, it is important to note that not all damages occurred on the surface of material are necessarily considered as wear. To be able to make distinction between surface damage and wear, first we categorize different surface damages.

Based on ASM handbook [4] surface damage is defined as “topographical or microstructural changes, or both, in a surface layer”. Idealized classification of different surface damages are explained briefly as in follow:

a) *Structural changes:* such as phase transformations, recrystallization, amorphization, tempering, aging and etc. This surface damage might yield to a shape change of material. Structural changes do not necessarily imply damages to the surface. It is suggested to use the word “deterioration” in this case (suggested by Ghabchi).

b) *Plastic deformation:* Local or global (macro-scale) permanent deformation of material. Sever plastic deformation might yield to a shape change of material.

c) *Surface cracking:* Surface crack emanating can be caused by localized excessive thermo-mechanical strains or cyclic loading.

d) *Surface damage involving loss or gain of materials:* Different origins can be considered for loss of material from one surface. However, main processes that yield to material loss can be fracture (shear, brittle, ductile and fatigue), chip formation, extrusion and tearing. In some situations sticking of loose particles to one surface and transferring the material from one to another surface in contact can cause gain of material. Note all surface damages explained in number “d” which involve gain or loss of materials is due to thermal or mechanical stimuli. However, chemical reactions and corrosion can also cause gain or loss of materials.

It is noted that tribo-surfaces exhibit complex combination of different types of surface damages and generally single type of surface damage is not involved.

2.3 Wear

Defined by Almen [5] wear is loss of material from one surface, displacement of material within single surface or transfer of material from one surface to another. This can be considered as the widest definition of wear which covers an extensive range of engineering applications. By comparing the Almen’s definition of wear with different surface damages introduced previously, it is noted that he considers the loss of materials (involves thermo-mechanical and chemical causes) and plastic deformation (displacement of material) as general definition of wear. Surface cracking is not necessarily included in the wear definition but it could cause wear at some stages. Another narrower definition for wear is considered as “progressive

loss of substance of a body as a result of relative motion at the surface" [6–7]. In most recent standard terminology relating to wear and erosion wear, [8], wear defined as "alteration of a solid surface by progressive loss or progressive displacement of material due to relative motion between that surface and a contacting substance or substances". This definition is more close to the one presented by Almen and considers the material displacement as part of wear. In earlier version of same standard, [9] the definition for wear was more simplified as "damage to solid surface, generally involving the progressive loss of material".

Despite of wide applicability of these definitions none of them provide mechanistic information by which the material degradation has happened. The mechanisms of material degradation can be mechanical (plastic deformation or brittle fracture) and/or chemical (oxidation of metal or hydration of a ceramic) [10]. It is also possible that both mechanical and chemical mechanisms act simultaneously to degrade the material.

2.3.1 Classification of wear

There is no unique, globally well-accepted classification of wear and there are different ways proposed to classify the wear. In following, different proposed wear classifications are explained and possible deficiency of each classification is discussed. Blau [11] considers the wear classification based on three contact conditions (sliding, impact and rolling) between counterparts. In this classification, abrasive, adhesive, fatigue, fretting and polishing wear mechanisms are considered as subcategories and result of sliding wear. In this approach type of relative motion is more emphasized and the mechanism by which the material is removed or displaced is overlooked. Budinski [12] classified wear by considering four different material removal mechanisms (abrasion, erosion, adhesion and surface fatigue). Burwell [13], Rabinowicz [14], Bayer [15] and Furey [16] introduced four major wear mechanisms as adhesive, abrasive, corrosive and surface fatigue. Burwell [13] in his survey also added fifth category as "minor types" which involve erosion, cavitation and impact chipping.

Nevertheless, the fact that more than one mechanism at the time can be active in any given tribo- systems, makes it difficult to rely only on purely wear mechanism-based classifications. Another approach for classification of wear uses the nature of contacting materials and conditions of tribological experiments. As it is noted by Davis [17], the explained conditions might not be steady during the service or tribological experiments. Beside all explained classifications one should consider the presence or absence of lubricants that change the wear condition dramatically.

2.3.2 A systematic approach towards wear classification

Here we present an approach rather than a direct classification to systematically study and understand the wear in different tribological systems. This approach was first introduced by Blau [18] and further developed by Holmberg and Matthews [7]. In

this approach different aspects of wear such as mechanisms, type of relative motion of surfaces or contact conditions, environment and surface appearance after tribological contact have been considered. In fact this approach is an attempt based on previously proposed wear classifications to amend deficiencies of different classifications by incorporating the main logic behind each classification approach. To provide a systematic approach towards classification of wear three major terms needed to be defined:

2.3.2.1. Wear mode
2.3.2.2. Wear mechanism
2.3.2.3. Wear failure mode

More detailed definition of each above terms have been presented in following.

2.3.2.1 Wear modes

A wear mode defines the type of contact that is specified by kind of movement, geometry or environment.

Different wear modes are considered as:

a) Sliding
b) Rolling
c) Rolling + sliding
d) Impact (Large body, particle impact, liquid impact)
e) Cavitation.

All of these wear modes are shown in Figure 2.2 schematically. Some of these wear modes can be sub-divided further. For example, sliding and rolling can be continuous or with varying velocity (reciprocating). Relative motion normal to one of the bodies may lead to impact. Wear can be due to repeated particle impact or single large body impact. The wear can also be due to impact of large number of small particles or even liquid droplets over a surface area. Wear can also be the result of the collapsing of vapor or gas bubbles produced by local pressure fluctuations in a cavitating liquid close to a solid surface [19].

2.3.2.2 Wear mechanisms

A wear mechanism is considered as mechanisms by which material is removed or displaced from the surface.

Following mechanisms are considered as main and typical wear mechanisms:

a) Adhesive wear
b) Abrasive wear
c) Fatigue wear
d) Chemical wear.

a) Adhesive wear

In standard terminology [8], adhesive wear is defined as "wear due to localized bonding between contacting solid surfaces leading to material transfer between the two surfaces or loss from either surface".

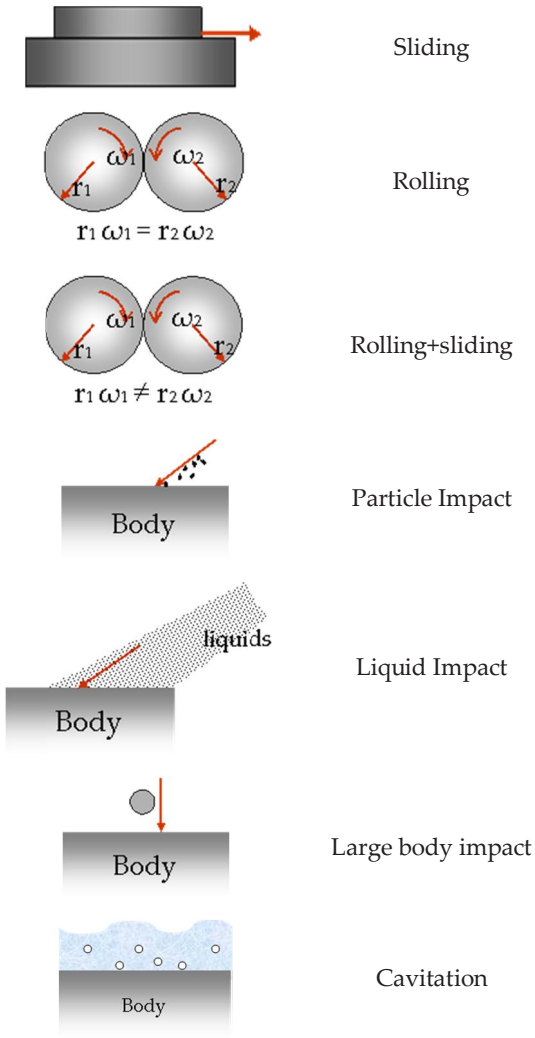

Figure 2.2. Schematic of different Wear modes. (Adopted from [19]).

To explain the fundamental of adhesive wear one should consider that material surfaces are not completely flat in microscopic level. In high magnification, even if they are polished perfectly, two surfaces will show ridges and valleys, asperities

and depressions. When two surfaces are brought together they touch only at the tip of a few asperities. Plastic deformation occurs locally and cold welding may form strongly bonded junctions between the two materials. When sliding begins (tangential motion is applied) the asperity of softer material will be separated from the bulk and material removal will occur. The adhesive wear mechanism is proposed by Bowden and Tabor [20] in 1950.

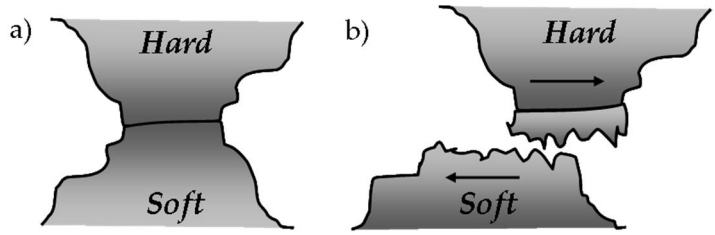

Figure 2.3. Schematic of adhesive wear mechanism: (a) Contact of asperities and possible cold welding. (b) Fracture of weaker material due to relative movement of surfaces in contact.

Further studies have criticized the original adhesive wear theory [21]. However, later on it was shown that the adhesive mechanism exists but not necessarily plays a dominant role in all wear conditions.

b) Abrasive wear

Abrasive wear based on ASTM standard terminology [8] is defined as: "Wear due to hard particles or hard protuberances forced against and moving along a solid surface." In case of hard and soft materials rubbing against each other, the harder surface asperities cause plastic deformation, plowing and cutting the surface of softer material.

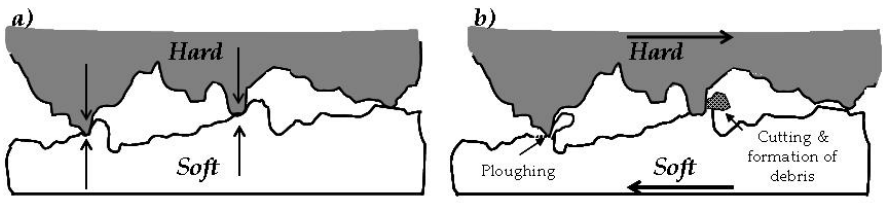

Figure 2.4. Schematic of abrasive wear mechanism of soft surface by hard surfaces in contact: (a) Contact of hard surface asperities with soft surface, (b) Plowing and cutting of soft material by asperities of harder surface.

When the tangential movement starts, the asperities of hard surface will plough the softer surface and will cause material removal or displacement. This is shown schematically in Figure 2.3.

Formation of abrasive grooves on the surface of soft material is result of this action.

Abrasive wear in most of the references is categorized to two-body and three-body abrasion. There are two completely different interpretations for definition of two-body and three-body abrasion. In one definition the primary concept is whether the abrasive particles are constrained (two-body) or free to roll (three-body) and in another one the primary concept is based on presence or absence of rigid counter surface backing the abrasives. These two concepts are explained and further criticized by Gates [22]. In the ASTM standard terminology relating to wear and erosion [8], two-body abrasive wear is defined as “form of abrasive wear in which the hard particles or protuberances which produce the wear of one body are fixed on the surface of the opposing body” and three- body abrasive wear is defined as “form of abrasive wear in which wear is produced by loose particles introduced or generated between the contacting surfaces”.

In this manuscript two-body abrasion is considered as there are no abrasive particles present in the tribo-medium between two sliding surfaces and three-body abrasion is considered as there are particles (hard or soft) intentionally introduced between two sliding surfaces. In most of references abrasion of softer surface by harder surface or harder particles are considered. In three-body abrasion the wear mode is not always necessarily sliding and the abrasive particles can be also in rolling mode. In the rolling mode depending on the hardness of softer surface, abrasive particles might leave indent marks along its rolling path. However, abrasion of hard surfaces by soft particles is also possible. In this case, surface roughness and surface open porosities play important role [23]. The rate of abrasion of surfaces depends on characteristics of each surface, the presence of abrasives between the first and second surfaces and the abrasive particles characteristics, speed of moving surfaces in contact, and other environmental conditions.

c) Fatigue wear

Fatigue wear based on ASTM standard terminology [8] is defined as:

“Wear of a solid surface caused by fracture arising from material fatigue.”

The available definition does not specifically refer to any aspects involved with fatigue. Cyclic loading which applies much lower load that yield or fracture limits of material can cause surface or subsurface crack nucleation and growth which can ultimately result in loss of material from the surface. Many of the wear modes have some elements of surface fatigue such as periodic impacts, repeated contacts or rubbing cycles [18]. Surface or subsurface fatigue mechanisms most commonly observed in rolling mode and is a life limiting failure mechanism in ball and roller bearings and in gear contacts [7]. As it is shown in Figure 2.2 the rolling can be considered as pure rolling and rolling + sliding. Assuming a perfect material (defect

free) in pure rolling mode (in absence of tangential force applied to the surfaces) maximum shear stress will evolve depending on contact width at some distance below the surface and one would expect that failure first starts in subsurface. However, in presence of tangential force (rolling + sliding) the maximum shear stress will move towards the surface of material and at higher friction (usually exceeding 0.32) will appear at the material surface [24]. Nevertheless, as not all materials can be considered defect free, other origins of surface or subsurface fatigue failure needs to be taken into account.

For an imperfect material in case of fatigue it is needed that a crack nuclei to be formed. The origin of crack nuclei can be due to pile-up of dislocations or presence of voids and inclusions as stress concentration locations. After growth of crack to some critical length, it will propagate rapidly and unite with other cracks and release surface material that yields to wear of surfaces.

In repeated sliding contacts, type of fatigue wear known as delamination wear occurs on a microscopic scale due to repeated sliding of surface asperities over each other. Due to tri-axial compressive stresses just below the contact region crack nucleation near the surface will not occur. The formed cracks below the surface tend to propagate parallel to the surface and uniting the cracks yield to formation of plate-like wear debris [7]. The theory of delamination wear was developed by Suh et al. [25] and by recourse to this theory, some of the effects in sliding wear that were considered as adhesive wear now can be more precisely described by delamination wear mechanism [25–27].

d) Chemical wear

The chemical wear is considered as a wear process which is mainly dominated by chemical reactions and usually is combined with effect of mechanical contacts. In most of the textbooks [3, 10, 24] this wear mechanism is called as “corrosive wear”. In ASTM standard terminology relating to wear and erosion the corrosive wear defined as “wear in which chemical or electrochemical reaction with the environment is significant”. However, one should consider that corrosion on its own might not necessarily cause the wear of surfaces. In that case (if no mechanical elements are involved) it is a pure corrosion and is no longer tribological problem.

The chemical reactions on the surface of materials can be detrimental in terms of surface properties and make the surfaces prone to cracking and plastic deformation. Such detrimental reactions in combination with mechanical loading due to contact might cause material removal and formation of wear debris. One of the most common chemical wear processes is formation of oxide layer. The thin oxide layer formed at top of the contacting metal surface reduces the friction and improves the wear performance. This layer can be removed due to mechanical contact and simultaneously be formed on the new metal surface. This continuous phenomenon is typical oxidation wear.

2.3.2.3 Wear failure modes

A wear failure mode defines the surface appearance after tribological contact. A wear failure mode usually is defined by post facto analysis of worn surface that describes a certain combination of wear mechanism with a material removal process. The most common wear failure modes are named as follow:

- plowing
- wedge formation
- cutting
- gouging
- grinding
- indenting
- surface craters
- pitting
- spalling
- delamination
- scuffing
- seizure.

However, it is always convenient to explain the observed wear failure mode rather using a single word as listed above. Use of single words rather than descriptive explanation makes confusions in different cases [19]. Figure 2.5 shows the conclusion of systematic approach towards the classification of wear that was proposed here. Inter correlation of wear mechanisms, and wear modes is more clear as different wear mechanisms can be observed in different wear modes individually.

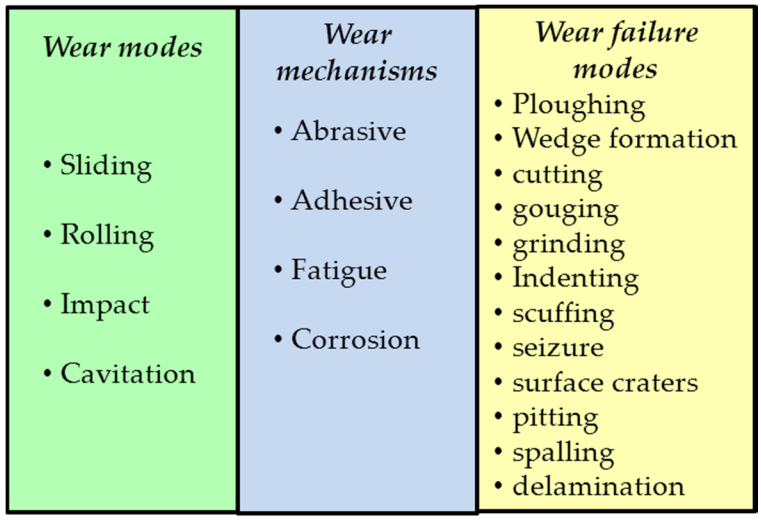

Figure 2.5. Presentation of proposed universal approach towards wear classification.

2.4 Conclusion

As discussed in chapter I there is a lack of universal wear classification for different tribological situations that limits the application and comparison of different evaluated wear resistant systems. To overcome such deficiencies different aspects of tribology were discussed and most cited definitions used in tribology communities were reviewed. The most generic definition of wear with widest application was chosen that is “loss of material from one surface, displacement of material within single surface or material transfer from one surface to another”. A tribo-system was defined and proposed as a primary tool to provide and identify most important variables of tribological problems. A universal wear classification approach rather than a classification based on single words was presented. It is concluded that to properly define any wear situations encountered in any tribological problems three main aspects needed to be defined: wear mode, wear mechanisms and wear failure modes.

References

1. Merriam-webster Online Dictionary. Available from: http://www.merriam- webster.com/dictionary/tribology.

2. Jost, P. Lubrication (Tribology) – A report on the present position and industry’s needs. 1966, Department of Education and Science, HMSO, UK.

3. Principles of tribology / Ed. by J. Halling, 1975, London: Macmillan.

4. ASM Handbook: Friction, Lubrication, and Wear Technology. ASM Handbook, ed. S.D. Henry. Vol. 18. 1992: ASM International. 942.

5. Almen, J.O. Surface Deterioration of Gear Teeth. in Mechanical Wear. 1950. Metals Park, Ohio: American Society for Metals.

6. Winer, M.B. and Peterson, W.O. Eds. Wear Control Handbook. 1980, American Society of Mechanical Engineers.

7. Holmberg, K. and Matthews, A. Coating Tribology: Properties, Mechanisms, Techniques and Applications in Surface Engineering. second ed. Tribology and Interface Engineering, ed. B. Briscoe. 2009: Elsevier Science. 560.

8. ASTM, Standard Terminology Relating to Wear and Erosion, G-40-10b. 2010, American Society for Testing and Materials.

9. ASTM, Standard Terminology Relating to Wear and Erosion, G-40. 2001, American Society for Testing and Materials.

10. Stachowiak, G.W. Ed. Wear: Materials, Mechanisms and Practice. Tribology in Practice. 2005, John Wiley and Sons Ltd. 458.

11. Blau, P.J. Ed. Wear Testing. Metals Handbook Desk Edition, ed. J.R.Davis. 1998, ASM International.

12. Budinski, K.G. Wear Modes. Surface Engineering for Wear Resistance. 1988: Prentice Hall.

13. Burwell Jr, J.T. Survey of possible wear mechanisms. Wear, 1957. 1(2): p. 119–141.

14. Rabinowicz, E. Friction and Wear of Materials. 1965: John Wiley.

15. Bayer, R.G. ASTM Standardization News. Vol. 2. 1974.

16. Furey, M.J. Tibology, in Encyclopedia of Materials Science and Engineering, M.B. Bever, Editor. 1986, MIT Press.

17. Davis, J.R. Surface Engineering for Corrosion and Wear Resistance, Maney Publishing.

18. Blau, P.J. Friction and Wear Transitions of Materials: Break-in, Run-in, Wear-in, ed. G.E.M. Rointan F Bunshah 1989: NOYES publication.

19. Hutchings, I., M. Gee, and E. Santner. Friction and Wear, in Springer Handbook of Materials Measurement Methods, H. Czichos, T. Saito, and L. Smith, Editors. 2007, Springer Berlin Heidelberg. p. 685–710.

20. Bowden F.P. and D. Tabot. The Friction and Lubrication of Solids. International Series of Monographs on Physics. 1986: Oxford Science Publications.

21. Jahanmir, S. On the Wear Mechanisms and the Wear Equations. In: Fundamentals of Tribology, N.P. Suh and N. Saka. Eds. 1980, MIT Press: London. p. 455–467.

22. Gates, J.D. Two-body and three-body abrasion: A critical discussion. Wear, 1998. 214(1): p. 139–146.

23. Ghabchi, A., et al. Behavior of HVOF WC-10Co4Cr Coatings with Different Carbide Size in Fine and Coarse Particle Abrasion. Journal of Thermal Spray Technology, 2010. 19(1): p. 368–377.

24. Bhushan, B. and B.K. Gupta. Handbook of Tribology: Materials, coatings, and surface treatments. Other Information: DN: From review by Robert D. Brown, Southwest Res Institute, in Applied Mechanics Reviews, Vol. 45, No. 1 (Jan 1992); PBD: 1991. 1991. Medium: X; Size: 1168 p.

25. Suh, N.P. and H.C. Sin. The genesis of friction. Wear, 1981. 69(1): p. 91–114.

26. Suh, P., N. The delamination theory of wear. Wear, 1973. 25(1): p. 111–124.

27. Suh, N.P. An overview of the delamination theory of wear. Wear, 1977. 44(1): p. 1–16.

3. Statement of problem

3.1 Process map and coating design

To achieve a multifunctional surface with desired performance and property characteristics, there is a need to understand effective parameters and develop a tool or approach to accurately control and tune the properties of the surface in form of a deposit. In fact the performance (chemical, thermal, electrical or mechanical) is the requirement defined for the system. Processing variables (starting material, hardware setting, gas flow and energy input), obtained coating microstructures and coating properties are tunable. However, it should be considered that obtained coating microstructure is affected and possible to control by process variables. Coating mechanical properties are defined and affected by microstructure. All of these properties and characteristics are highly inter-connected. Thus, to be able to achieve final performance, understanding each individual step and how they affect each other is decisive. Additionally, following this step-by-step, process map, (starting from process to final performance) approach provides indispensable knowledge on process control, state of in-flight particles and their interaction with the flame, coating formation mechanisms, microstructure evolution and how the mechanical properties are governed based on these parameters. Development of such knowledge-based chain makes it possible to design a coating and proper process based on its performance, simply by following the reverse route starting from system performance requirements.

Nonetheless, developing the full process map chain is a challenging task due to complex nature of thermal spray process and deposit structure. Additional complexity might arise in processing of Ceramic-Metallic (CerMet) material. In course of developing the process map for composite WC-CoCr coatings following questions can be addressed:

- How the in-flight particles temperature and velocity and consequently the particles state are affected by process variables?
- What are the best approaches to control the in-flight particles state?
- How different coating microstructures are formed and affected by different particle states?
- How generated microstructure is correlated with coating properties?

3.2 Importance of understanding the surface damage and wear mechanisms

A combination of good abrasion, erosion and corrosion resistance make the cermets in form of coatings as a widely used material in industrial and engineering components. Cermets (with general formula of Carbide or oxide-Metal) are composite materials that contain hard carbide or oxide particles dispersed within and held together by metallic matrix. As main application of this class of material is in wear combat, evaluation of wear performance quantitatively and identifying crucial parameters affecting the wear is important. On the other hand, qualitative description of encountered wear mechanisms under different tribological conditions is highly valuable as it provides a base for designing of improved wear resistant materials and processes. In this regard following questions needed to be answered:

- How body in relative motion interacts with the coating surface?
- How changes in abrasives particle characteristics can change the observed wear mechanism?
- What is the effect of different microstructural characteristics on wear mechanism?
- What are the damage mechanisms (not necessarily wear) under controlled tangential loading of coating surface?

3.3 Carbide size effect

Another crucial parameter in carbide-based coatings that needs to be considered carefully is the carbide size. In last few years the main interest has been on reducing the carbide size. There are reports available showing the enhancement in mechanical properties and wear performance in smaller carbide coatings. However, reducing the carbide size down to nano-scale has not returned reasonable improvements. The main proposed reason is the formation of secondary carbide phase that is highly brittle. However, the effect of carbide size reduction on respond of material to external loading in absence of secondary brittle carbides remains unanswered. In studying the carbide size effects following questions need to be addressed:

- What is the effect of carbide size on wear performance and mechanisms?
- What is the effect of carbide size on wear performance and mechanism with no secondary carbide's parasitic effect?

4. Process control and coating formation: a process map approach

4.1 Introduction

Recent advances in thermal spray technology are driving this technique to be used as a part of the engineering design for different components rather than an additive surface treatment technique that has been used for dimensional repair or life extension purposes. In last decades development of process monitoring and diagnostics tools and devices improved the understanding of particle-flame interaction and provided significant information regarding to in-flight particles state [1–3]. Advancement in characterization of complex defective microstructure of TS coatings has been achieved employing 3D microstructural characterization techniques such as small angel neutron scattering and X-ray [4, 5]. Development of in-situ coating property measurement sensor provided indispensable knowledge regarding to coating build up process and development of intrinsic stresses within different coating/substrate systems [6–8]. Availability of modeling software and computational capabilities enabled the modeling of thermal spraying process and coating complex microstructure-related mechanical properties such as indentation response and anelasticity of coatings [9–11].

To be able to use the thermal spraying technique as a part of engineering component design addressing the reliability and reproducibility aspects of TS technique is compulsory. Additionally, successful implementation of this technique in engineering design requires adequate knowledge regarding to properties and performance of thermal sprayed coatings. The measure of properties, performance evaluation and how properties and performance are affected by different microstructural and processing variables can be achieved through developing and understanding the correlation between process-particle state-microstructure-property and performance. By developing such knowledge it is possible to choose the most proper and efficient design and manufacturing route for an engineering component with desired properties and performance (mechanical, chemical, thermal and electrical). This step by step, process map, approach helps to improve repeatability and reproducibility of the process. However, due to different available processes, hardware settings and feedstock materials, the obtained in-flight particles state will be extensively diverse that results in many different microstructures.

Such variations in obtained deposits make filling the process to performance know-how chain a challenging and complicated task that takes enormous efforts. These complex interrelated variables are shown briefly in Table 4.1.

Table 4.1. Brief description of interrelated parameters in TS process.

Hardware Variables	Gas dynamics governing variables	Particle, Flame interaction variables	Particle, substrate interaction variables
Different torches	Fuel type	Powder density, morphology	Substrate roughness, temperature
Noxxle characteristics	Volume flow of fuel & oxygen	Particle size distribution	Standing off distance
Power injection location	Fuel to oxygen ratio	Volume flow of carrier gas	Raster speed
		Feeding rate of particles	Spraying pattern

Nevertheless, such a vast variation in process hardware, conditions and feedstock materials provides possibilities to tailor the microstructures and properties.

4.2 1st and 2nd order process maps

Process map is a systematic manner to determine the relationship between process parameters, in-flight particles characteristics, microstructure and properties. Proposed by Sampath et al. [12] process map is an schematic representative that examines the role of process variables on the properties and performance of sprayed coatings. Process maps provide fundamental insight to thermal spray process and ultimately offer suitable tool to identify the optimized process, microstructure and property for specific performance/application. In fact developing the “process map” for any system/application enables the “process, material and structure design” based on system requirements. The concept and ideology of process map and ultimate goal of process mapping, coating design, is represented in Figure 4.1.

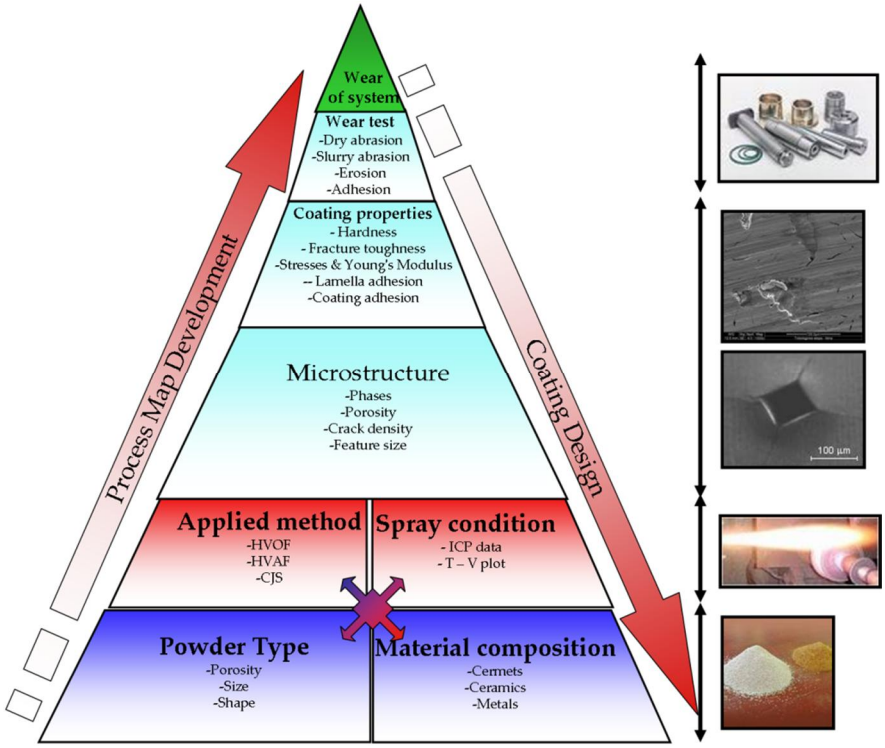

Figure 4.1. Process map, bottom up, and coating design route, top down for wear performance of a coating/substrate system.

By developing process maps in thermal spray addressing some questions will be attempted:

- How the in-flight particles temperature and velocity and consequently the particles state are affected by process variables? (1st order process map). At this stage understanding the flame formation and effect of its chemistry on in-flight particles state and developing effective strategies and tools to control particles state are of main concern. However, developing the knowledge in this level is challenging task as the nature of processes inside the spray torch are complex and involve two-phase (gas, liquid and solid particles) turbulent flow, heat transfer, chemical reactions, and supersonic/subsonic flow transitions [13].
- How different coating microstructures are formed and affected by different particle states? (1st and 2nd order process map). At this level, evolution of different microstructural features such as carbide shape and size, porosities as well as phases within the coatings and how they are affected by state of in-flight particles are of main objectives. Interaction of in-flight parti-

cles with substrate (first layer of deposit) that defines the coating/substrate adhesion characteristics as well as continuous coating build up that is incorporated with development of stresses will be addressed by state-of- the-art in-situ coating property (ICP) sensor. Such studies provide essential knowledge regarding to coating formation mechanisms and enable to identify crucial parameters controlling microstructural features.

- How generated microstructure is correlated with coating properties? (2nd order process map). The obtained microstructure representing specific microstructural features such as carbide size and shape, binder mean free path, phases available within the coating and porosities govern the mechanical properties. Different stresses developed during spraying and coating build up will have significant effects on mechanical response of material.

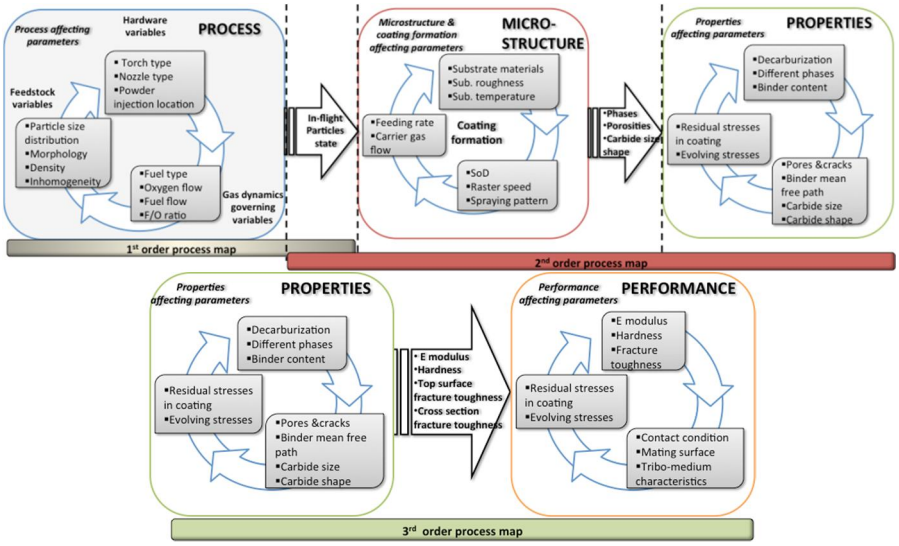

Figure 4.2. Presentation of process map route, 1st, 2nd and 3rd order process map.

The process map route for carbide based cermet thermal sprayed coatings is represented schematically in Figure 4.2. The route is divided to process, microstructure and properties and at each sub-level most crucial affecting parameters are illustrated.Measured outcome at each sublevel is described by connecting arrows.

Number of reports are available in literatures studying the correlation between particle state – splat formation – microstructure and properties of plasma sprayed zirconia [14], plasma sprayed molybdenum [12, 15], plasma sprayed YSZ and HVOF sprayed CoNiCrAlY bond coat [16] and HVOF sprayed dense alumina coating [17]. It is noted that degree of melting (fully molten, semi-molten and unmolten) specifically for ceramic materials and the kinetic energy are the most crucial factors which have effect on microstructure of deposits. Thus, measured in-flight particles temperature and velocity are not defining the particle state properly

as they are unable to represent the real particle's thermal history and kinetic energy. The fundamental idea for degree of melting, melting index, is explained by Vaidya et al. [15] and developed further by Xiong et al. [18].

In this chapter at first we aim to establish a correlation between process variables and in-flight particles temperature and velocity and further analyze the diagnostics data to understand the real in-flight particles state represented by non-dimensional group parameters. Two approaches were employed to control the process variables. The first approach is based on fuel/oxygen ratio and total volume flow control and the second approach is based on fuel/oxygen ratio and back pressure control. Based on in-flight particles state few points were chosen and coatings were deposited. Microstructures of coatings were studied to address the effect of processing conditions on developed microstructure. Effect of in-flight particles state on decarburization, W_2C formation and carbide size distribution in the coating was studied.

4.3 Experimental techniques and material

4.3.1 Feedstock material and coating processing

A commercially available WC-14(CoCr) powder was used in this study (WOKA 3652, Sulzer Metco, Germany). Detailed characteristics of employed powder are available in Table 4.2. Figures 4.3a and 4.3b show the morphology and cross section of powder used in this study.

Table 4.2. Detailed powder characteristics used for diagnostics and coating deposition.

Apparent density g/cm^3	WC gain size, µm	Size distribution-µm d10–d90%	Chemical composition, wt.%		
			C	Co	Cr
4.91	1–3	24–45	5.34	9.68	3.79

The cross section of powder (Figure 4.3b) reveals the porosity within the powder structure. Presence of different grey scales in the binder of powder is an indication of heterogeneity (cobalt and chromium rich regions) of the binder. The low density and heterogeneity of powder are due to the employed powder manufacturing technique. An HVOF DJ-2600 torch (Sulzer-metco, Westbury, NY, USA), with water cooling and hydrogen fuel was used. Nitrogen was used as powder carrier gas. Detailed specifications of the torch were noted in chapter I.

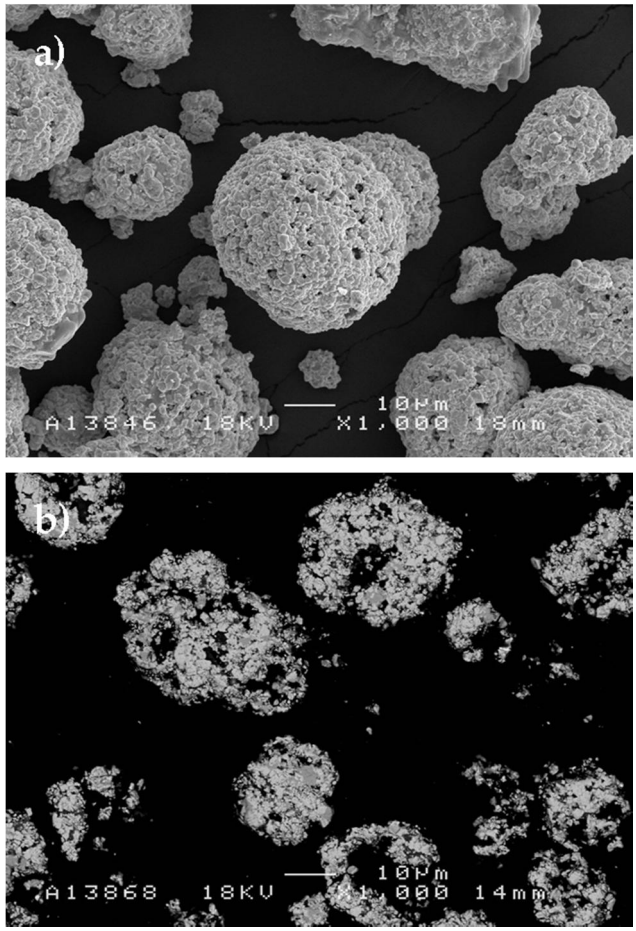

Figure 4.3. (a) SEM image of powder morphology and (b) powder cross section.

4.3.2 Process diagnostics

In-flight particles temperature and velocity was measured by Spray Watch 2i diagnostic device (Oseir Oy, Tampere, Finland). Spray Watch uses a digital CCD camera with special spectrally resolving optics. The ultra-fast electronic shutter camera and dedicated real-time image processing software enables on-line measurement of the velocity. Velocities are measured by image analyzing the length of the traces drawn by in-flight particles during the exposure time. The average particle temperature is measured by two colors pyrometry. The camera was located at 250 mm from exit of the nozzle (the same distance where the substrate is located for coating deposition). The data collection procedure was continuous and average of data point collected in one minute was used as a representative of

temperature and velocity for each spraying parameter. Details of this diagnostic tool used in this study can be found elsewhere [2].

4.3.3 Design of experiments – 1st order process map

There are different variables that can be manipulated to control the flame conditions in high velocity oxygen fuel which enables the control of in-flight particles temperature and velocity. Flame controlling variables were considered as hydrogen (fuel gas), oxygen, and air. Nitrogen was used as powder carrier gas. Beside oxygen and hydrogen, 21% of air (as oxygen) was considered to contribute in combustion and nitrogen cools the flame down with no contribution in combustion process but it contributes to the particle momentum. To simplify the complexity of controlling parameters in all spraying conditions the volume flow of air and nitrogen were kept constant. Therefore, by changing the fuel and oxygen value the in-flight particles temperature and velocity (T & V) were manipulated. The fuel/oxygen ratio was calculated as follow:

$$\gamma = \frac{fuel\ flow}{oxygen + 0.21 \times air\ flow} \quad (1)$$

The stoichiometric ratio for hydrogen combustion is 2.0.

4.3.4 Microstructure

For microstructural studies coatings were characterized by x-ray diffraction (Phillips PW3710) with Mo-K-α radiation for detection of different phases. Using XRD data the W_2C /WC intensity peak ratios were extracted. These values were used as an indication of the level of decarburization. Coatings cross sections were studied by scanning electron microscopy (SEM), JEOL JSM-6400 and Zeiss FEG-SEM.

4.3.5 Coating build up monitoring by in-situ coating property measurement sensor

Recently a new method based on substrate curvature and temperature measurement has been developed at Center for Thermal Spray Research at SUNY Stony Brook that enables to extract the residual stresses and Elastic modulus of deposits and monitor the dynamics of deposit formation in real time [6, 7, 19]. Fundamental of stress development in thermal spray coatings is presented elsewhere [20, 21].

4.4 Results and discussion

4.4.1 Correlation of process parameters with in-flight particles temperature and velocity

4.4.1.1 Total volume flow and fuel to oxygen ratio control approach

In first set of diagnostics experiments it was attempted to control the in-flight particles temperature and velocity by controlling the fuel/oxygen ratio and total volume flow of gases. The motivation to control the process by controlling the total volume flow is coming from the easiness of this approach as the total volume flow is basically the result of summing up the volume flow of all processing gases. Four different total volume flow values and 10 different fuel/oxygen ratios for each total volume flow value (40 spraying conditions) were tested. Figure 4.4 shows the in-flight particles temperature and velocity at different total volume flows and normalized F/O ratios (γ*).

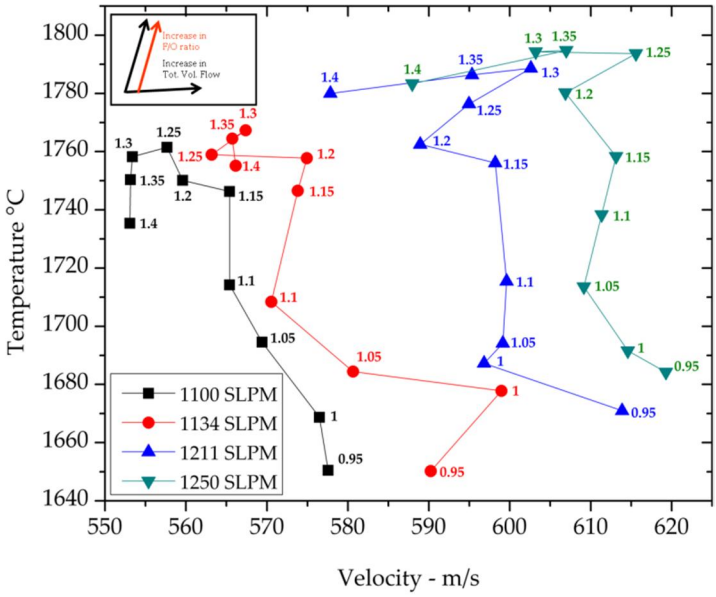

Figure 4.4. In-flight particles temperature and velocity with controlled total volume flow and γ*. SLPM: Standard Liter Per Minute (total volume flow) and numbers next to each point represent the normalized Fuel/Oxygen ratio.

It is noted that by increasing the total volume flow, overall temperature and velocity levels are increasing. However, velocity trend at each constant total volume flow is not clear as it increases and decreases with no logical trend. Temperature at

each total volume flow is reached to its maximum at γ*~1.3. It is noteworthy that in ambient pressure the adiabatic combustion temperature of hydrogen reaches its maximum (~2850°C) at γ*=0.8. This difference between γ* values to reach the maximum adiabatic combustion temperature and real spraying conditions might be due to the ability of burning the excessive hydrogen with assistance of ambient oxygen. With further increasing the γ* the temperature starts to drop down. Drop in temperature by further increasing of γ* hypothesized to be due to quenching of flame by unburned fuel. Temperature versus different normalized F/O ratios for total volume flow controlled spraying set is shown in Figure 4.5. The increase of temperature by increasing the γ* to 1.3 and decreasing the temperature with further increase of γ* is consistent in all total volume flow levels. A similar prediction for temperature behavior at different γ* ratios by modeling has been made by Shamim et al. [22]. Figure 4.5 shows that in general temperature increases by increasing the total volume flow. The figure shows that temperature is not only affected by F/O ratio, also affected by total volume flow of gases in this set of experiments. As the moving of each point in temperature and velocity space is not predictable, controlling the temperature and velocity by total volume flow will not be feasible with enough accuracy. Deficiency of this approach might be due to the assumption that each processing gases have equal contribution to flame dynamics. However, as discussed previously for example contribution of oxygen, hydrogen and air to burning process and thermal energy of flame are different.

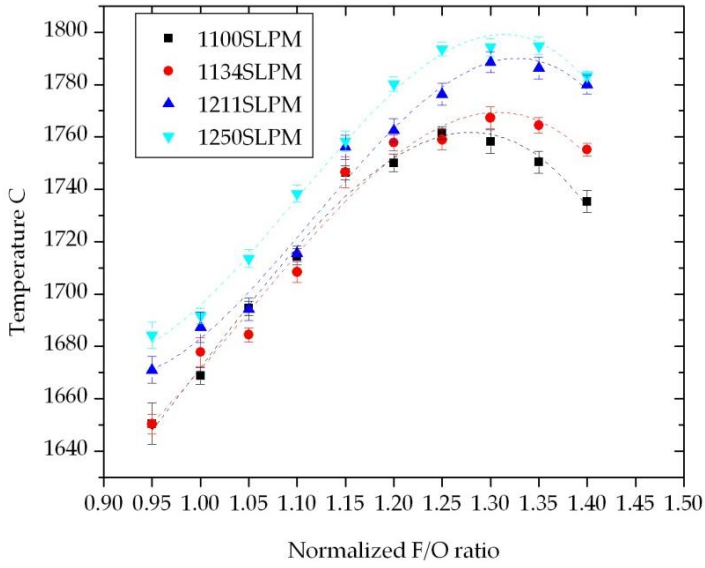

Figure 4.5. Temperature versus normalized F/O ratio under controlled total volume flow condition.

The same discussion can be considered for effect of each gas on kinetic energy of flame as their density and mass for instance are completely different.

4.4.1.2 Backpressure and fuel to oxygen ratio control

In second experimental set it was attempted to control the in-flight particles temperature and velocity by controlling the fuel/oxygen ratio and backpressure[1]. Four different backpressure values and five different fuel/oxygen ratios for each backpressure value (20 spraying conditions) were tested. Figure 4.6 shows the temperature and velocity values measured by diagnostic device at different backpressure and fuel/oxygen ratio values. Each line indicates a particular backpressure value.

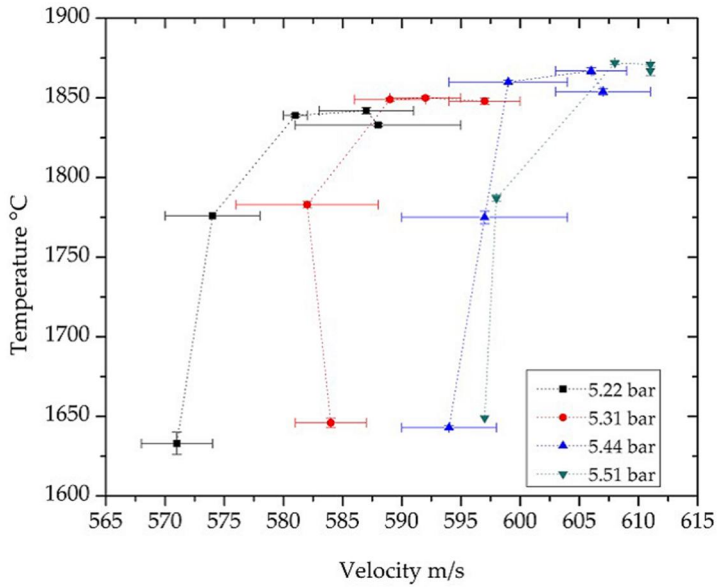

Figure 4.6. In-flight particles temperature and velocity with controlled γ* and back pressure.

Unlike the previous case, total volume flow control, there is a clear trend in controlling the temperature and velocity by back pressure and F/O ratio. It is shown that in-flight particles temperature at each backpressure level is reached its maximum around γ*~1.3 and by increasing γ* value temperature starts to drop down. The same temperature trend was observed in case of total volume flow control approach with similar γ* for maximum temperature. By increasing backpressure the

[1] Backpressure was measured from powder feeder line. This is not a direct measure of combustion pressure, but provides a comparative tool for different spraying parameters.

overall velocity has been increased with repeating the trend at different backpressure levels. Also, at each individual backpressure level a gradual increase in velocity by increasing the γ* was observed. At individual backpressure levels, points with higher γ* are incorporated with higher total volume flow. This suggests that velocity is not a single function of backpressure and it might be affected also by total volume. According to this observation it was hypothesized that velocity of particles is a function of both backpressure and total volume flow. To examine this hypothesize a simple function of backpressure and total volume flow is proposed as backpressure multiply by total volume flow of gases to explain the velocity of particles. Figure 4.7 shows the resultant velocity versus the proposed function. As Figure 4.7 shows velocity is linearly proportional to proposed function and by increasing the backpressure and/or total volume flow the velocity of particles will be increased.

Figure 4.8 shows the temperature versus γ* for backpressure controlled spraying set. It is noted that deviation between temperature values at each γ* level compared to the similar graph with total volume flow control approach is small. Nevertheless, this deviation increases at higher γ* values. This suggests that temperature is more dependent only on γ* in back pressure controlled regime.

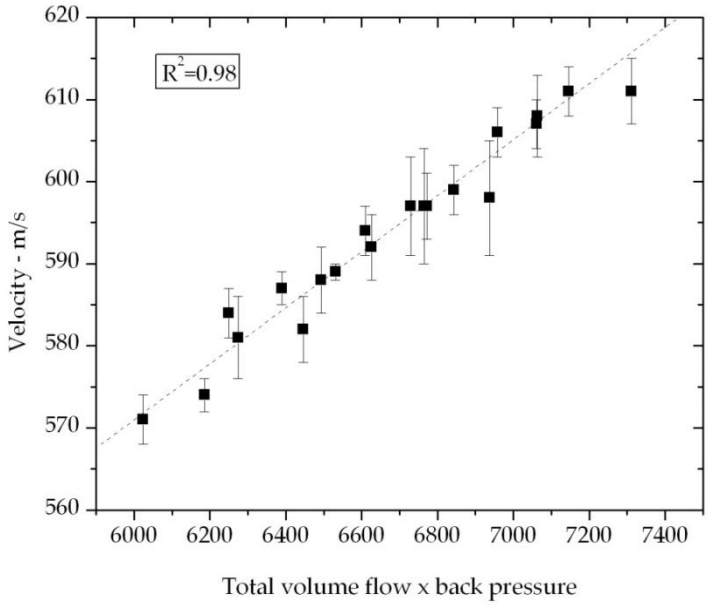

Figure 4.7. A function showing the correlation of velocity with total volume flow and back pressure.

Comparing two examined approaches suggests there is a possibility to control the in-flight particles temperature and velocity by controlling the fuel to oxygen ratio

and backpressure. The effectiveness of backpressure control approach owing to the fact that back pressure reflects the state of flame inside the combustion chamber as a result of interaction of gases.

4.4.1.3 Isolating the effects of hydrogen and oxygen

In previous section it was noted that each processing gas has different contribution to flame dynamics owing to their different chemical and physical characteristics. In this section an attempt has been made to evaluate the contribution of hydrogen and oxygen to measured in-flight particles temperature and velocity.

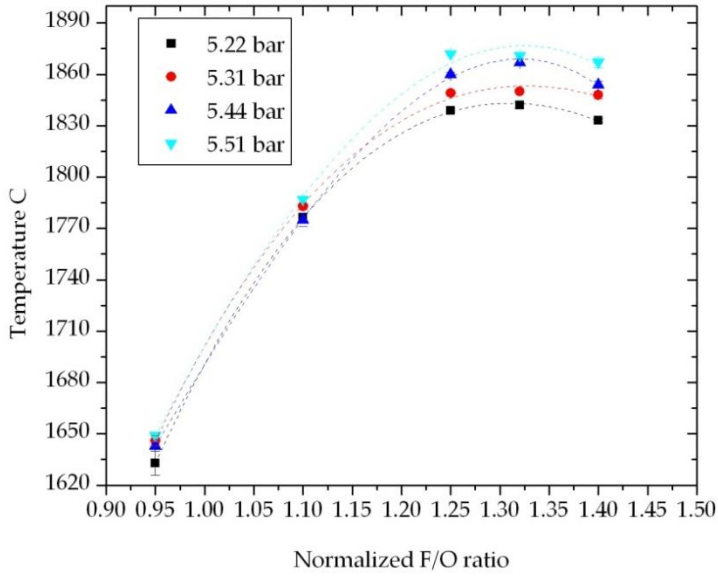

Figure 4.8. Temperature versus normalized F/O ratio under controlled back pressure condition.

To study the effects of hydrogen and oxygen separately on measured backpressure as well as on in-flight particles temperature and velocity, it was attempted to control the γ* ratio in two different manners. In one set it was attempted to keep the oxygen constant and change the hydrogen (hydrogen controlled). In second set it was attempted to keep the hydrogen constant and change the oxygen (oxygen controlled). In both cases targeted fuel/oxygen ratios were achieved except for γ*=1.4 in hydrogen controlled and γ*=0.95 for oxygen controlled conditions. The reason not to be able to cover whole range was the limits of torch and employed gas feeding systems. Figure 4.9a shows the effect of hydrogen and oxygen flow (total volume flow) on backpressure. It is shown that changing in oxygen flow has larger impact on backpressure than hydrogen (the slope of oxygen controlled curve is 0.008 and hydrogen controlled curve is 0.002). Figure 4.9b depicts that

small changes in back pressure caused by hydrogen provides bigger changes in velocity values. Figure 4.9c examines the validity of same function proposed previously (back pressure multiplied by total volume flow).

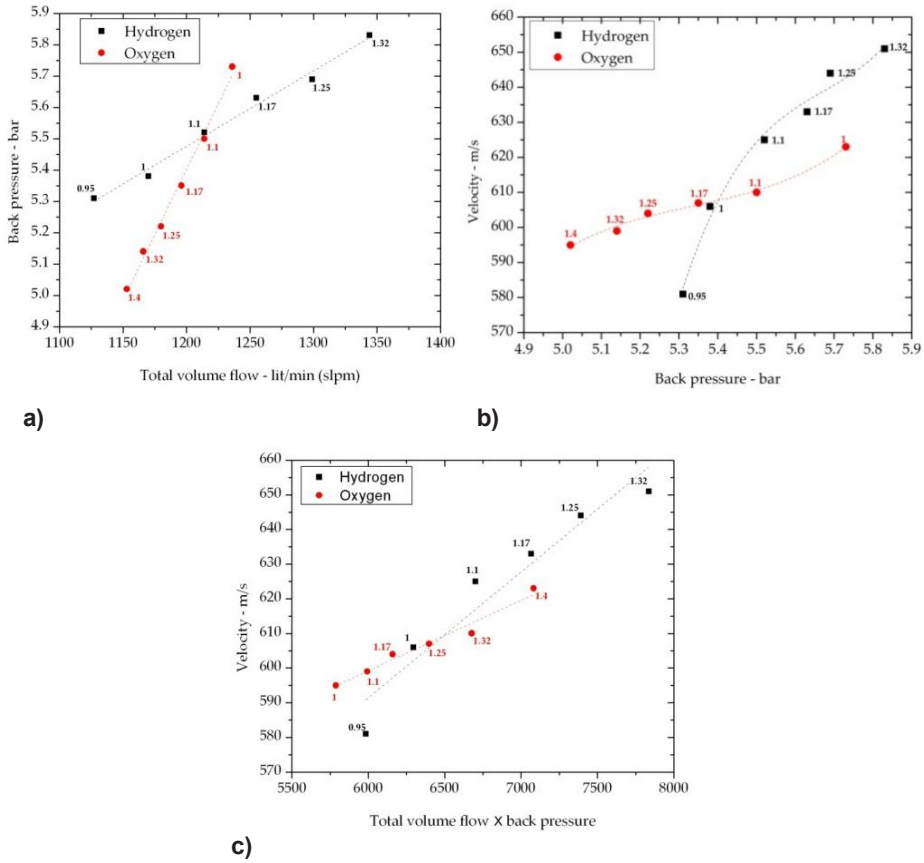

Figure 4.9. (a) Back pressure versus total volume flow for hydrogen and oxygen controlled conditions (b) velocity versus back pressure for hydrogen and oxygen controlled conditions (c) velocity versus function of total volume flow and back pressure.

The same linear trend was observed for both hydrogen and oxygen controlled regimes but with different slopes.

Figure 4.10 shows the effect of normalized γ* on in-flight particles temperature for both oxygen and hydrogen controlled regimes. In lower γ* values measured temperature for both cases are almost the same but with further increasing of the γ* value the oxygen controlled set reaches its maximum at γ*~1.25–1.3.

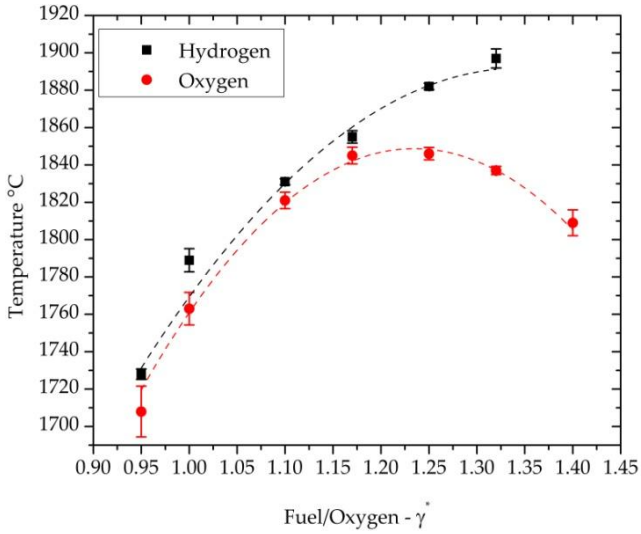

Figure 4.10. Effect of γ* on in-flight particles temperature with controlled hydrogen and oxygen.

However, for hydrogen controlled spraying set the maximum value reaches around γ*~1.36–1.4 (calculated based on trendline). This might be due to burning of excessive hydrogen even outside of the nozzle that provides more heat to the powders.

4.4.1.4 Guideline for controlling back pressure and particles temperature and velocity

In this section two approaches for controlling the in-flight particles temperature and velocity were studied. The back pressure and γ* (fuel/oxygen ratio) control provides more accurate and reliable manner to control in-flight particles temperature and velocity. By considering air and carrier gas flow constant, it is possible to control the process with hydrogen and oxygen flows. However, obtaining in-depth knowledge on controlling the back pressure and γ* by hydrogen and oxygen is a challenging task as of different gases at various temperatures and pressures on measured back pressure is not fully clear. Beside all the information provided regarding to back pressure, values were not controlled as a predefined value as there are no guidelines available to do so. Thus, a guideline for process control, based on back pressure and γ* is provided shown in Figure 4.11 which is developed to illustrate how it is possible to get desirable F/O ratio and back pressure values by changing the oxygen and hydrogen. The same logic was persuaded to develop a guideline to control the in-flight particles temperature and velocity by F/O ratio and backpressure. In Figure 4.11b the color contour shows the back pressure and white dotted lines represent the γ* values. As it is shown by this figure it is possible to estimate the hydrogen and oxygen necessary to obtain any desired γ* ratio and back pressure values. Further to be able to estimate in-flight

particles temperature and velocity based on γ* and back pressure values another map was developed shown in Figure 4.11a. The color contour in this map shows the backpressure and white dotted lines show the γ* values. The color contour is limited to the spraying window. In fact, starting from process variables (hydrogen and oxygen) and going all the way to in-flight particles temperature and velocity have been done by following the process map route. However, two graphs presented here can be used in process design by following the reverse route of process map. For instance it is possible to simply estimate what is the necessary backpressure and γ* to obtain a particular in-flight particles temperature and velocity. Further it is possible to estimate what is the necessary fuel and oxygen flow to reach the desired γ* and back pressure. Through this route it is possible to directly control process variables (fuel and oxygen) to reach the proposed temperature and velocity.

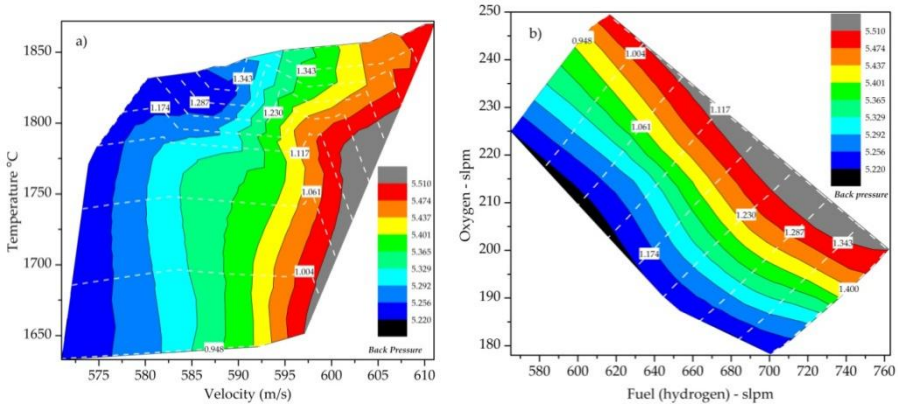

Figure 4.11. Guideline for estimation of (a) required back pressure (bar) and γ* to obtain particular T&V and (b) a guideline for esimation of required fuel and oxygen value to obtain particular back pressure (bar) and γ*. (b) to (a) is process map route and (a) to (b) is process design route.

4.4.2 Non-dimensional parameters for description of in-flight particles state

Temperature and velocity are two characteristics of in-flight particles measured by diagnostics that are highly affected by process parameters. However, these two parameters (temperature and velocity) do not represent the real thermal and kinetic history of particles at the time of their impingement to the substrate. Descriptive deficiency of temperature and velocity for ceramic materials was addressed by Vaidya et al. using an index defining the fraction of melting content of in-flight particles. This index simply is defined by time of particle flight over the time needed to fully melt the particles. The melting index in its simple form is defined as [23]:

$$Ml = \frac{T\Delta_{ny}}{D} \tag{2}$$

Further modified version of MI equation developed by Zhang et al. [24]:

$$MI = A\frac{24k}{\rho h_{fg}}\frac{1}{1+4/Bi}\frac{(T_s-T_m)\Delta t_{fly}}{D^2} \quad (3)$$

In which time of particle flight is $\Delta t_{fly} = \frac{2s}{v}$, s is standing off distance and v is particle velocity. In this equation A is the ratio of $T_f - T_m/T_s - T_m$, T_f is the flame temperature, T_s is the particle surface temperature measured by diagnostics and T_m is the particle melting point. In this estimation flame temperature and particle surface temperature has been considered the same. K is the thermal conductivity, ρ is the density, h_{fg} is the enthalpy of fusion, Bi is the Biot number and D is the particle diameter.

The melting state represents the thermal history of in-flight particles and the kinetics of particles have been represented by kinetics energy of in-flight particles as it is a simple term to be identified by experimental data and is related to velocity and mass of particles. As the particle size was not available for every single in-flight particles due to employed diagnostic device, the overall average size of particles was used in calculation of melting state and kinetic energy. Figure 4.12a shows the in-flight particles temperature and velocity at different F/O ratios. The same T&V points are presented in melting index and kinetic energy space (Figure 4.12b). Lower melting index means that bigger fraction of particle is in its solid form and as the index increases and gets closer to unity, molten fraction of particles increases.

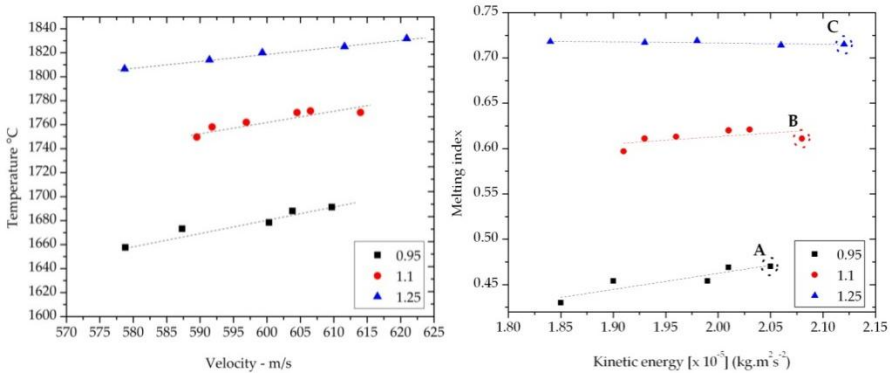

a) b)

Figure 4.12. (a) Measured in-flight particles temperature and velocity at three different γ* levels and (b) same points converted to MI-KE space.

4.4.3 Significance of in-flight particles state in microstructure

4.4.3.1 Decomposition, dissolution and W_2C formation

In terms of carbide-based composite materials higher melting index promotes decomposition of carbide as it works in favor of diffusion of carbides into the binder.

Also, higher melting index can help the structure to be more homogenized which guarantees the improved cohesion of splats to each other and yield coatings with improved mechanical properties. Figure 4.13 shows the W_2C /WC ratio as a comparative function to define the level of decarburization and W_2C formation versus melting index. As it is shown in this figure increase in melting index cause an increase in formation of W_2C phase. To further analyze the microstructure and demonstrate the effect of decarburization on final coating microstructure three coatings were chosen based on their melting index.

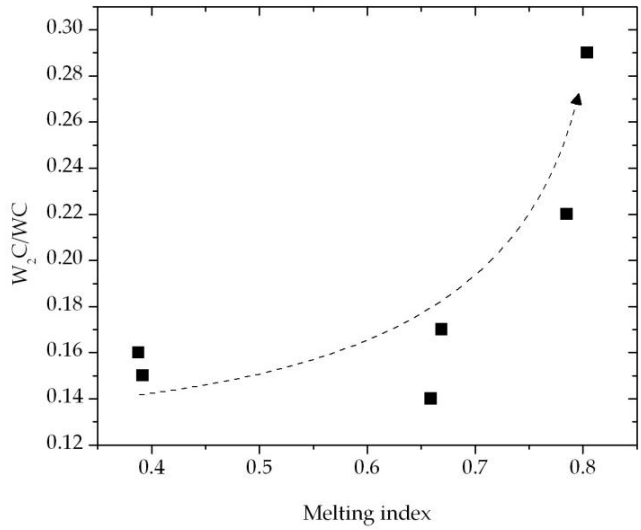

Figure 4.13. W_2C /WC ratio as a function of melting index.

Locations of these three coatings (A,B and C) have been shown on MI-KE spaces in Figure 4.12b. Figure 4.14a shows the SEM cross sectional images of the coatings with corresponding melting index indicated on top left and sample names on bottom right side of each image. From lower to higher melting index the finer carbides in the microstructure disappear and rounding of carbides have been observed. It is hypothesized that decarburization of carbides is responsible for both phenomena. Carbide rounding due to decarburization was reported previously by Usmani et al. [25]. There are limited techniques available to quantify decarburization of carbides. One is extraction of W_2C /WC ratio using XRD data that was reported in Figure 4.13 and another technique that has been used here is measuring carbide particle size within the microstructure employing image analysis technique. Figure 4.14b shows series of graphs explaining the decarburization quantitatively. The first graph in Figure 4.14b shows the average measured particle size in coating “A” and “C”, corresponding to lowest and highest melting index respectively.

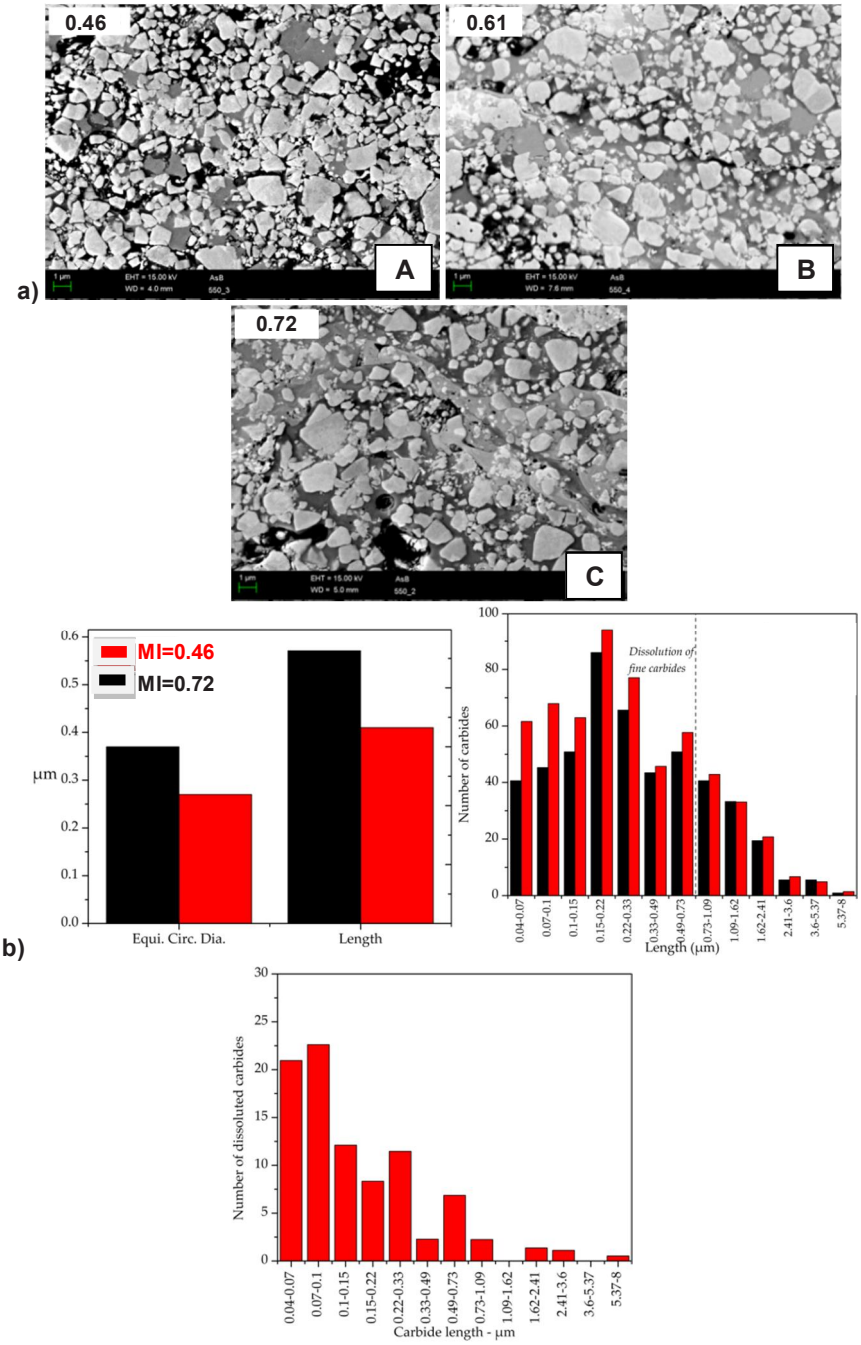

Figure 4.14. (a) SEM microstructural cross section image of three coatings with different MI and (b) quantification of decarburization using image analysis software.

As it is noted the average particle size in coating “C” is higher than coating “A”. This indicates that fine carbides due to sever decarburization in coating “C” have been dissolved into the matrix and disappeared and only bigger carbides remained in the structure. To further illustrate the size dependency of dissolution of carbides, the second graph in Figure 4.14b is presented that shows the number of dissolved carbides versus carbide length histogram. This figure highlights that bigger number of carbides with smaller size have been dissolved into the binder and with increasing the carbide size the dissolution effect diminishes. The third graph in Figure 4.14b simply shows the susceptibility of finer carbides to dissolution.

4.4.3.2 Chemical heterogeneity in the coating

As it was mentioned previously high thermal input might cause excessive W_2C formation in the microstructure and this brittle phase might have some detrimental effects on coatings performance. However, this does not necessarily mean that reduced heat input to the in-flight particles improves the performance of material as thermal input is decisive in improvement of splat/splat cohesion and obtaining the coating with more homogenized microstructure. If the heat input is not enough during the process, the microstructure of the coating will be similar to the starting material that is usually heterogeneous (coating “A” in previous section). Such heterogeneous structure will be detrimental in fine particle wear and corrosion performance of material. To further understand the nature of heterogeneities within the microstructure and examine these phases, Energy Dispersive Spectroscopy (EDS) was done on different spots for sample “A” shown in Figure 4.12b. EDS results show five main distinguishable phases with different chemical compositions. WC grains, Cobalt rich, Chromium rich and tungsten rich regions and a region that was originally WC and has undergone diffusion and changed its nature. Figures 4.15 and 4.16 show backscattered images and EDS studies with corresponding tables. In Figures 4.15 spectrum 1 and 5 that are taken from darkest areas in the microstructure reveal highest Cr/Co ratio (2.52–2.62) indicating a chromium rich area in the microstructure. Spectrum 3 and 4 are taken from another area within the binder that is slightly brighter than first spot with Cr/Co ratio between 0.26–0.27. This is an indication of Co rich area with higher W concentration compared to spectrums 1 and 5. This also suggests some W diffusion to the binder as these spots are surrounded with finer WC particles. Spectrum 2 shows a WC grain as there is no Cr or Co was detected.

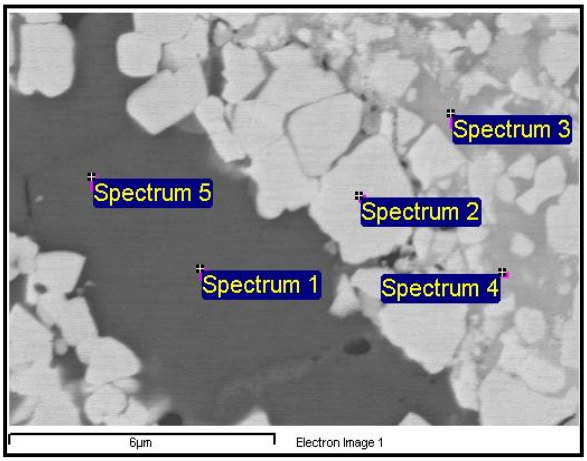

Spectrum	C	Cr	Co	W	Total	Cr/Co
Spectrum 1	35.87	43.96	17.43	2.74	100.00	2.52
Spectrum 2	70.78			29.22	100.00	-
Spectrum 3	41.46	8.70	32.17	17.68	100.00	0.27
Spectrum 4	45.58	7.82	29.40	17.20	100.00	0.26
Spectrum 5	40.60	41.28	15.75	2.38	100.00	2.62

Figure 4.15. EDS study of WC-CoCr coating and corresponding table.

Spectrum 2 was taken from a WC grain. Spectrum 1 in Figure 4.16 shows another phase which is just slightly darker than WC grains. The shape of this phase is similar to WC grains but EDS result shows this phase contains cobalt and chromium as well. It is hypothesize that this phase originally was WC grain and due to partial diffusion W and C have diffused to the binder. This explains higher cobalt and chromium and lower W compared to spectrum 2 that is taken from a WC particle. It is also noted binder areas that are poor in W are in vicinity of large WC grains but binder areas richer in W are in vicinity of medium size WC grains and binder areas in vicinity of fine carbides are saturated in W or the whole WC is dissolved. it means less W diffuses to the binder from larger carbides and more W diffuses from finer carbides to the binder. It can be concluded in the powder manufacturing step, the powder exhibits chemical heterogeneity (as it is shown in Figure 4.3) and spraying powder with colder parameter will return a coating with the microstructure similar to the one in the powder.

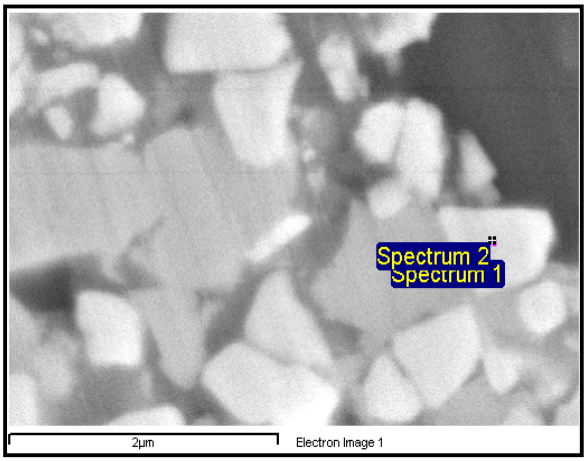

Spectrum	C	Cr	Co	W	Total
Spectrum 1	80.07	3.82	8.40	7.71	100.00
Spectrum 2	87.89	1.10		11.01	100.00

Figure 4.16. EDS study of WC-CoCr coating and corresponding table.

4.4.3.3 Porosities

To further analyze the effect of in-flight particles state on microstructure, porosities for each coating was measured. Figure 4.17 shows the low magnification microstructural images of the coating and corresponding porosity value. As it is shown in this figure, increasing M.I. results in deposition of denser coating. However, the effect of K.E. is not clear as the velocity window for these sets of samples is narrow.

4.4.3.4 Stress formation during deposition and cooling the coating/substrate system

Stresses during the coating deposition and cooling of coating/substrate system were monitored using the ICP sensor. The considered stresses are called deposition stress, thermal stress, residual stress and evolving stress. Figure 4.18 shows an example of outcome of ICP sensor on which different stresses are shown.

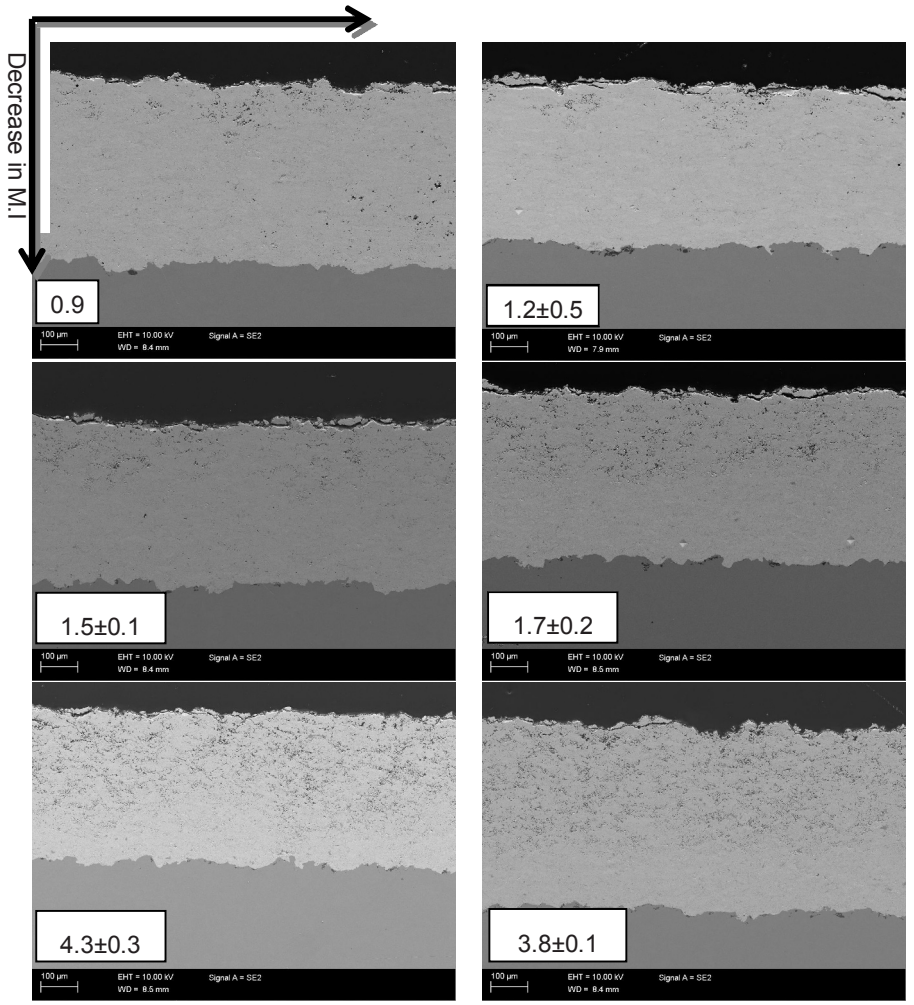

Figure 4.17. Low magnification microstructural SEM images with different M.I. and K.E. values.

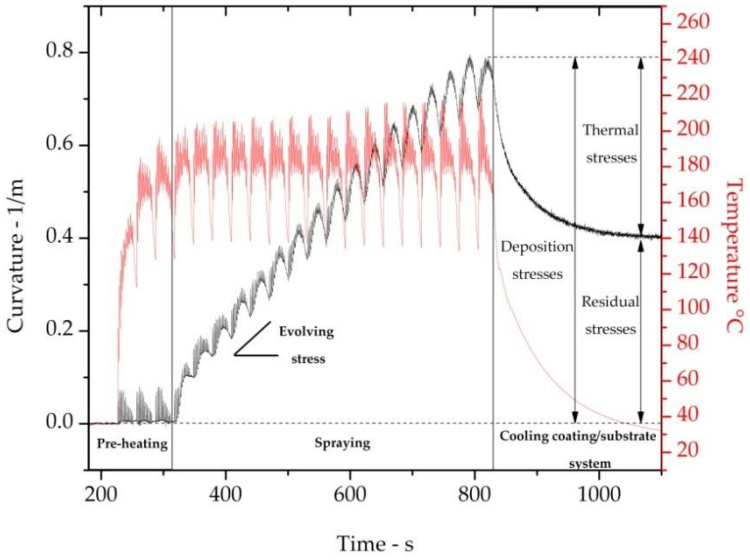

Figure 4.18. An example of curvature, temperature measurement data from ICP and stresses.

Among the stresses named above residual stress and evolving stress might have significant impact on performance of thermal sprayed coatings. For instance, tensile residual stress might limit the fatigue life of material or promote the material removal under the wear condition. On the other hand, evolving stress is reflection of quality of the splat/splat cohesion. Splat debonding or detachment is one of the key wear mechanisms in wear of thermal sprayed coatings. Figure 4.19 shows the dependency of evolving stress and residual stress on in-flight particles temperature and velocity. Figure 4.19 shows that lowest residual stresses obtained for coating with highest velocity and lowest temperature. However, highest residual stresses are obtained for coating with highest temperature and lowest velocity. Evolving stresses do not show any dependency on the velocity and it is directly correlated with temperature. This can be explained by recourse to improved splat/splat bonding. As by increasing the temperature higher degree of melting is obtained and subsequently better bonding between splats will be observed.

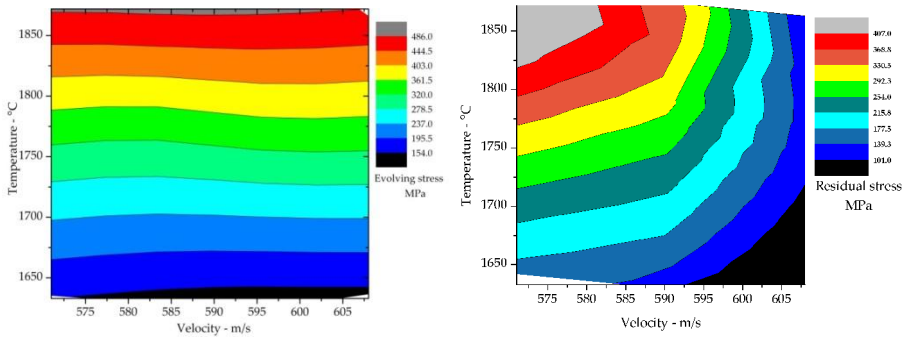

Figure 4.19. Dependency of (left) evolving stress and (right) residual stress on in-flight particles temperature and velocity.

4.4.4 Effect of in-flight particles state and microstructure on mechanical properties and performance

As the possible measures of microstructural characteristics are very limited, establishing direct correlation between microstructure and mechanical properties will be difficult. Thus, it is attempted to find a correlation between in-flight particles state and mechanical properties. Elastic modulus (based on ICP), hardness, indentation fracture toughness from cross section and top surface were measured. Sand abrasion rubber wheel test was performed as a measure of wear performance. Figure 4.20 shows this correlation as contour plots regarding to temperature and velocity. These countour plots are generated from 6 to 9 data points for each graph. Coatings deposited by low velocity and low temperature show the lowest elastic modulus, hardness and cross section indentation fracture toughness as well as low wear performance. From previous section it was shown that the same coating shows very porous structure. Note that hardness and elastic modulus have been measured by indentation technique from cross section.

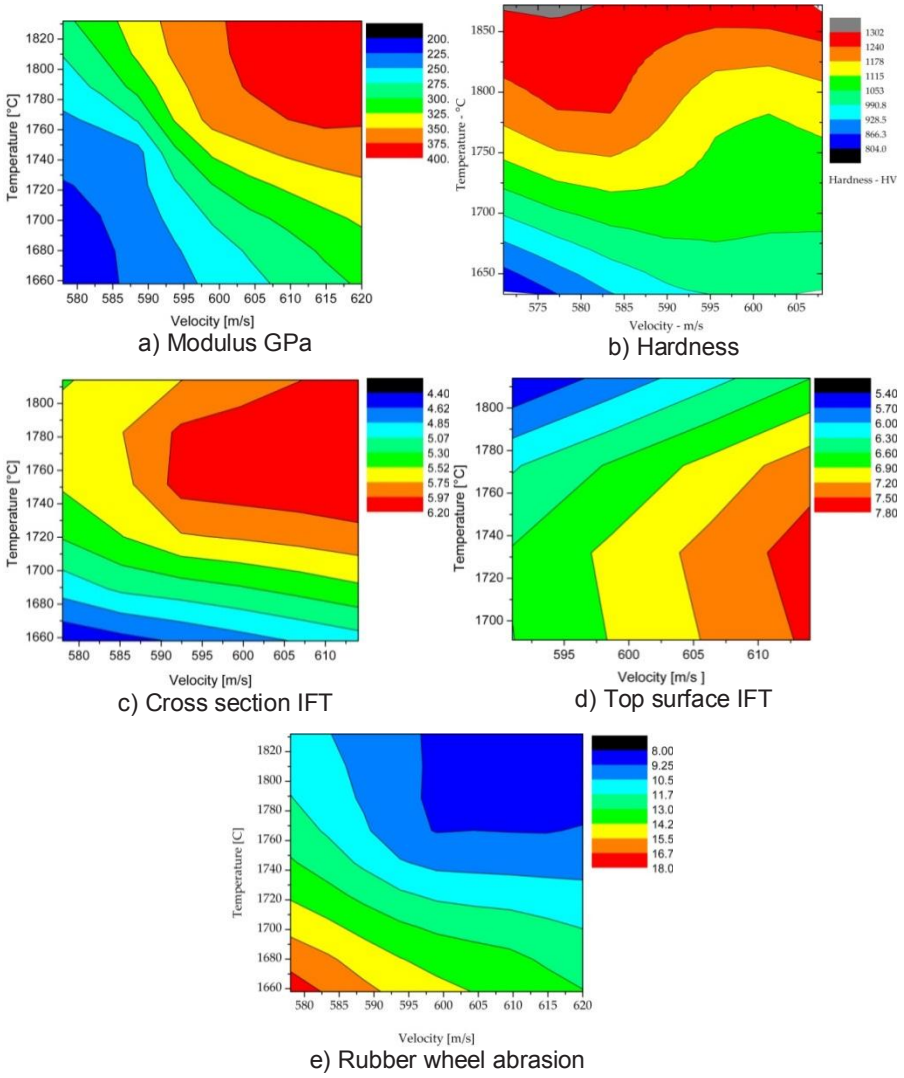

Figure 4.20. Correlation of in-flight particles temperature and velocity to properties and performance; (a) ICP elastic modulus (GPa), (b) hardness, (c) cross section indentation fracture toughness (MPa.m0.5), (d) top surface indentation fracture toughness (MPa.m0.5) and (e) rubber wheel abrasion in (mg/30 min).

The low mechanical properties can be attributed to low degree of melting, poor splat/splat cohesion and low kinetic energy of particles upon impact. It is also noteworthy that porosities have detrimental effect on mechanical properties and wear performance of coating. However, best mechanical properties and wear performance were obtained for coatings deposited with high temperature and velocity.

Top surface indentation fracture toughness is correlated directly with residual stress level of coatings (Figure 4.19). At higher tensile residual stresses crack formation and propagation will be easier compared to lower tensile residual stresses.

References

1. Swank, W.D., J.R. Fincke, and D.C Haggard. HVOF particle flow field characteristics. In: 7th National Thermal Spray Conference: Thermal Spray Industrial Applications. 1994, ASM International. p. 319–324.

2. Vattulainen, J., et al. Novel method for in-flight particle temperature and velocity measurements in plasma spraying using a single CCD camera. Journal of Thermal Spray Technology, 2001. 10: p. 94–104.

3. Fincke, J.R., et al. Diagnostics and control in the thermal spray process. Surface and Coatings Technology, 2001. 146-147: p. 537–543.

4. Deshpande, S., et al. Application of image analysis for characterization of porosity in thermal spray coatings and correlation with small angle neutron scattering. Surface and Coatings Technology, 2004. 187(1): p. 6–16.

5. Kulkarni, A., et al. Computed microtomography studies to characterize microstructure-property correlations in thermal sprayed alumina deposits. Scripta Materialia, 2000. 43(5): p. 471–476.

6. Matejicek, J. and S. Sampath. In situ measurement of residual stresses and elastic moduli in thermal sprayed coatings: Part 1: apparatus and analysis. Acta Materialia, 2003. 51(3): p. 863–872.

7. Matejicek, J., et al. In situ measurement of residual stresses and elastic moduli in thermal sprayed coatings: Part 2: processing effects on properties of Mo coatings. Acta Materialia, 2003. 51(3): p. 873–885.

8. Matejicek, J., et al. Quenching, thermal and residual stress in plasma sprayed deposits: NiCrAlY and YSZ coatings. Acta Materialia, 1999. 47(2): p. 607–617.

9. Liu, Y., et al. Anelastic Behavior of Plasma-Sprayed Zirconia Coatings. Journal of the American Ceramic Society, 2008. 91(12): p. 4036–4043.

10. Kulkarni, A., et al. Comprehensive microstructural characterization and predictive property modeling of plasma-sprayed zirconia coatings. Acta Materialia, 2003. 51(9): p. 2457–2475.

11. Wang, Z., et al. Effects of pores and interfaces on effective properties of plasma sprayed zirconia coatings. Acta Materialia, 2003. 51(18): p. 5319–5334.

12. Sampath, S., et al. Development of process maps for plasma spray: case study for molybdenum. Materials Science and Engineering A, 2003. 348(1–2): p. 54–66.

13. Cheng, D., et al. A numerical study of high-velocity oxygen fuel thermal spraying process. Part I: Gas phase dynamics. Metallurgical and Materials Transactions A, 2001. 32(7): p. 1609–1620.

14. Prystay, M., P. Gougeon, and C. Moreau. Correlation between Particle Temperature and Velocity and the Structure of Plasma Spray Zirconia Coatings. In: Thermal Spray: Practical Solutions for Engineering Problems, S. Sampath, Editor. 1996, ASM International. p. 517–523.

15. Vaidya, A., et al. An integrated study of thermal spray process-structure-property correlations: A case study for plasma sprayed molybdenum coatings. Materials Science and Engineering: A, 2005. 403(1–2): p. 191–204.

16. Sampath, S., et al. Sensing, Control, and In Situ Measurement of Coating Properties: An Integrated Approach Toward Establishing Process-Property Correlations. Journal of Thermal Spray Technology, 2009. 18(2): p. 243–255.

17. Turunen, E., et al. On the role of particle state and deposition procedure on mechanical, tribological and dielectric response of high velocity oxy-fuel sprayed alumina coatings. Materials Science and Engineering: A, 2006. 415(1–2): p. 1–11.

18. Xiong, H.-B., et al. Melting and oxidation behavior of in-flight particles in plasma spray process. International Journal of Heat and Mass Transfer, 2005. 48(25–26): p. 5121–5133.

19. Sampath, S. Method And Apparatus For Determining Process-Induced Stresses And Elastic Modulus Of Coatings By In-Situ Measurement. 2002, The Research Foundation of State University of New York, Stony Brook, NY (US): UNITED STATES. p. 6.

20. Clyne, T. and S. Gill. Residual Stresses in Thermal Spray Coatings and Their Effect on Interfacial Adhesion: A Review of Recent Work. Journal of Thermal Spray Technology, 1996. 5(4): p. 401–418.

21. Kuroda, S., T. Fukushima, and S. Kitahara. Significance of quenching stress in the cohesion and adhesion of thermally sprayed coatings. Journal of Thermal Spray Technology, 1992. 1(4): p. 325–332.

22. Shamim, T., C. Xia, and P. Mohanty. Modeling and analysis of combustion assisted thermal spray processes. International Journal of Thermal Sciences, 2007. 46(8): p. 755–767.

23. Vaidya, A., G.B., S. Sampath and H. Herman. In: International Thermal Spray Conference (ITSC). 2001, ASM International, Materials Park, OH, 2001: Singapore.

24. Zhang, H., et al. Melting Behavior of In-Flight Particles and Its Effects on Splat Morphology in Plasma Spraying. ASME Conference Proceedings, 2002. 2002(3638X): p. 309–316.

25. Usmani, S., et al. Effect of Carbide Grain Size on the Sliding and Abrasive Wear Behavior of Thermally Sprayed WC-Co Coatings. Tribology Transactions, 1997. 40(3): p. 470–478.

5. Carbide size effect and wear mechanisms in different contact conditions

5.1 Introduction

In last two chapters effect of process variables on in-flight particles state, microstructure, properties and performance were studied. However, there is another crucial non-process parameter, powder characteristics, that has significant impact on in-flight particles state, microstructure and properties. Employing different powder manufacturing techniques result in powders with diverse density and morphology range. Most often employed techniques for manufacturing powders are; agglomerating and sintering, plasma densification, fusion and crush and mechanical blending. Other powder characteristics that can be modified are chemical composition (e.g. Carbon contents in one set of powder materials), carbide grain size (for carbide based cermets) and size distribution of powders. Different morphology and powder density affect the in-flight particles temperature and velocity. Temperature and velocity of the powder particles define the microstructure of deposits that affect the mechanical properties as well as performance. Such interrelated powder characteristics are depicted schematically in Figure 5.1. In general, it is considered that starting powder characteristics with the microstructure and mechanical properties govern the coatings wear performance.

In this chapter at first effect of two main characteristics of starting material, particle size distribution and carbide size, have been studied to address the microstructure, properties and wear performance. In second part of this chapter encountered wear mechanisms regarding to carbide size have been addressed in different tribological contact conditions including slurry abrasion, dry abrasion and sliding. Slurry and dry abrasion tests were conducted by rubber wheel and sliding adhesive condition was simulated using pin-on-disk technique.

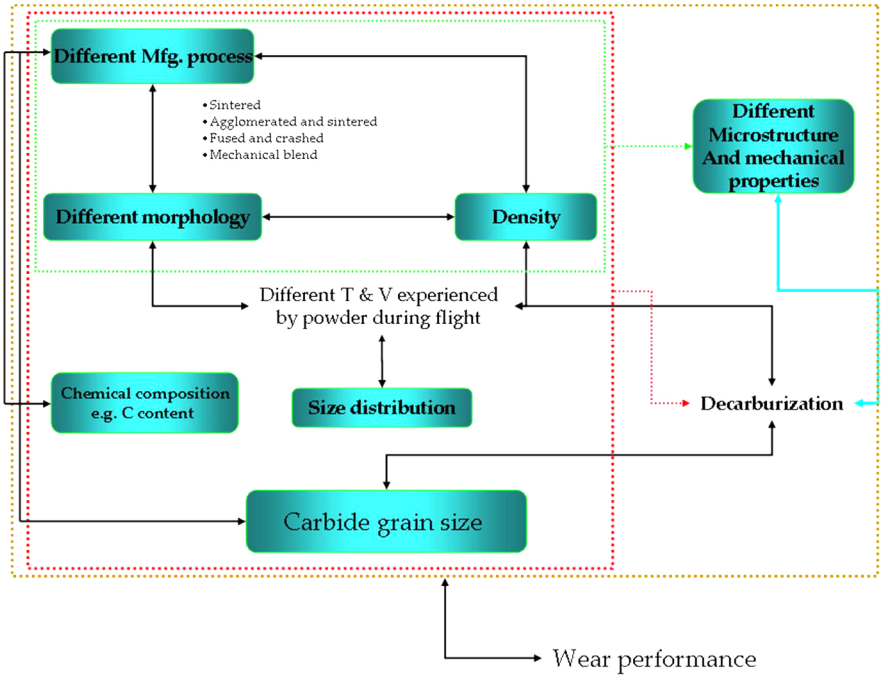

Figure 5.1. Interrelated powder characteristics affecting the mechanical properties and wear performance.

5.2 Experimental techniques

5.2.1 Materials

WC-CoCr powders with different WC grain size were deposited using DJ and CJS torches. Starting materials based on their carbide size were called conventional, sub-micron and nano. Detailed characteristics of the powders used in both torches are provided in Table 5.1. To study the effect of powder size distribution, conventional powder used in DJ process was sieved to obtain two batches of powders with size distribution of 24–32 µm and 32–45 µm. For both batch the same spraying parameter was employed.

Table 5.1. Details of employed powders in this study.

Powders	Apparent density, g/m^3	WC gain size, µm	Size distribution d10–d90%	Chemical composition, wt.%		
				C	Co	Cr
Conventional	4.91	1–3 µm	24–45	5.34	9.68	3.79
Sub-micron	5.71	0.4–1 µm	20–39	5.13	9.98	4.0
Nano	–	<0.02 µm	19–40	5.37	8.52	3.10

Table 5.2. Spraying parameters. * Standard Liters per Minute.

Parameters	H_2 (SLM*)	O_2 (SLM)	N_2 (SLM)	Air (SLM)	Fuel/Oxygen	Stand Off Distance
A	635	215	14	350	2.2	230 mm

5.2.2 Coating deposition

Three coatings (conventional, sub-micron and nano) were deposited by HVOF DJ-Hybrid gun using the hydrogen as the fuel gas and nitrogen as the carrier gas and three coatings (conventional, sub-micron and nano) were deposited by CJS torch using hydrogen and kerosene as fuel gases. Two sets of spray parameters were selected for deposition of each coating material. Parameters used for DJ and CJS torches are shown in Table 5.2. Coatings were deposited on steel that was grit-blasted with 590–710 µm alumina particles at 4.5 bar pressure followed by ultra-sonic cleaning in the acetone. Enough air cooling was applied to keep the sub-strate temperature at 150 °C during spraying. Substrate temperature was meas-ured during the spraying to assure the minimal fluctuation from intended substrate temperature (±50 °C).

5.2.3 Characterization techniques

Coatings were evaluated by x-ray diffraction with a Phillips PW3710 with Mo-K-α radiation for detection of different phases and the W_2C /WC intensity peak ratio was used as an indication of the level of decarburization. Powders and coatings cross-sections were studied by scanning electron microscopy (SEM), JEOL JSM-6400. The shape of abrasive particles utilized in this work was analyzed by SEM. Hardness values and elastic modulus values were obtained by an instrumented microhardness tester (Zwick ZHU 0.2). A Vickers indenter was employed using a 300 g load for hardness and elastic modulus measurement. Wear performance was evaluated by volume loss in a wet abrasion test using a Sensofar surface

profilometry instrument and by weight loss in a dry sand abrasion test. The volume loss was measured in pin-on-disk test to evaluate the wear performance.

5.2.4 Abrasive wear test

There are different test methods for evaluation of wear performance of a coating system. In each particular method, testing variables have diverse and significant effects on the evaluation of wear performance and the associated wear mechanisms. It is important to choose proper test methods and test parameters to mimic real working conditions. By simulating the actual wear condition in different applications, laboratory-based results will be more useful and reliable. One of the important testing variables in abrasion is abrasive particle size. In some applications, such as paper and pulp industries, there are nano-sized abrasive particles varying in shape which exist in the medium and can be softer or harder than the coating material. Most of the investigations for abrasive wear study of thermal spray coatings have been done by employing abrasive particles on the order of tens of microns which are significantly larger than reinforced hard particles and binder mean free path of coatings [1–3]. Changes in wear performance as well as wear mechanisms by changing the abrasive particle size from micro to nano are expected. There are different apparatus for abrasion test based on ASTM standards such as ASTM G65 and B611 [4, 5] specifically designed for cemented carbides. We used two different modified abrasion test techniques to carry out both dry and wet abrasion tests. Figure 5.2 shows two modified settings used in this study. In both cases, a rubber wheel was used to provide low stress level in dry and wet conditions.

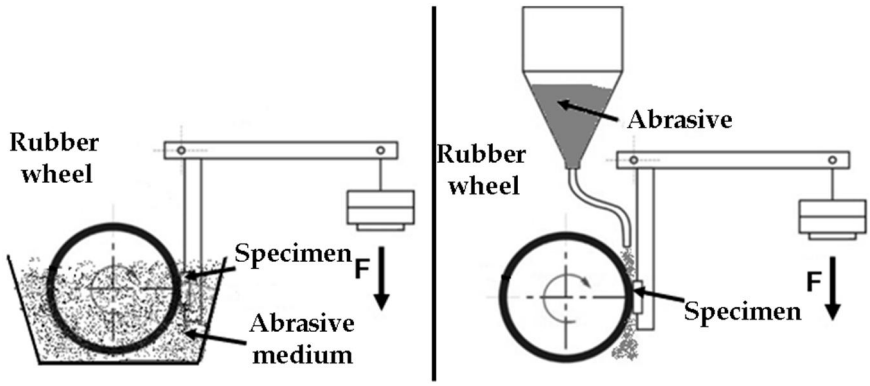

Figure 5.2. Schematic of settings used in this study for slurry abrasion test (left) and dry abrasion test (right).

The abrasive particles that were used in the dry rubber wheel tests were casting sand particles (99.5% SiO_2) with a 368 μm diameter. SiC particles were only used to study the very early stage of wear and no complete wear test was conducted

using SiC particles. Figure 5.3 shows the SEM image of abrasive particles used in this study. It is notable that sand abrasive particles contain both irregular- and spherical-shape particles. The SEM image of titania particles shows fine spherical particles. SiC abrasive particles are in the same size range of sand particles with sharp irregular shape. No recycling of abrasive particles was done during the dry rubber wheel abrasion test. Mass loss of samples was measured at different time intervals (10, 20, and 30 min) as an indication for wear performance during dry rubber wheel abrasion testing. Wheel speed was 200 rpm and feeding rate of sand particles was 260 g/min. Both tests, dry and slurry abrasion, were done under 5 kg load. For wet abrasion testing, a mixture of 10% mass titania in water was used. Average particle size of employed titania was 220 nm. Size distribution of titania particles in the water mixture was measured to make sure no permanent bonding of particles has happened in the mixture.

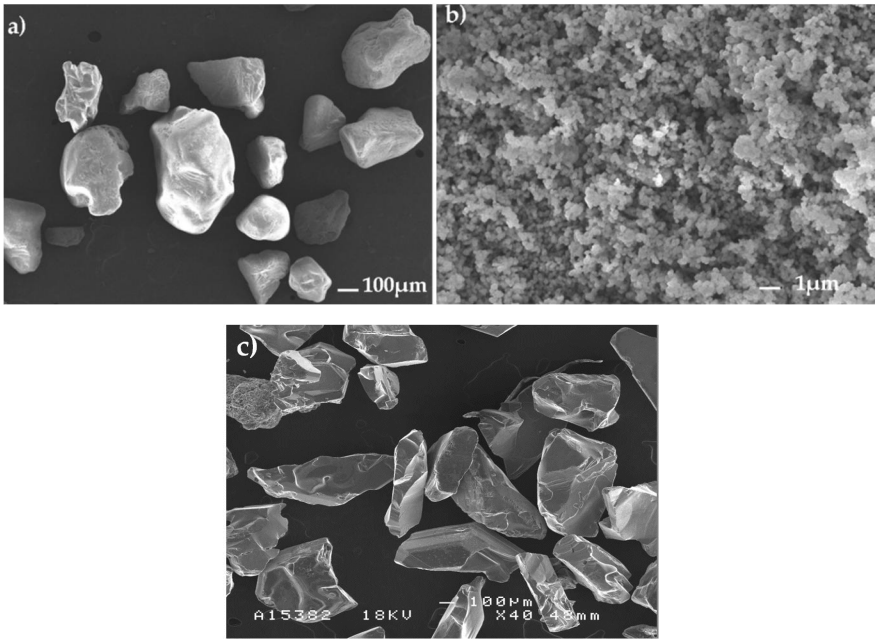

Figure 5.3. Abrasive particles used in this study, (a) sand particles, (b) titania particles and (c) SiC particles.

Hardness of titania and casting sand particles are relatively the same (750–950 HV). However, the hardness of SiC is much higher (2400 HV). A wheel speed of 100 rpm was used for wet abrasion test. The volume loss of coating was measured after 6-h tests as an indication of wear performance.

5.2.5 Pin-on-disk

In pin-on-disk test 4 tests were done on each sample. The counter parts were mushroom-shaped (50 mm radius) samples that were coated with the same coating and alumina balls (5 mm radius). Test parameters are shown in Table 5.3.

Table 5.3. List of pin-on-disk tests and parameters.

Counterpart		Self-mated mushroom		Alumina bal
Test duration (min)	10	30	120	120
Normal load (N)	10	10	10	10
Sliding speed (m/s)	0.1	0.1	0.1	0.1
Radius (mm)	50	50	50	5

After each test material loss was measured based on volume loss of material on mushroom samples. The material loss of tests carried out by alumina ball was measured from the disk.

5.3 Results and discussion

5.3.1 Effect of particle size distribution on microstructure, mechanical properties and wear

Based on modeling it is shown that powders regarding to their sizes experience different temperature and velocity inside and outside the nozzle. It is common to have a size distribution in starting material that is fed into the spray torch. Therefore, during processing each individual particle regarding to its size will have different velocity and temperature. This fluctuation in temperature and velocity yields different level of melting state in the powder before hitting the substrate. By modeling approach it is shown that fine particles are accelerated and heated to higher temperature in the nozzle much faster than coarser ones. However, fine particles decelerated and cooled faster than coarser particles in the jet [6]. The significance of melting state in terms of powder particle size is shown in Figure 5.4 for WC-CoCr assuming same in-flight particles temperature and velocity for all particle size.

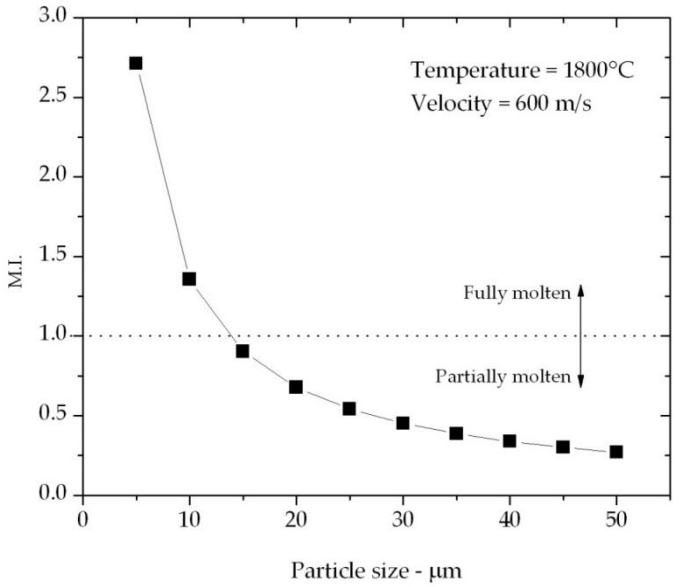

Figure 5.4. Melting index for same material with different particle size assuming same temperature and velocity.

As it is shown in Figure 5.4 fine powder particles undergo higher level of melting. To study the effect of particle size distribution on microstructure, properties and wear performance conventional powder was sieved to two different size distribution, 24–32 micron and 32–45 micron. For deposition of coatings same spraying parameters were employed. Figure 5.5 shows the SEM cross section of these two coatings. Obtained microstructures from these two coatings are distinctly different. As it is depicted in cross sectional images, coating deposited using fine particle size shows more white regions in the microstructure that are indication of severe decarburization and formation of W_2C in the microstructure. Two main reasons are hypothesized to explain the sever decarburization of fine particles. First, as it was shown in Figure 5.4 finer particles undergo higher level of melting. Higher melting index, as it was shown in chapter 4, promotes higher decarburization of WC particles. Second explanation is that finer the particle size higher the temperature experienced by particles especially inside the nozzle.

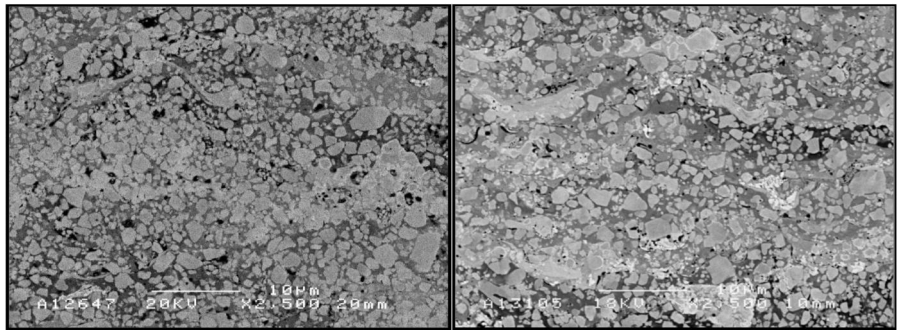

Figure 5.5. Cross section of coatings produced with left, coarse powders and right, fine powders.

Such observation can be validated by recourse to W_2C/WC intensity peaks ratio in the XRD results. Comparison of these two ratios reveals higher level of decarburization for fine coating as it was shown in SEM cross sectional images. W_2C/WC ratio for fine coating was measured to be 0.37 and for coarse coating was measured to be 0.22. As a result of higher decarburization and formation of higher amount of W_2C the coating will exhibit higher degree of brittleness as the W_2C phase is harder and more brittle than the WC phase. The effect of brittleness on mechanical properties can be seen in indentation fracture toughness values. Brittle material returns lower indentation fracture toughness. Figure 5.6 shows the both W_2C /WC ratios and indentation fracture toughness values. Another mechanical property that is directly affected by amount of W_2C phase within the structure is hardness value.

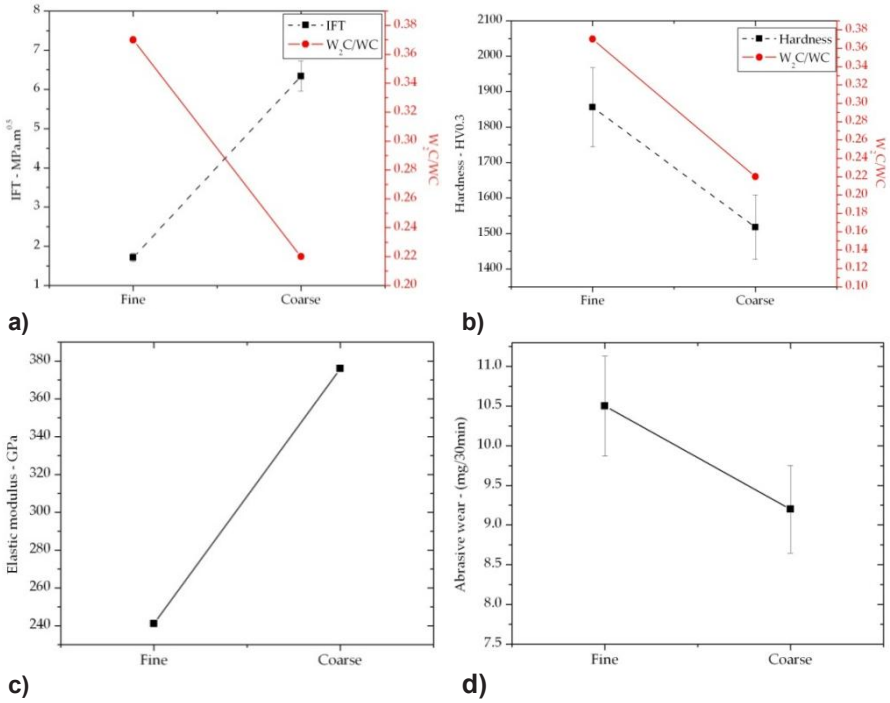

Figure 5.6. Microstructural and mechanical properties and wear performance of coatings deposited using fine and coarse particles, (a) IFT, (b) W_2C and hardness, (c) elastic modulus and (d) abrasive wear.

As W_2C phase is a hard phase (harder than WC) by introducing more W_2C phase in the microstructure the hardness of overall coating will be increased. However, presence of higher W_2C lowers the fracture toughness due to its brittle nature. Increase of hardness by increasing the W_2C is evident in Figure 5.6. Coating deposited by finer particles shows lower elastic modulus compared to coating deposited by coarse particles. In terms of performance coating deposited using coarse powder shows better abrasion wear in dry condition. The lower wear performance for fine powder coating might be due to very low fracture toughness value compared to coarse coating. In this case it is hypothesized that wear mechanism is dominated by fracture.

5.3.2 Effect of carbide size on microstructure, mechanical properties and wear – WC-CoCr coatings processed by DJ-2600

One of the most crucial parameters that affects mechanical properties and wear performance of carbide-based cermet coatings is carbide grain size. For carbide-based cermets, researchers have shown a gain in wear performance by reducing

the carbide size [7]. The driving force for reducing the carbide grain size comes from the fact that as the carbide size becomes smaller, the binder mean free path is decreased, resulting in higher resistance against deformation and material loss. Many researchers [1, 8–17] have pursued such a hypothesis to improve the wear performance of HVOF WC-Co by reducing the WC grain size to the nanoscale. Nevertheless, for thermal spray coatings, different researchers have shown sometimes contradictory wear performance results for the effect of reducing carbide size from conventional to nano [2, 18]. In chapter I a comprehensive review of the work on this topic is given. The main obstacle that is faced in processing the nano-carbide coatings is difficulty to maintain the original phases in the powder as the fine carbides have higher tendency to decarburize and dissolve into the binder. Therefore, the main conclusion drawn from previous works is that nano-carbide coatings mainly fail in the wear performance due to excessive decarburization and excessive brittleness. Nevertheless, addressing the pure structural effect of nano-carbide on mechanical properties remains unanswered unless to be able to process a nano-structured coating with no parasitic effect of W_2C phase. Figure 5.7 shows the microstructural SEM cross section of conventional (Figure 5.7a), sub-micron (Figure 5.7b) and nano (Figure 5.7c). Distinct difference between carbide size and spacing between carbides is detectable.

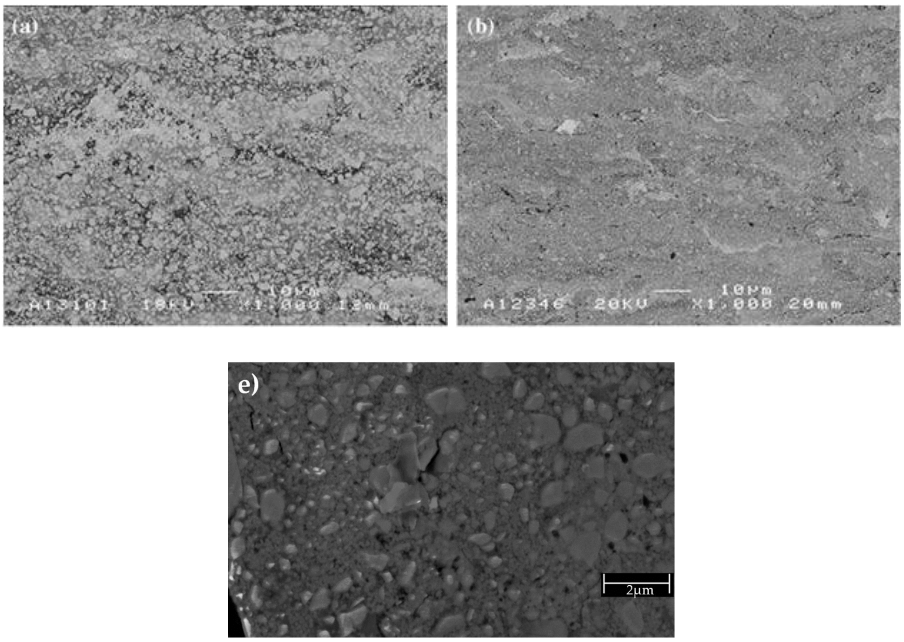

Figure 5.7. SEM microstructural images of (a) conventional, (b) sub-micron and (c) nano coatings.

Figure 5.8 shows W_2C/WC ratio, indentation hardness, indentation elastic modulus, and wear performance of coatings with different carbide size. The level of decarburization (W_2C/WC ratio) for coatings deposited using nano powder is higher than conventional and sub-micron powder. In Figure 5.8 dry abrasion rubber wheel test results are shown for conventional, sub-micron and nano coatings. The spraying parameters have been chosen to be the same. Among these three coatings, wear performance of sub-micron coating is the best.

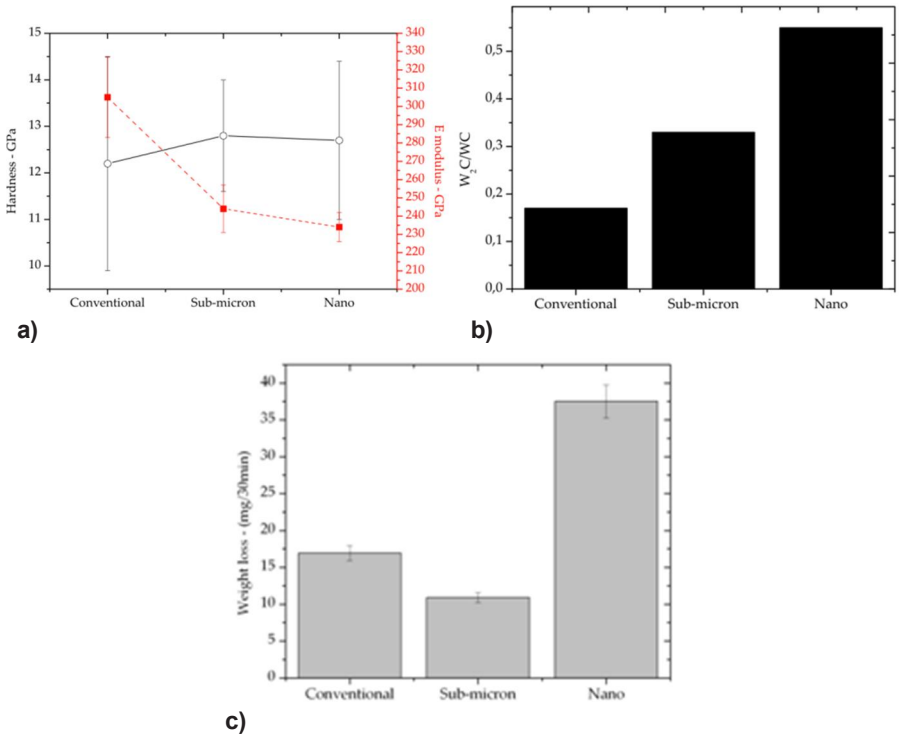

Figure 5.8. (a) Mechanical properties, (b) W_2C contents and (c) Dry abrasion performance of coatings with different carbide size.

Nano-coating shows very poor wear performance that is hypothesized to be related to excessive decarburization and brittle behavior of this coating.

5.3.3 Effect of carbide size on microstructure, mechanical properties and wear – WC-CoCr coatings processed by CJS

As it was mentioned in first chapter a new generation of HVOF torches have been developed that enable to apply coating with less amount of heat input and higher kinetic energy to powder particles. Employing this technique enables to process

finer powder particles and finer carbide powders with negligible or no decarburization and W_2C phase formation. In this section it is attempted to purely study the effect of carbide size on microstructure, properties and performance in absence of W_2C. Figure 5.9 shows the SEM microstructural images of coatings with different carbide size deposited employing CJS torch. All coatings have dense microstructure and by decreasing the carbide size the binder mean free path decreases Darker areas in the microstructure similar to the DJ coating processed with cold parameters are chromium rich regions. Figure 5.10 shows the elastic modulus, hardness and dry abrasion rubber wheel test results for CJS sprayed coatings and the results for coatings processed with both CJS and DJ torches are compared. It is shown in Figure 5.10a that sub-micron coating has slightly higher hardness and elastic modulus values. Figure 5.10b shows slight improved performance in sub-micron coating.

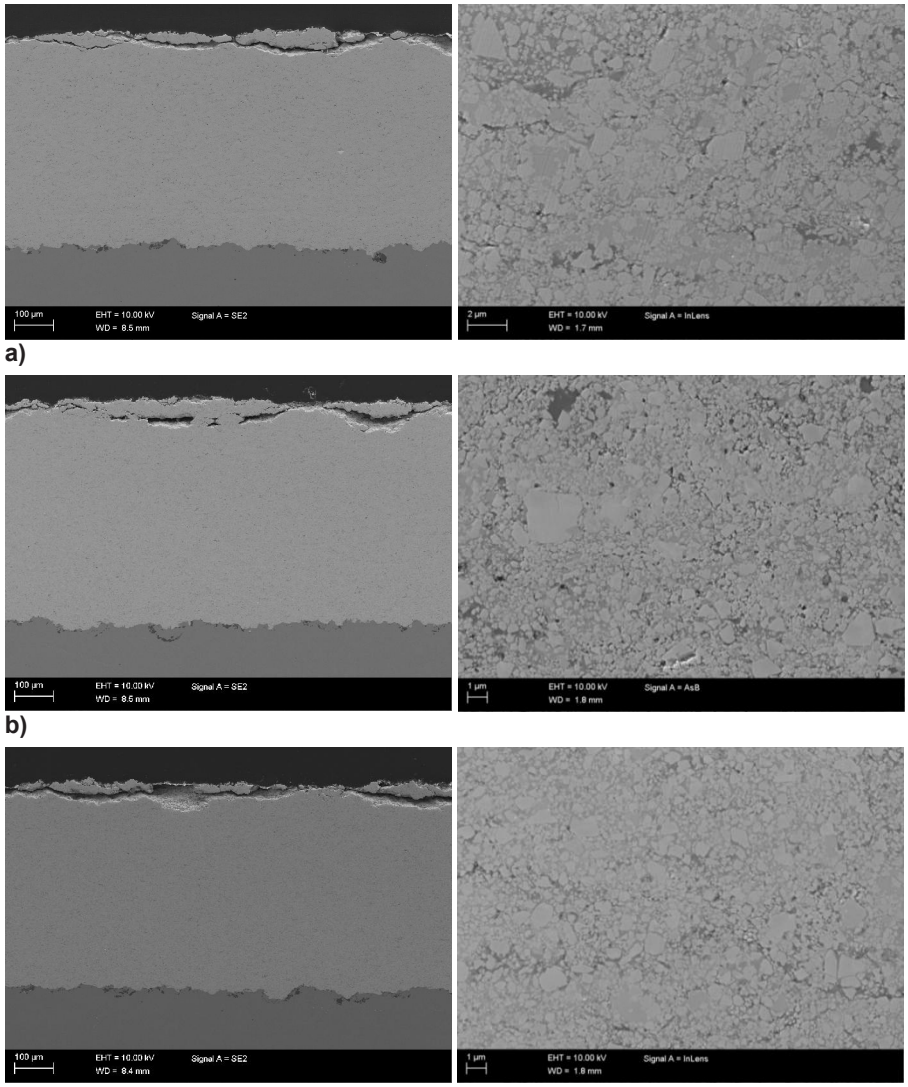

Figure 5.9. SEM microstructural images of (a)conventional, (b) sub-micron and (c) nano caotings deposited by CJS.

However, differences in both mechanical properties and wear performance are small. Figure 5.10c and 5.10d compare both mechanical properties and wear performance of coatings processed by DJ and CJS torches.

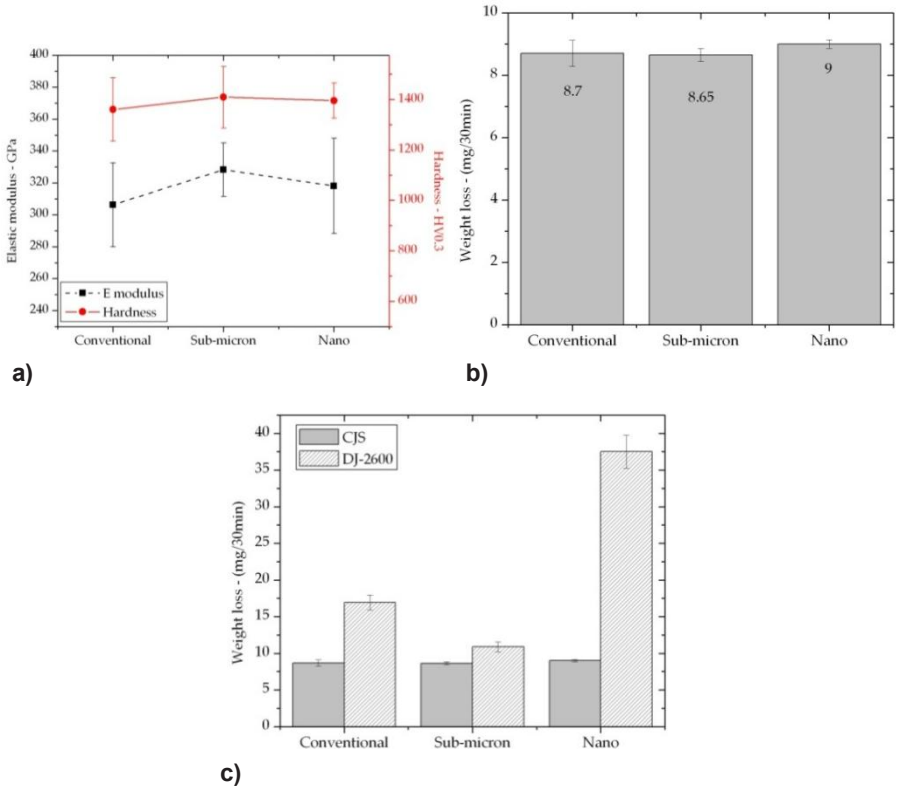

Figure 5.10. (a) mechanical properties (b) dry abrasion wear performance and (c) performance comparison with DJ of coating with different carbide size deposited by CJS torch.

Figure 5.10d shows significant gain in terms of wear performance of coatings processed by CJS torch disregarding to the carbide size. In addition to dry sand rubber wheel test set of pin onf disk tests were performed on CJS-processed coatings. The test consisted of a mushroom shape pin sliding on disk specimen and both were coated with the same material. The volume loss measurement was done on mushroom pins. Figure 5.11 shows the volume loss for conventional, sub-micron and nano coatings at 10, 30 and 120 minutes test intervals. As it is shown in this figure sub-micron coating shows the best wear performance and nano-coating exhibits low wear performance. At smaller sliding time the difference between conventional and sub-micron coating is the minimal. However, with further progress of the test the difference becomes bigger and sub-micron shows better wear performance. It is noteworthy that in these coatings there was no W_2C detected. However, similar to DJ-processed coatings the nano coating shows low wear performance. It is hypothesized that not only presence of brittle W_2C phase might be detrimental in terms of wear performance also binder mean free path can

play significant role in level of generated excessive stresses within the deformed and loaded structure. In conventional coating microstructure there is more spacing available between carbides (binder mean free path) and upon loading the material can accommodate the deformation within the binder.

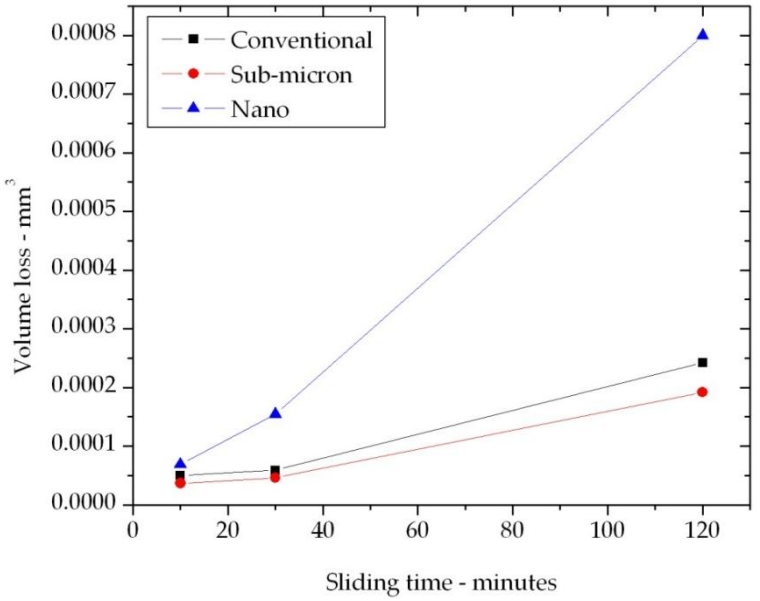

Figure 5.11. Volume loss measured on mushroom sample for conventiona, sub-micron and nano coatings at different sliding durations.

With decreasing the binder mean free path accommodation of deformation within binder will be more limited. This structure will result in a behavior similar to work hardening in metals. As long as the accumulated stresses within the binder or binder/carbide interface do not exceed the yield strength or do not cause fracture in the structure, reducing the binder mean free path will have positive effect as for further deformation such structure requires further stresses to be applied (this positive effect is seen in improved wear performance of sub-micron coating over conventional coating). Nevertheless, further decrease in binder mean free path results in development of even higher stresses within the structure upon deformation or loading. In this scenario deformation of binder will be very limited and high stresses will be generated in the binder. With extra loading of structure, individual carbide particles will start to interact with each other and stresses will be generated within carbides as well. This high level of stresses in such structure results in early yielding or fracture of material or facture of individual carbides that all these are detrimental for wear performance or any performance that consists of loading.

5.3.4 Abrasive wear mechanisms

5.3.4.1 Wear mechanism in fine particle slurry abrasion test

To systematically study the wear mechanism, a visualization approach was employed by means of studying the same spot on the wet abrasion wear track with low and high resolutions. Patterned indents using a Vickers indenter were made with a 10 kg load on the surface of sample to serve as landmarks for relocating purpose. Using this marking technique, we were able to relocate the same spot in the electron microscope. This technique enables us to relocate individual carbides with high resolution in the microstructure by interrupting the abrasion test and examining the sample using SEM. This technique allowed for studying the wear mechanism on different scales. Figure 5.12 shows a schematic of this procedure.

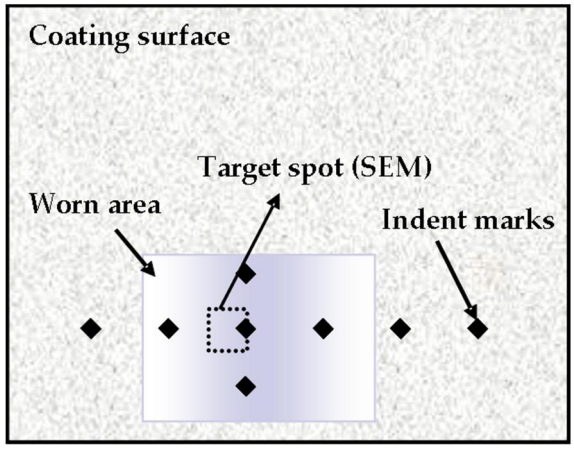

Figure 5.12. Schematic of relocating process and sample preparation.

After marking the sample, the SEM images were taken before the wet abrasion test, after 3 h of testing and after 6 h of testing exactly from the same spot. The SEM images taken from the targeted spot before the test did not reveal any features of microstructure due to poor surface quality (not presented here). Because of the sample size, we were not able to apply polishing on the samples and only lapping was applied prior to wet abrasion wear test. Figure 5.13 shows the same spot after 3 hours and 6 hours of testing. In the microscale range, it was observed that some of the pores became bigger and some others became smaller (shown by arrows in Figure 5.13a and 5.13b). We hypothesize this is due to non-uniform material removal from the surface. In some areas, the whole material is worn (similar to cutting) and the porosity became smaller. On the other hand, in other areas abrasive particles interacted with the edges of pores and caused removal of material. The interaction of abrasive particles with the edge of pores leads to their

widening. In addition, in images with 1000X magnification (Figure 5.13c and 5.13 d), removal of a group of carbides or splats is illustrated.

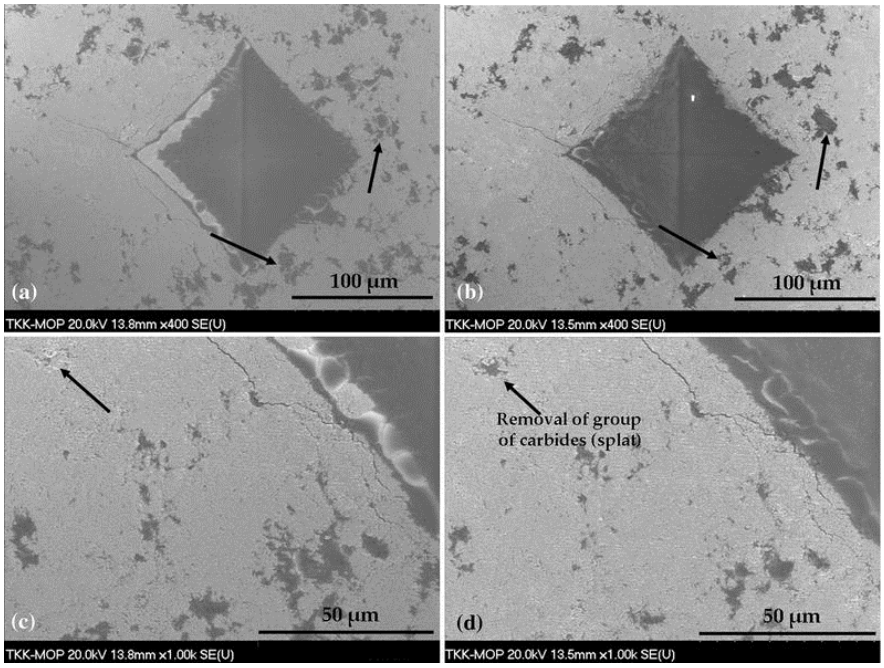

Figure 5.13. Same spot after 3 hours and 6 hours of slurry abrasion test.

However, higher magnification studies revealed additional wear mechanisms related to the interaction of abrasive particles with carbide grains. Figure 5.14a shows one spot after 3 h of wet abrasion testing and Figure 5.14b shows exactly the same spot after 6 h of wet abrasion testing. The following mechanisms that can happen step by step or simultaneously in the case of soft abrasive particles in wet abrasion test on WC-CoCr thermally sprayed materials are suggested:

1. Removal of soft metallic binder phase.
2. Fragmentation of carbide grains as a whole or in part.
3. Removal of fragments by removing the binder.

Larssen-Basse et al. reported similar wear mechanism for soft abrasives [19]. For a more detailed study, each carbide size shown in Figure 5.14a was measured employing the image analysis software (Leica Qwin) and the above mechanisms were addressed by recourse to the relative size of the carbide grains to abrasive particles (average 220 nm). When this ratio is <0.5, cutting of binder and the removal of carbides with the binder occurs (Figure 5.15a). When this ratio is between 0.7 and 1.3, fragmentation of carbides occurs (Figure 5.15b). Note that when this ratio is close to the lower limit (0.7) fragmentation of whole grain happens

and when it is close to higher limit (1.3) partial fragmentation of carbide grain occurs. With the ratio larger than 1.4, no significant effect on the carbides was observed. All the above mechanisms were observed for spherical-like soft abrasive particles (in comparison to the coating material) in the wet abrasion test and might not be applicable for abrasives with different shape and different characteristics.

5.3.4.2 Wear mechanism in coarse particle dry abrasion

Due to the formation of rough surfaces and high volume loss after dry sand abrasion test, study of the wear track in high magnification provides limited insight into underlying wear mechanism. One solution to overcome such limitations is studying the single scratches that have been made by individual abrasive particles in the very early stages of material removal.

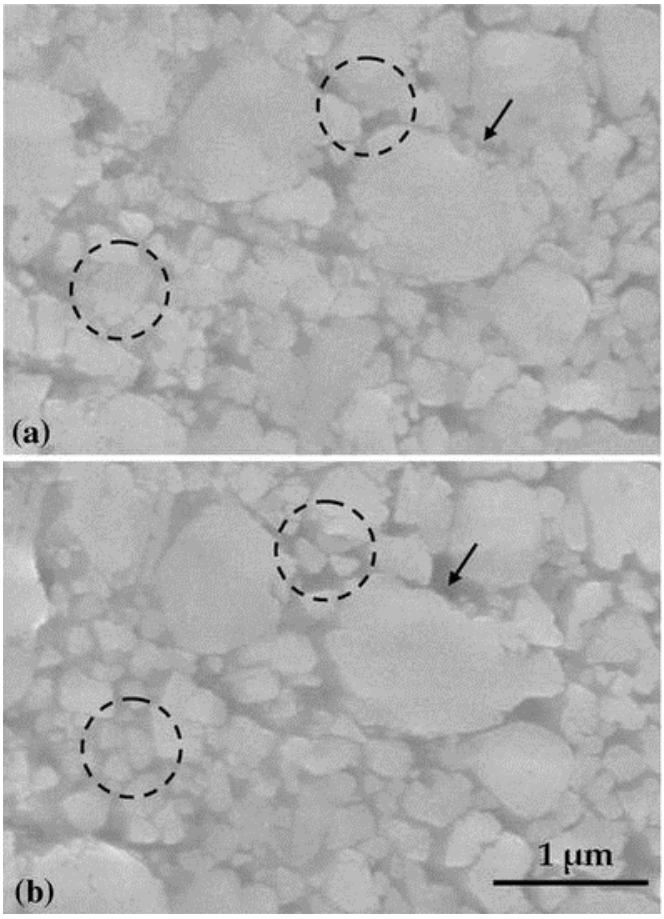

Figure 5.14. (a) high magnification image after 3 hours slurry abrasion test and (b) the same spot after 6 hours slurry abrasion.

To be able to analyze the initial scratches and material removal caused by abrasive particles, the sample was exposed to the sand abrasion rubber wheel test for a very short time (one complete rotation of wheel at 30 rpm). The outcome of this test was a surface with single scratches. Scratches were studied by SEM.

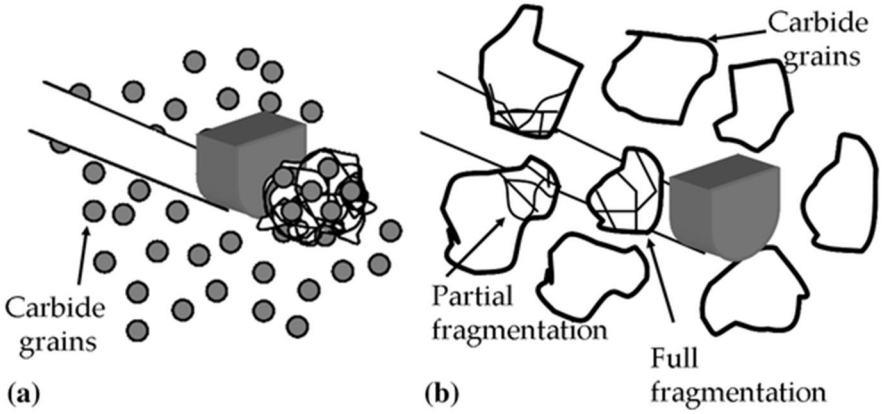

Figure 5.15. Schematic of wear mechanisms observed in slurry abrasion, (a) removal of small carbides with the binder and (b) partial or full fragmentation of carbides.

When a rubber wheel (a cylinder) comes to the contact with a flat surface based on Hertzian theory [20], the contact pressure may have an elliptical distribution which has its maximum value in the center and the lowest values at its two ends. This contact pressure can be calculated as follows:

$$P(x) = P_{max}\sqrt{\frac{x^2}{a^x}} \tag{4}$$

$$a = \sqrt{\frac{4RF}{\pi E_R}} \tag{5}$$

$$P_{max} = \frac{2F}{\pi a} \tag{6}$$

where P(x), R, F, a, and E_R are pressure distribution, radius of rubber wheel, contact force per unit length of the cylinder during the test, half of contact length, and elastic modulus of rubber wheel, respectively. Figure 5.16a and 5.16b show one example of the starting point of the scratches within the contact area and the continuance of same scratch, respectively. Similar to all other scratches, the scratches originated from surface open porosities and continued to the direction of rubber wheel movement. It is noteworthy that starting points of single scratches are not at the same pressure level in the contact region (based on pressure distribution of the rubber wheel in contact with rigid surface). This observation indicates that pressure level does not necessarily define the penetration point of abrasive particles into the material in this case. The schematic of scratches formed on the surface within the contact region are shown in Figure 5.16c.

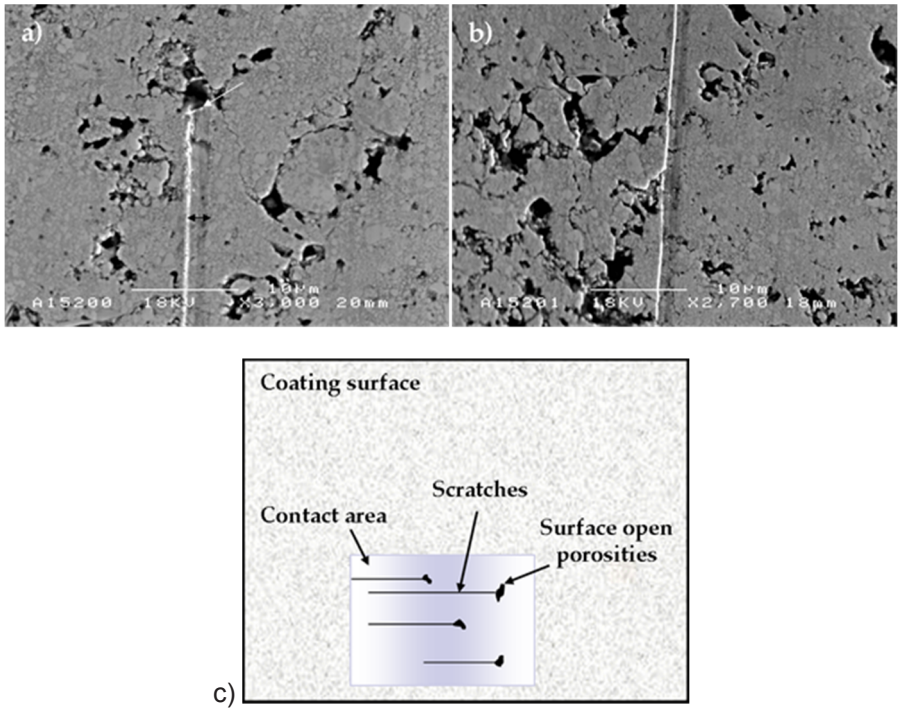

Figure 5.16. (a) single scratch caused by SiO_2 abrasive particle started from surface open porosities, (b) continuation of same scratch and (c) schematic of scratches formed on the surface of material and started from surface open porosities.

To remove material by abrasive particles, penetration of abrasives into the material and high enough shear force (parallel to the surface) acting on penetrated particle is necessary. In the case of relatively soft sand particles moving in between soft rubber wheel and hard coating surfaces, penetration of particles to the hard surface will be very limited. Nonetheless, in the current experiment, entrapment of the corner of an abrasive particle (which is sharp on the micro-scale) into the surface open porosities provides a condition similar to the already-penetrated particle. At this stage, a bigger portion of particle is gripped by rubber wheel and a smaller portion of particle is locked into the pore. Entrapment of a corner of an abrasive particle into the pore (similar to penetration of particle) and shear force provided by rotation of rubber wheel acting on abrasive particle satisfy two conditions for material removal by abrasive particles. Formation of grooves (Figure 5.16a and 5.16b) with much smaller width than actual abrasive particle size (groove width 2–3 μm, abrasive particle size ~368 μm) provide evidence of the above explained mechanism which is based on entrapment of a corner of abrasive particle into the surface open porosities. The observed grooves are more likely microplowing and microcutting of material due to the single pass of an abrasive particle [21]. In microplowing, the material does not detach from the surface and just displaces side-

ways. It can be displacing the hard WC within the soft binder. Microcutting can be cutting a shallow thickness of WC and cutting the binder which has been extruded from between the WC grains. The microplowing was not pronounced to form significant ridges at the edges of grooves. This explanation is more plausible in the absence of debris and microcracking inside and around the wear grooves. In this experiment, microfatigue was not addressed as only one pass of single abrasive particle was considered and studied.

A similar experiment was carried out using SiC abrasive particle to address the early stage material removal mechanisms. Figure 5.17a shows the starting point of penetration of SiC particle to the material surface. As it is shown unlike to sand abrasive particles case the scratch groove is not originated from surface open porosities and they originate at the location in which the contact pressure is high enough to cause penetration of SiC particles to the material surface. The continuance of scratch groove shows the chipping of material (Figure 5.17b).

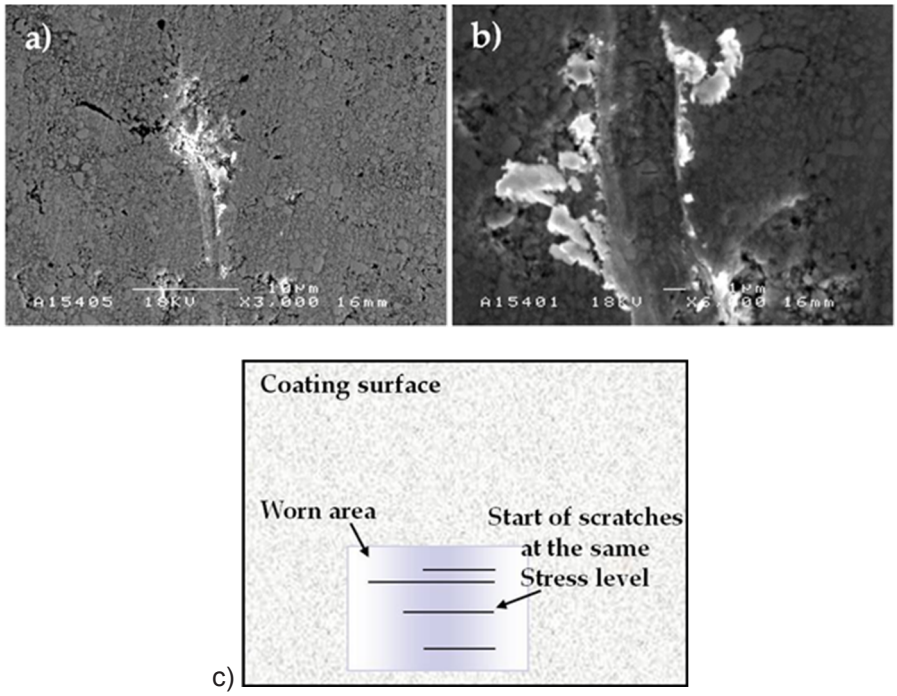

Figure 5.17. (a) single scratch caused by SiC abrasive particle started from regions with high enough stress level, (b) continuation of same scratch and (c) schematic of scratches formed on the surface of material that shows pressure dependency of starting point of scratch.

Chipping of material is mainly due to sharp shape of abrasive particles and shallow depth of cut. Interestingly chipping is observed in machining the relatively soft

materials. However, to machine the hard brittle materials it is common to use a cutting tool with sharp attack angel and set it to low feed rate (similar case to sharp SiC abrasive particles). In that case chipping also was observed and the brittle material behaves like ductile. Figure 5.17c shows the schematic of scratch formation mechanism under SiC abrasives.

5.3.4.3 Effect of surface open porosities on wear performance

When the surface open porosity size is smaller than the abrasive particle size, the pores will have a negative effect on wear performance as explained above (a corner of abrasive particle can be locked into the pore and start to scratch). Nonetheless, when the pore size is larger than the abrasive particle, the pore will act as a reservoir and abrasive particles will be deposited into that pore and the concentration of abrasive particles in contact with surface of material will be decreased. Consequently, the wear performance will be improved. It can be seen in Figures 5.13a and 5.13b where the indent imprint acts as a big pore that abrasive particles can be deposited into the pore, resulting in less effected surface to the left side of indent mark (smooth with no pore produced by wear). Voyer and Marple observed the same positive effect of porosity on wear performance [22].

5.3.5 Sliding wear mechanisms

To better understand the encountered wear mechanism under sliding condition (pin on disk), the wear tracks formed on the disk were studied by SEM and debris were collected on a carbon tape from the mushroom surface after the test and were studied by SEM microscope as well. Wear track studies of disk revealed a smeared layer of material on original material surface. The smeared layer seems to be fairly thin as it is possible to see the original material microstructure through the smeared layer. The smearing happened on all coating surface disregarding of their carbide size and test duration. Figure 5.18 shows three images of smeared layer at different magnifications. The observed smearing suggests there is an interaction of sliding bodies and binder phase as the binder attaches to the disk surface as a smeared layer. In polished surface of WC-CoCr material carbide particles stand higher than binder. Thus it is hypothesized that after two surfaces are brought to contact carbide particles are pushed to the binder and binder extrudes out from between the carbide particles. Then extruded binder in contact with counterpart is smeared on the surface.

Based on collected debris on carbon tape it was noted that debris tend to be accumulated at trail of contact region. Figure 5.19 shows the images of debris collected from region A and region B that show both individual particle and dense layered structure. Debris that is collected from the sides of contact region (region A in Figure 5.19) is made of individual single particles. Nevertheless, debris produced from the center of contact (region B in Figure 5.19) show a layered dense

structure. The region B debris dense structure might be because of compressing the loose debris due to exposure to high contact pressure.

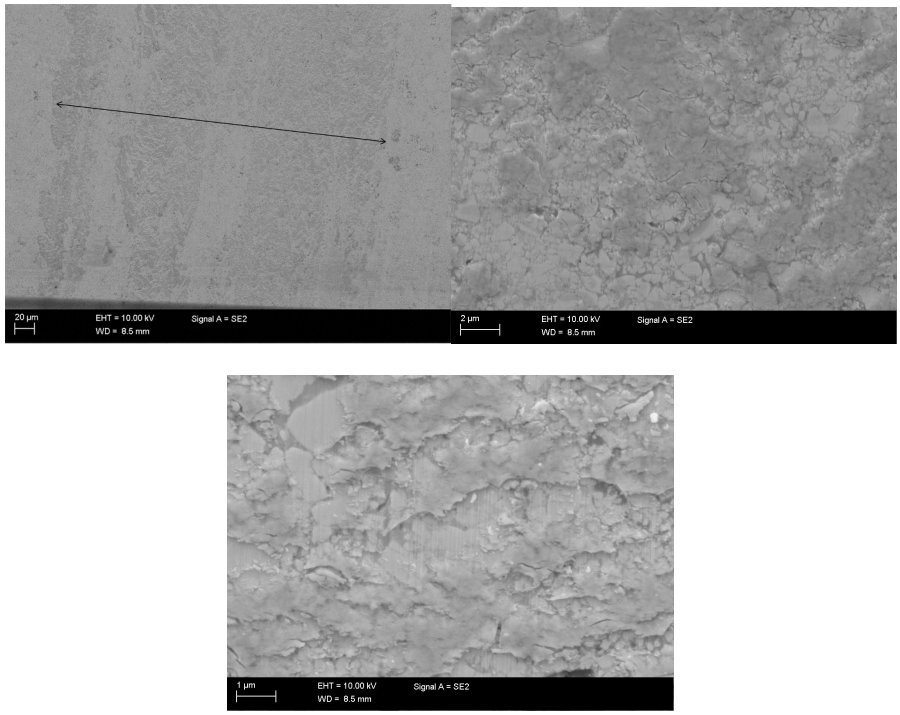

Figure 5.18. Images of smeared layered in wear track at different magnifications.

Debris from region A collected on carbon tape from conventional, sub-micron and nano coatings are shown in Figure 5.20.

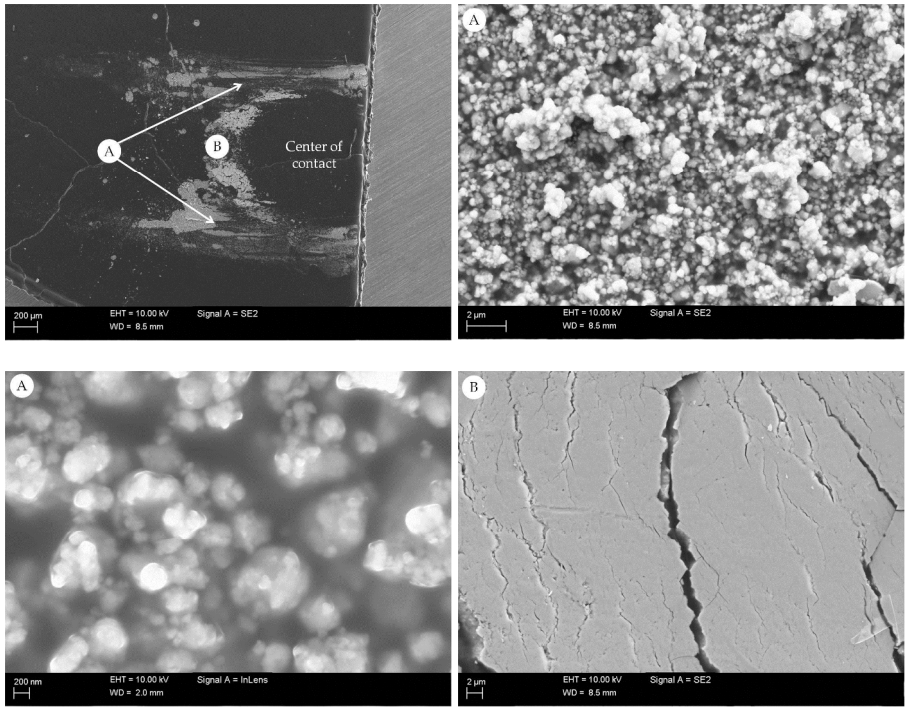

Figure 5.19. Debris collected from two different regions of contact area on carbon tape.

It is noted that debris particle size is correlated with carbide size. Smaller the carbide size, smaller the debris particle size. The observed debris might be detached carbide particles or the binder that was extruded, smeared and fractured. Nonetheless, debris collected from region B disregarding to the coating carbide size show similar dense structures.

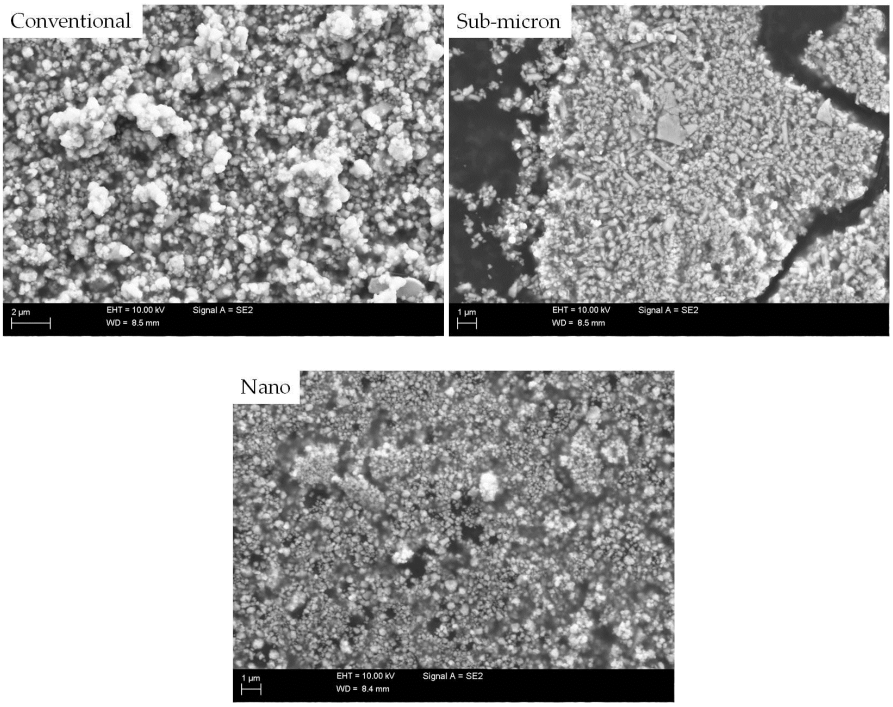

Figure 5.20. Debris collected from region "A" of contact showing different sizes for coatings with different carbide size.

5.4 Conclusions

The behavior of WC-CoCr coatings with different carbide size produced with two different torches (DJ-2600 and CJS) under abrasive and adhesive wear conditions were studied. Dissolution of WC into the matrix is more sensitive to spraying parameters compared to sub-micron or conventional coating processed by DJ-2600. On the other hand, disregarding to carbide size no W_2C formation was observed for coatings processed by CJS torch. In DJ-processed coatings hardness is a function of W_2C phase. In both CJS and DJ processed coating sub-micron coating exhibits the best wear performance in abrasion rubber wheel and pin-on-disk test. It can be concluded not only the excessive amount of W_2C can be detrimental also minimizing the binder mean free path in the structure that cause accumulation of stresses in loaded structure can have negative impact on wear performance of material. The wear mechanism in slurry abrasion test consists of partial and/or full fragmentation of WC grains, removal of binder and removal of carbide fragments or small carbides within the binder. These steps can happen simultaneously or step-by-step. In the early stages of material removal, under dry abrasion condition, abrasive medium contains sand particles which are bigger than the carbides or

binder mean free path. In this case, penetration of abrasive particle to the dense region of coating will be difficult. However, open surface pores will serve as origins for wear scratches made by individual abrasive particles. Porosities which have been formed during the deposition process and can be found within the coatings have an effect on some of the mechanical properties such as elastic modulus, shear modulus, Poisson's ratio, and hardness that may indirectly affect the wear performance by changing the material's elastic-plastic response to the external loading. Dependency of mechanical properties on the porosity has been discussed extensively in literature [23–26]. Nevertheless, when the porosities appear on the surface of a coating or are generated on the surface due to cutting or polishing process, the contact condition will be changed which causes the change in wear performance. The early stage wear mechanism under SiC particles suggests that due to high hardness and sharp shape particle they do not need surface open porosities to start removing material. Instead, as soon as enough stresses applied on SiC particles the particles penetrate to the material and cause scatching the material. The wear mechanism under pin-on-disk is hypothesize to consist of two steps. At first the binder extrudes from between the carbide particles. Further removal binder leaves the carbide particles unsupported on the surface and as next step carbides start to detach from the material surface.

References

1. Stewart, D.A., P.H. Shipway, and D.G. McCartney. Abrasive wear behaviour of conventional and nanocomposite HVOF-sprayed WC-Co coatings. Wear, 1999. 225- 229(Part 2): p. 789–798.

2. Shipway, P.H. and J.J. Hogg. Dependence of microscale abrasion mechanisms of WC- Co hardmetals on abrasive type. Wear. 259(1–6): p. 44–51.

3. Qiao, Y., Y. Liu, and T. Fischer.liding and abrasive wear resistance of thermal-sprayed WC-CO coatings. Journal of Thermal Spray Technology, 2001. 10(1): p. 118–125.

4. Standard Test Method for Measuring Abrasion Using the Dry Sand/Rubber Wheel Apparatus, ASTM.

5. Standard Test Method for Abrasive Wear Resistance of Cemented Carbides. 1991, ASTM.

6. Kreye, H., F.Gärtner, and H.J. Richter. High velocity oxy-fuel flame spraying – state of the art, new developments and alternatives, in HVOF colloquim. 2006: Germany.

7. Jia, K. and T.E. Fischer. Abrasion resistance of nanostructured and conventional cemented carbides. Wear, 1996. 200(1–2): p. 206–214.

8. Bartuli, C., et al. Parametric study of an HVOF process for the deposition of nanostructured WC-Co coatings. Journal of Thermal Spray Technology, 2005. 14(2): p. 187–195.

9. Dent, A., S. DePalo, and S. Sampath. Examination of the wear properties of HVOF sprayed nanostructured and conventional WC-Co cermets with different binder phase contents. Journal of Thermal Spray Technology, 2002. 11(4): p. 551–558.

10. Guilemany, J., et al. High-velocity oxyfuel Cr3C2-NiCr replacing hard chromium coatings. Journal of Thermal Spray Technology, 2005. 14(3): p. 335–341.

11. He, J. and J.M. Schoenung. A review on nanostructured WC-Co coatings. Surface and Coatings Technology, 2002. 157(1): p. 72–79.

12. Marple, B. and R. Lima. Process temperature/velocity-hardness-wear relationships for high-velocity oxyfuel sprayed nanostructured and conventional cermet coatings. Journal of Thermal Spray Technology, 2005. 14(1): p. 67–76.

13. Qiao, Y., T.E. Fischer, and A. Dent. The effects of fuel chemistry and feedstock powder structure on the mechanical and tribological properties of HVOF thermal-sprayed WC-Co coatings with very fine structures. Surface and Coatings Technology, 2003. 172(1): p. 24–41.

14. Shipway, P.H., D.G. McCartney, and T. Sudaprasert. Sliding wear behaviour of conventional and nanostructured HVOF sprayed WC-Co coatings. Wear. 259(7–12): p. 820–827.

15. Stewart, D.A., P.H. Shipway, and D.G. McCartney. Microstructural evolution in thermally sprayed WC-Co coatings: comparison between nanocomposite and conventional starting powders. Acta Materialia, 2000. 48(7): p. 1593–1604.

16. Yang, Q., T. Senda, and A. Ohmori. Effect of carbide grain size on microstructure and sliding wear behavior of HVOF-sprayed WC-12% Co coatings. Wear, 2003. 254(1–2): p. 23–34.

17. Watanabe, M., et al. Effect of WC size on interface fracture toughness of WC-Co HVOF sprayed coatings. Surface and Coatings Technology, 2006. 201(3–4): p. 619–627.

18. He, J., et al. Near-nanostructured WC-18 pct Co coatings with low amounts of non-WC carbide phase: Part I. Synthesis and characterization. Metallurgical and Materials Transactions A, 2002. 33(1): p. 145–157.

19. Larsen-Basse, J. and E.T. Koyanagi. Abrasion of WC-Co Alloys by Quartz. Journal of Lubrication Technology, 1979. 101(2): p. 208–211.

20. Timoshenko, S.P. and J.N. Goodier. Theory of elasticity. 3rd ed. 1970, New York: McGraw- Hill Book Comp. 567.

21. Gahr, K.H.Z., Wear by hard particles. Tribology International, 1998. 31(10): p. 587–596.

22. Voyer, J. and B.R. Marple. Sliding wear behavior of high velocity oxy-fuel and high power plasma spray-processed tungsten carbide-based cermet coatings. Wear, 1999. 225- 229(Part 1): p. 135–145.

23. Ramakrishnan, N. and V.S. Arunachalam. Effective elastic moduli of porous solids. Journal of Materials Science, 1990. 25(9): p. 3930–3937.

24. Hunter, O. and G.E. Graddy. Porosity Dependence of Elastic Properties of Poly- crystalline Cubic Lu2O3. Journal of the American Ceramic Society, 1976. 59(1–2): p. 82–82.

25. Arnold, M., A.R. Boccaccini, and G. Ondracek.Prediction of the Poisson''s ratio of porous materials. Journal of Materials Science, 1996. 31(6): p. 1643–1646.

26. Nakamura, T., G. Qian, and C.C. Berndt. Effects of Pores on Mechanical Properties of Plasma-Sprayed Ceramic Coatings. Journal of the American Ceramic Society, 2000. 83(3): p. 578–584.

6. Development of a damage mechanism map based on scratch testing

6.1 Importance of understanding the wear mechanisms

It is shown that abrasive and erosive wear performance of material depends on material resistance to penetration of particles and its resistance to removal or displacement of material from the surface due to fracture and/or plastic deformation. The abrasive wear controlling parameters of material can be defined by elasto-plastic properties and fracture toughness of the material. In fact these characteristics are the main motivations to employ ceramic-metallic coatings in wear resistance applications as they exhibit a combination of high hardness and high toughness. The hardness is provided by hard, brittle WC phase and toughness is provided by metallic, ductile binder [1–3].

Understanding the wear mechanisms in any tribological systems provides indispensable information on material response to loading which causes failure and material removal. Such understanding is a crucial step towards material and process optimization in design of wear resistant surfaces.

Evaluation of wear performance and addressing the associated mechanisms are challenging tasks as most of the testing methods are based on either volume loss or mass loss measurements that provide quantitative means rather than mechanistic means for evaluation of wear performance of material. Besides, providing mechanistic insight into wear requires careful and extensive post facto inspection on wear event traces. Recently Ghabchi et al. visualized the wear mechanism of WC-CoCr thermal- sprayed coatings subjected to fine slurry abrasion [4]. In the same study it was also shown the very early stage of material removal caused by action of single abrasive particles on the surface. In spite of obtaining information on how a single abrasive particle interacts with the material surface, such observation provides limited insight into the wear mechanism as many imperative factors associated with wear event are not taken into account adequately such as exact applied load on single particle and the morphology and the size of abrasive particle which caused the wear. Providing reliable and accurate mechanisms needs the material to be loaded in a controlled mode with known load and known geometry of counterpart (abrasive particle) in contact with the material surface.

One method to load the material with known geometry and controlled load is indentation technique. Instrumented indentation technique provides practical information regarding to elasto-plastic properties of material [5]. Nonetheless, this technique has deficiency to characterize the interaction of indented material to moving indenter tip in lateral direction as it only applies the load normal to the material surface. It is well demonstrated that measured indentation hardness or elastic modulus individually are unable to predict the wear performance of material [6].

The scratch testing can be employed to load the material in a controlled manner and take into account the interaction of surface and indenter in lateral movement of indenter.

In general, scratch testing consists of moving a stylus on the surface of a material with increasing normal load [7] . Researchers have reported the scratch testing as a potential tool for evaluation of adhesion of thin coatings to the substrate [8–12]. Despite all proposed techniques for coating adhesion measurement by scratch testing one should consider that not all of the failure mechanisms observed in scratch testing are necessarily related to the interfacial adhesion. The failures that take place in scratch testing usually have a complex nature and associated with different mechanisms that are activated simultaneously. Thus, the scratch testing reliability to evaluate coating- substrate adhesion has been argued furthermore by other researchers [13–15]. A failure modes map developed by Bull for scratch testing of thin films shows different failure modes taking place during the scratch testing [16].

One term that has been used extensively in scratch testing reports is “critical load” (L_c). In fact critical load is defined as a load in which the first particular failure mechanism occurred. For example Laukkanen et al. used the concept of critical load for introducing first visible crack on the material surface under scratch testing to extract the fracture toughness of coated surfaces [17].

In current study damage mechanisms of thermal sprayed WC-14(CoCr) coatings are addressed. Additionally, the effect of WC particle size on observed damage mechanisms is discussed.

6.2 Fundamental considerations regarding to scratch testing of thermal spray coatings

6.2.1 Contact condition

When the coating on a substrate in contact with a spherical counterpart is thick enough and the maximum penetration depth does not exceed the 10% of coating thickness, the plastic as well as elastic field beneath the contact will be limited to the body of coating. Therefore, unlike the thin films some of the interfacial (coating/substrate) failure mechanisms will not be present [18]. However, there might be other interfacial failures in thermal sprayed coatings that arise from splat/splat bonding interfaces.

In response of material to increasing sliding loading three mechanisms can be considered; plowing, friction and fracture of material. These steps are shown schematically in Figure 6.1 and are explained as follow:

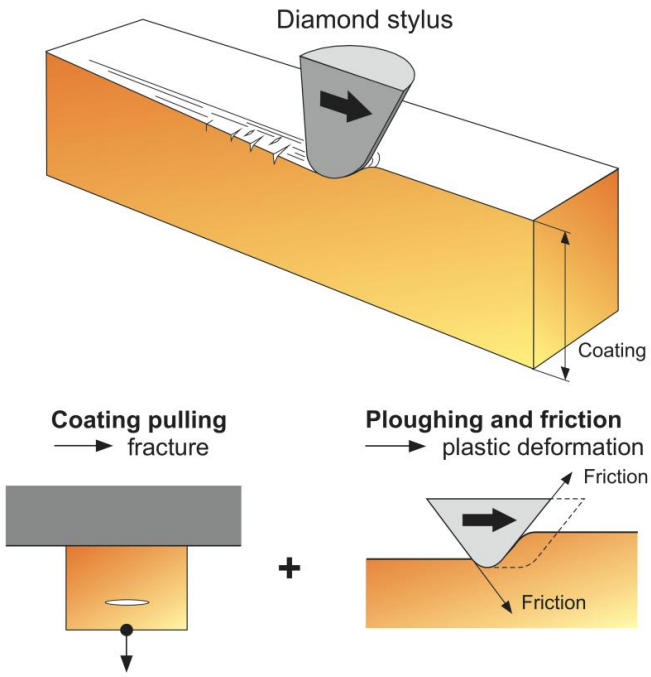

Figure 6.1. Three mechanisms, plowing, friction and material fracture in response of material to increasing sliding load.

1. *Material plowing* includes the elasto-plastic deformation of material under and in front side of the moving tip. Behind the moving tip only plastic deformation is left which is observed as scratch groove.
2. *Friction* is considered to have two contributing components; plowing and adhesive. The material deformation results in the plowing component of friction. Adhesion between the material and the moving tip results in adhesive friction. The adhesive friction force causes pushing the top layer of material in front of moving tip and pulling the top layer of material behind the moving tip. These two actions, pushing the material in front and pulling it behind the moving tip, cause formation of pile up and sink-in of material in front and behind of moving tip, respectively. The friction forces pulling and pushing the material behind and front of moving tip is shows in Figure 6.1.

3. *Fracture* can be caused by formation of stresses in front, beneath and behind the moving tip. Behind the moving tip cracks usually are formed in highest tensile stress regions. The crack formation beneath the indenter is mainly due to loading (plastic and elastic deformation) and unloading (elastic deformation) which cause lateral cracking parallel to the material surface.

This approach is same as explained by Holmberg et al. [19] but modified to fit the thick composite coating concepts such as thick WC-based thermal sprayed coatings.

6.2.2 Stresses around the moving tip

The origins of stresses around the moving tip in thick coatings are schematically shown in Figure 6.2a and can be considered as follow:

1. *Friction* in front side of sliding tip causes compressive stresses and in trail of the sliding tip generates tensile stresses.
2. *Tip geometry* affects the stress state on the material surface and beneath the indenter (e. g. sharper indenter generates higher stresses than a blunt indenter)
3. *Residual stresses:* Generally, two sources for residual stresses are considered called as *intrinsic* and *extrinsic residual stresses*:

   Intrinsic residual stress in thermal spraying is the sum of deposition stresses (peening and/or quenching stresses) and thermal stresses. The peening and quenching strresses are developed during the deposition and thermal stress is developed during the cooling of coating/substrate system from deposition temperature to room temperature.

   Extrinsic residual stress is considered to be as a result of plastic deformation introduced to material surface. However, the original material surface in our experiments is considered with no extrinsic residual stresses.

The formation of intrinsic residual stresses during the thermal spraying can be evaluated by a non-contact curvature measurement technique. The formation of these stresses and their significance explained by Kuroda et al. [20] and further developed by Sampath and Matejicek [21]. The details and fundamentals of this technique can be found elsewhere [22].

6.2.3 Scratch testing

In scratch testing the indenter tip first acts as a pure indentation to apply the preloading with no lateral movement. At this stage the material beneath the indenter deforms elastically and/or plastically. Depending on material's work hardening characteristics, sink-in or pile-up of material around the indent imprint will be observed [23]. With moving the tip and increasing the load a groove with increasing depth will be formed. In front side of moving tip compressive stresses are generat-

ed due to friction force. The friction force between the front side of the tip and material surface pushes the material upward to form a pile-up. At top of the highest pile-up point, tensile stresses will be generated. At the trail of the tip the same friction force causes the material to sink in and generates a tensile stress behind the tip. The pile-up and sink-in that are formed in front side and behind the moving tip are due to friction forces but the pile-up and sink-in that can be formed in indentation are more related to material's hardening characteristics.

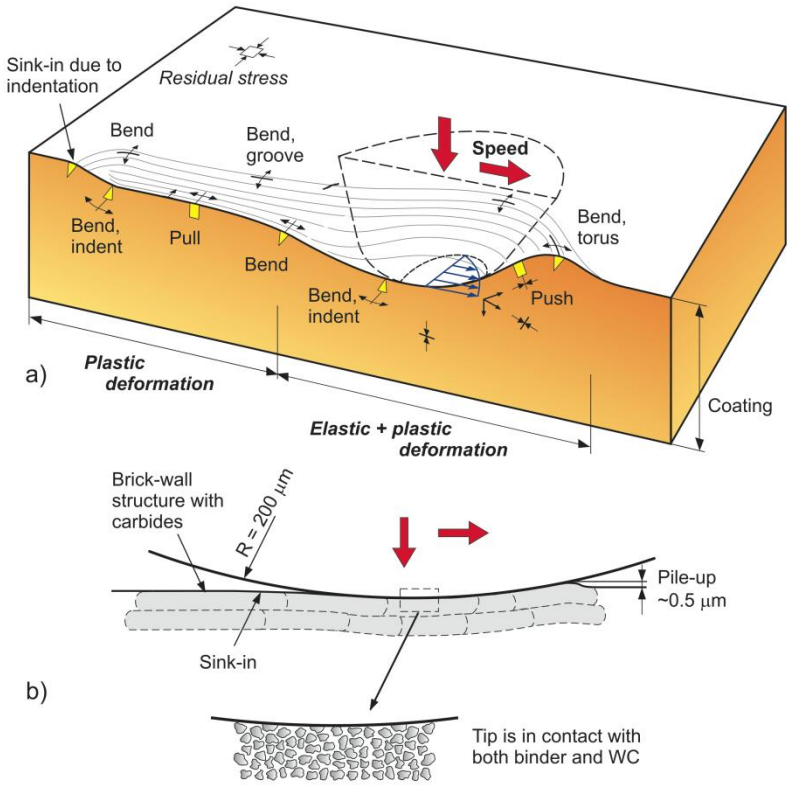

Figure 6.2. The origin of stresses around the moving tip and groove formation mechanism in a) macro and b) micro scales.

The groove formation mechanisms are shown in Figure 6.2 in macro- and micro scales in thick thermal sprayed composite coatings.

6.3 Experimental techniques

6.3.1 Materials and coating deposition

Three WC-CoCr and one WC-Co powders were employed as starting materials (Table 6.1) to deposit coatings. Depending on carbide size of WC-CoCr starting powders they were called as conventional, sub-micron and nano. WC-CoCr coatings were deposited with Diamond Jet (DJ) High Velocity Oxygen Fuel (HVOF) system using hydrogen and nitrogen as fuel gas and carrier gas respectively. WC-Co coatings were deposited using Jet Kote (JK) Deloro Stellite. WC-CoCr coatings were used to study the effect of process parameters and carbide size on scratch test respond and WC-Co coatings were used to evaluate the effect of residual stresses.

Table 6.1. Detailed characteristics of employed powders in this study.

Powders	Apparent density, g/m^3	WC gain size, µm	Size distribution d10–d90%	Chemical composition, wt.%		
				C	Co	Cr
Conventional	4.91	1–3	24–25	5.34	9.68	3.79
Sub-micron	5.71	0.4–1	20–39	5.13	9.98	4.0
Nano	–	<0.2	18–52	5.37	8.52	3.10

Different spraying parameters were used for deposition of conventional coatings. Coatings were deposited on steel that was grit-blasted with 590–710 µm alumina particles at 4.5 bar pressure followed by ultrasonic cleaning in the acetone. Enough air cooling was applied to keep the substrate temperature at 150 ˚C during spraying.

6.3.2 Characterization techniques

Coatings sections and scratch grooves were studied by scanning electron microscopy (SEM), (JEOL JSM-6400 and Zeiss FEG-SEM) and optical multifocus (Olympus) microscope. Hardness and elastic modulus were evaluated by instrumented micro-indentation tester (Zwick ZHU 0.2). A Vickers indenter was employed using 300 g load.

6.3.3 Scratch testing

Scratch testing was done using a conical diamond tip with 200 µm tip radius. The test was carried out applying 5 N preload, increasing to 100 N. Average scratch length was measured to be ~9 mm in all cases. For each sample three scratches were carried out.

6.4 Results and discussion

In HVOF thermal spray system there are different variables to control the flame conditions. In current study flame controlling variables considered as hydrogen (fuel gas), oxygen, nitrogen and air. To simplify the complexity of controlling parameters in all spraying conditions the volume flow of air and nitrogen have been kept constant. Therefore, by changing the fuel and oxygen coating with different microstructures and properties were deposited. Spraying parameters used for deposition of coatings are presented in Table 6.2. Table 6.3 tabulates the hardness and elastic modulus of coatings measured by instrumented indentation.

Table 6.2. Spraying parameters used for deposition of WC-CoCr coatings.

Sample code	Nominal carbide size	Spraying parameters			
		N_2	H_2	O_2	Air
C1	Conventional	14	635	215	350
C2	Conventional	14	708	210	350
C3	Conventional	14	615	250	350
C4	Conventional	14	655	230	350
S2	Submicron	14	635	215	350
N2	Nano	14	635	215	350

Table 6.3. Hardness and elastic modulus of sprayed coatings.

Sample	Hardness GPa	Elastic modulus GPa	W_2C/WC
C1	12.2±2.3	305±22	0.17
C2	12.8±2.5	321±30	0.29
C3	9.9±1.3	274±28	0.15
C4	11±2.2	280±33	0.14
S2	12.8±1.2	244±13	0.33
N2	12.7±1.7	234±8	0.55
High tension	11.5±1.1.	126±9	–
Low tension	11.8±1.6	220±16	–
Comparession	13.5±1.3	372±31	–

6.4.1 Macro and micro-damage mechanisms

After running three scratch tests on each sample, the generated scratch grooves were studied by multi-focus optical microscope to address overall failure mechanisms and to develop a failure map for WC-CoCr thermal sprayed coatings. Five

general mechanisms were realized and their origin regarding to loading conditions are explained as follow:

a) Localized collapsing of material: In the range of low to intermediate loads in some regions where the surface open porosities have higher concentration and spaced closely, sliding tip suddenly penetrates into the material. Fine-structured crack networks which connect the surface pores were observed in that region. In fact, presence of surface open porosities lowers the local load carrying capacity of the material. This observation is called as local collapsing of material (Figure 6.3). Surface pores might be formed during the deposition of coating or during the surface preparation and polishing procedure. Note that at higher loads in which the contact width is much bigger than pore size, this surface phenomenon was not observed.

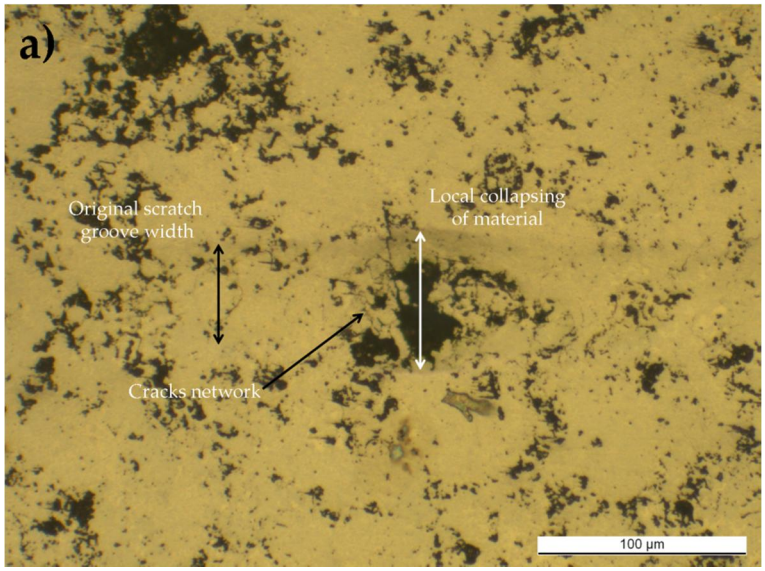

Figure 6.3. Localized collapsing of material under moving stylus due to presence of surface open porosities (moving direction from right to left).

However, sudden changes in groove width at higher loads (localized collapsing of material) that were observed might be due to formation of subsurface cracks or collapsing of subsurface pores along the scratch path. Sudden change in scratch groove width at higher loads that is due to collapsing of sub-surface pores is shown in Figure 6.4.

This figure is taken from split sample that shows both cross section and top surface of scratch groove. It can be seen the change of scratch groove width attributed to collapsing of pore beneath the surface.

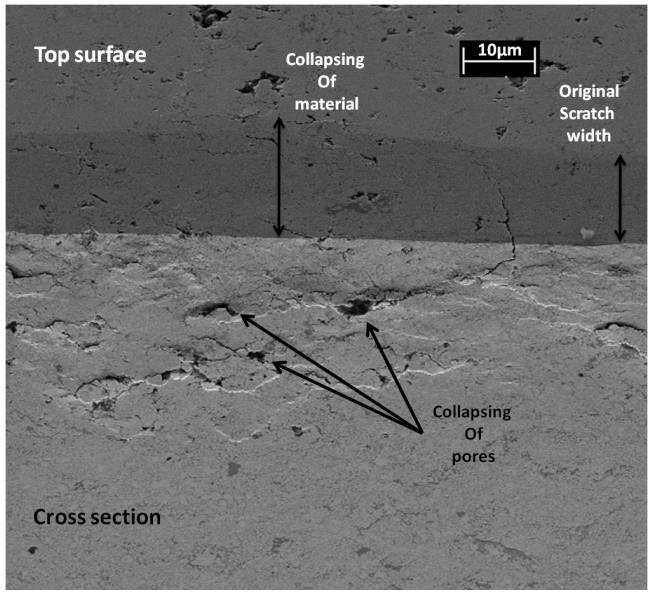

Figure 6.4. Sudden change of scratch groove width (running of tip into the material) due to collapsing of subsurface pores (moving direction from right to left).

b) Angular cracks: Angular cracks were observed at the edge of scratch grooves. These cracks are formed due to combination of moving action (providing tensile stresses parallel to the scratch groove behind the moving tip) and bending action (providing tensional stress perpendicular to scratch track) around the moving tip at the edge of groove. At lower loads the angular cracks are finer but at higher loads they become more visible (Figure 6.5). Similar angular cracks have been reported for thin coatings [16, 19].

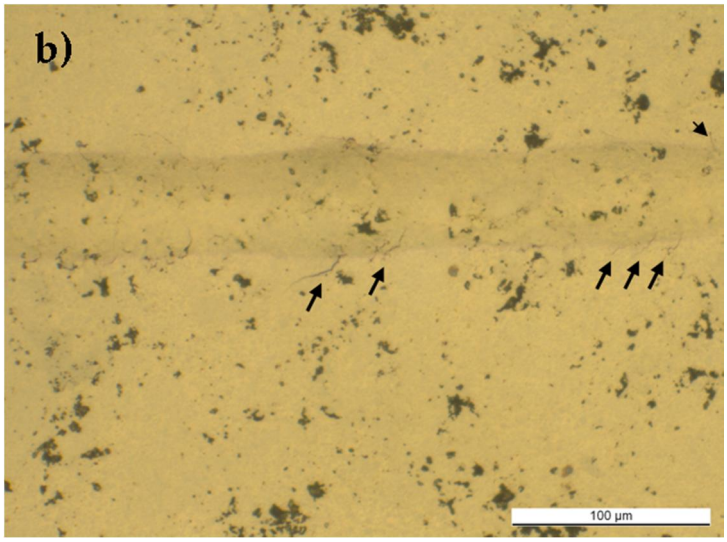

Figure 6.5. Angular cracks observed at the scratch groove edge.

c) Semi-circular cracks: In absence of friction, maximum tension will be occurred below the material surface. Nevertheless, with increasing friction these maximum tensile regions tend to appear at the contact surface. The cracks might follow the maximum tensile stress contours on the surface of material that is developed in trail of moving tip. At lower loads this kind of cracks are not developed fully and are mainly limited to the scratch groove (Figure 6.6). Also, similar semi-circular cracks have been reported for thin coatings [16, 19].

d) Developed semi-circular cracks: At higher loads semi-circular cracks are developed and are expanded outside of scratch groove. In some areas both angular and developed semi-circular cracks can be observed alongside the scratch groove (Figure 6.7). The main difference between semi-circular cracks observed in thin coatings and thermal sprayed thick coatings is that in thin coatings cracks penetration depth can be down to the substrate/coating interface but in thick coatings it will be limited to one splat thickness.

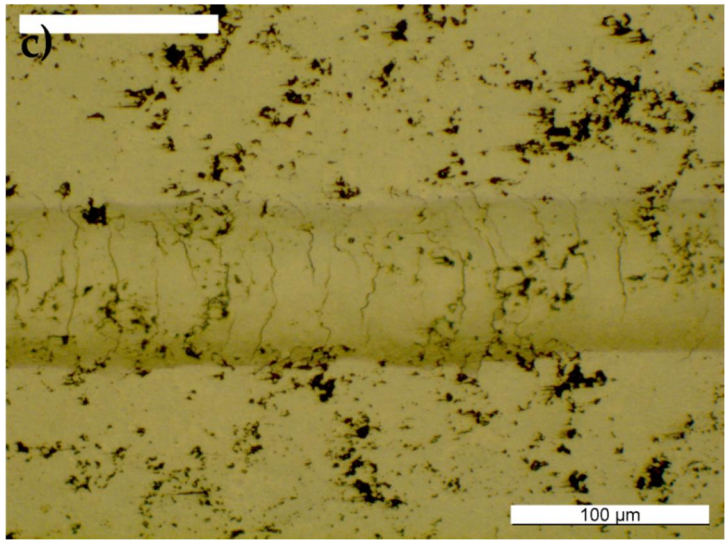

Figure 6.6. Semi-circular cracks formed at the trail of moving tip due to tensile stresses.

For instance, Figure 6.8 shows the split sample cross section and top surface that confirms the penetration depth of semi-circular cracks are limited to very top surface of coating. The average penetration depth is in the range of one or two splat thickness. Usually, the semi-circular cracks tend to get parallel to the surface. Such crack path is attributed to the unique lamellar structure of thermal sprayed coatings.

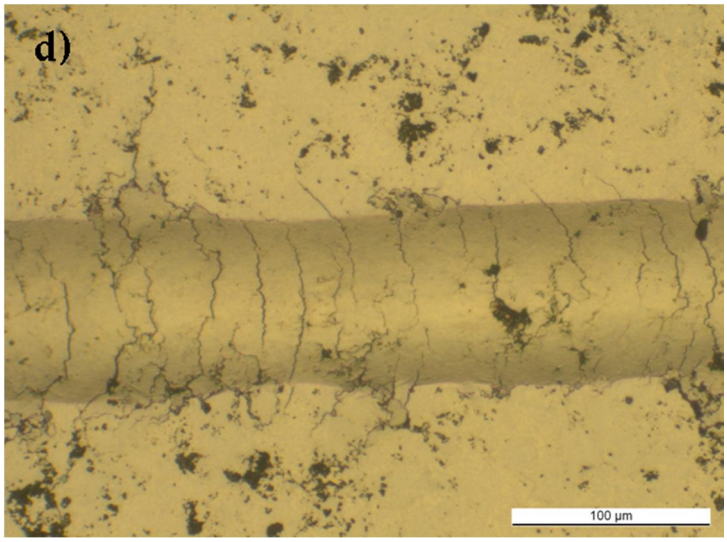

Figure 6.7. Developed semi-circular cracks propagating out of the scratch groove.

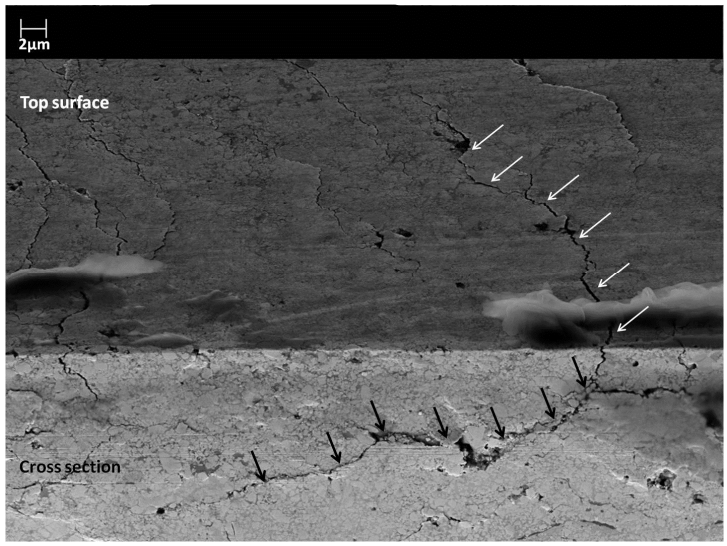

Figure 6.8. Top surface and cross section view of semi-circular crack, arrows are following the same crack at top surface and cross section.

e) Splat delamination: At higher loads in which the semi-circular cracks are well developed they reach each other at the splat boundaries and such interaction between cracks and splat boundary cause detachment of single splat. This explanation is more plausible by considering the splat boundaries as weak regions in

the coatings. It is also hypothesized that splat delamination might occur in front of moving tip due to formation of tensile stress at highest point of pile up. Note that this delamination mechanism is not same as outlined for thin coatings. In thin coatings, one would consider the detachment or delamination of whole coating from the substrate. Nonetheless, delamination in this case considered as full or partial detachment of one splat from the underlying splat (Figure 6.9).

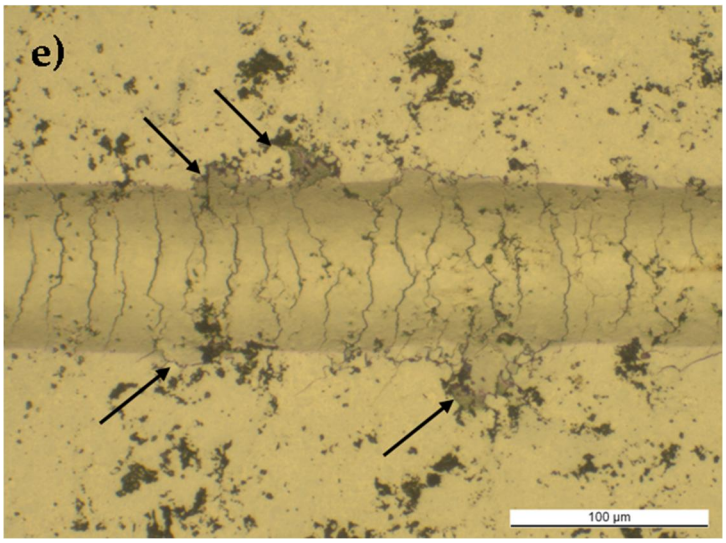

Figure 6.9. Delamination of splat at the edge of scratch groove.

Based on observed damage mechanisms a schematic illustration was developed as damage mechanism map that is shown in Figure 6.10.

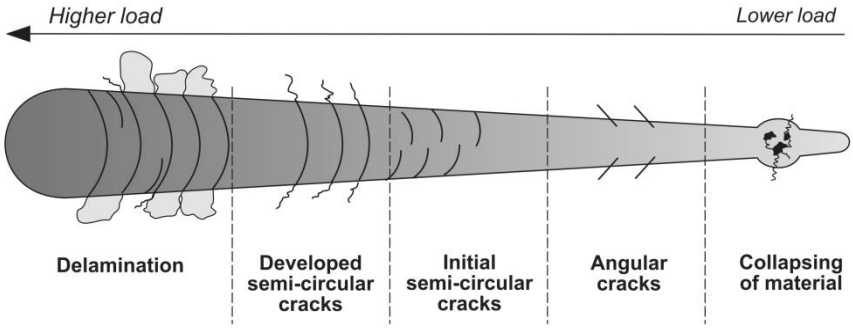

Figure 6.10. Schematic of damage mechanism map for WC based thermally sprayed coatings.

Obtaining quantitative values such as different critical loads can help to evaluate performance related properties of the coating. For example the critical load for delamination can lead us to quantify splat boundary strength (splat cohesion) or the critical load for formation of angular or semi-circular cracks can be used for determination of fracture toughness.

As an example two samples, C2 and C3 (hottest and coldest spraying parameters respectively at relatively same velocity range) were selected to further examine the possibility of quantifying the scratch test. The critical loads for formation of angular cracks, semi-circular cracks and delamination were measured optically for these two coatings are shown in Figure 6.11. The LC1, LC2 and LC3, represent the critical load for angular cracks, semi-circular cracks and delamination, respectively.

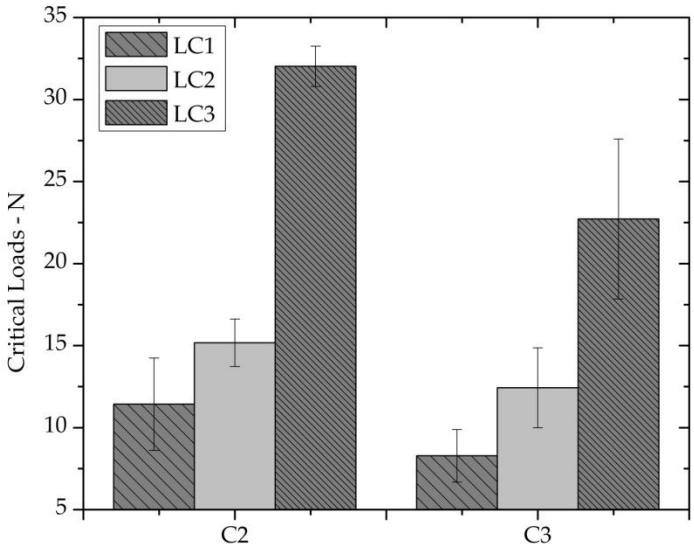

Figure 6.11. Critical loads for coatings deposited with low and high temperature.

As it is depicted in this graph overall loads necessary to form different kind of damages (angular, semi circular and delamination) are higher in coating C2 which has experienced highest deposition temperature and highest velocity. For instance higher load for formation of delamination can be attributed to higher melting state of material and subsequently to improved splat cohesion. Determination of splat cohesion based on delamination critical load is addressed more in detail in next section.

To address cracking behavior (shape, size and path of cracks) in micro scale, the cracks which were formed during scratch testing were analyzed by FEG-SEM. Figures 6.12a and 6.12b depict the comparative low magnification images taken from ~8.4mm, ~45 N, from starting the scratch grooves for samples C3 and C2 (lowest and highest spraying temperature respectively). As it is shown in Figures

6.12a and 6.12b, sample C2 exhibits less cracking than sample C3. This means at the same loading level, cracks in sample C3 are in the range of “well-developed semi-circular” cracks but the cracks in sample C2 are in the range of “semi-circular” cracks (refer to Figure 6.11). Thus, cracks in sample C3 are well-developed and wider than sample C2. In other words the critical load for formation of semi-circular cracks in sample C2 is higher than sample C3. The similar trend was observed in determining the delamination. Delamination occurred at lower loads in sample C3 compared to sample C2. The cracks that were formed at the middle of scratch groove, semi-circular cracks, mainly go through the binder and do not pass through the carbides (Figure 6.12c). Also individual cracks within the carbides were observed which might be due to high stresses and high friction in contact with diamond tip. As it is shown in Figure 6.12d, the first angular cracks that were formed at the edge of grooves in all samples are sharp and usually follow straight line through the binder and carbides. Vertical dashed line in Figure 6.12d is approximate location of groove edge. The critical load for angular crack or semi-circular cracks formation might be used for indication of cracking resistance of coating or in another term, fracture toughness of coating.

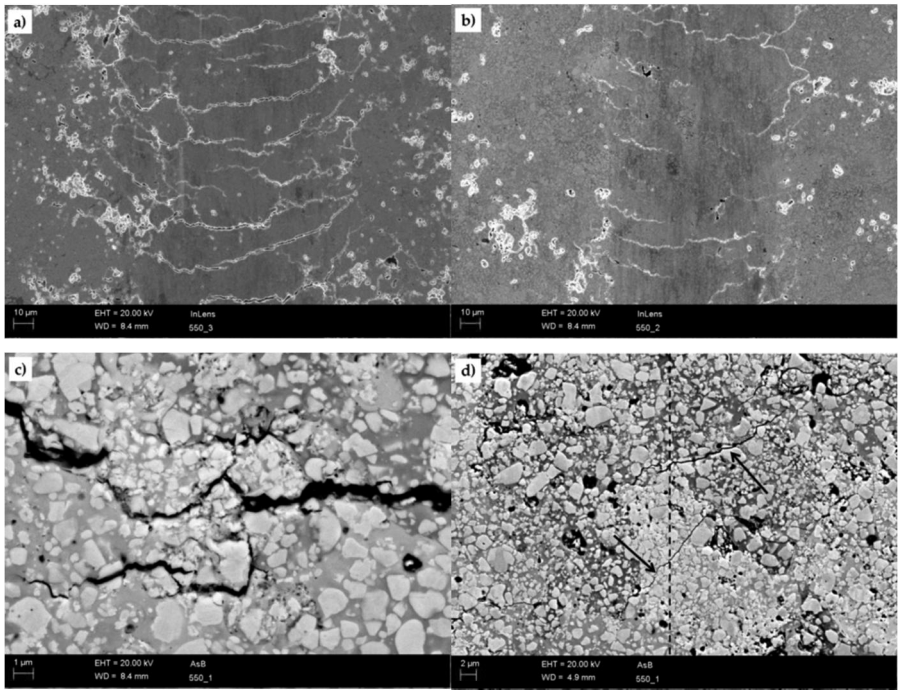

Figure 6.12. SEM studies of scratch groove for coatings deposited with cold (a) and hot (b) and (c) details of semi-circular crack and (d) angular cracks (scratch direction bottom to top).

Figure 6.13 shows the indentation fracture toughness values versus the angular critical loads. As it is shown in this figure there is a direct correlation between indentation fracture toughness and angular crack critical load. However, to be able to extract the actual fracture toughness values based on angular crack critical load it is needed to estimate the stresses at that normal load.

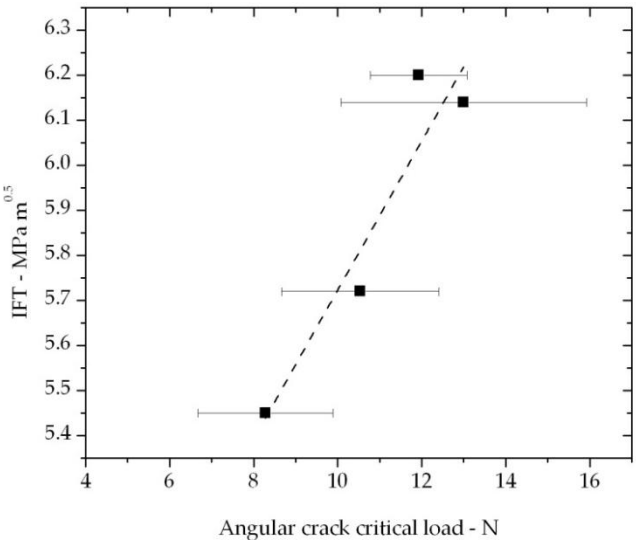

Figure 6.13. Correlation of indentation fracture toughness values versus angular crack critical load.

6.4.2 Effect of carbide size on damage mechanisms

To analyze effect of carbide size on cracking behavior S2 and N2 samples (with submicron and nano-sized carbides) were scratched and scratch grooves were analyzed by optical microscope and FEG-SEM. Three regions of the scratch groove, starting, middle and end part were compared with each other as shown in Figures 6.14a to 6.14f. At the starting of scratch, Figure 6.14a shows cracking of nano coating. Nevertheless, sub-micron coating, Figure 6.14b, unlike the nano-coating shows more of plastic deformation. The plastic deformation is observed as formation of scratch groove in this figure. With further progressing of the scratch (Figures 6.14c and 6.14d), the cracking of nano coating (Figure 6.14c) becomes more pronounced. In nano coating at low to intermediate loading, cracks have no particular orientation or structure (Figure 6.14c).

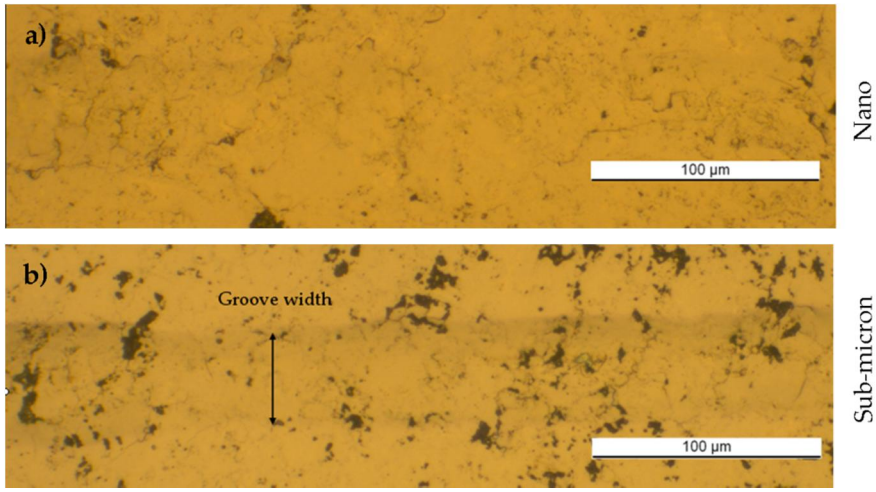

Figure 6.14. Starting of scratch on (a) nano coating and (b) sub-micron coating.

However, in sub-micron sample cracks tend to be formed in shape of semi-circles (similar to conventional coatings) (Figure 6.14d). At higher loading conditions towards the end of scratch grooves, more cracking was observed in the nano sample and sever delamination at the groove edge is evident. Nevertheless, for submicron coating less of delamination was observed. This observation suggests that nano sample exhibits more brittle behavior compared to submicron or conventional sample. Three main reasons for excessive brittleness of nano coating are hypothesized:

- It is well shown that nanocarbide coatings undergo more dissolution of W and C that cause formation of higher amount of brittle W_2C phase in the coating. The W_2C phase is prone to cracking.
- Dissolution of W and C hardens the binder and hinders the binder to undergo plastic deformation freely. Same amount of deformation can cause generation of higher stresses in comparison to non-hardened binder.

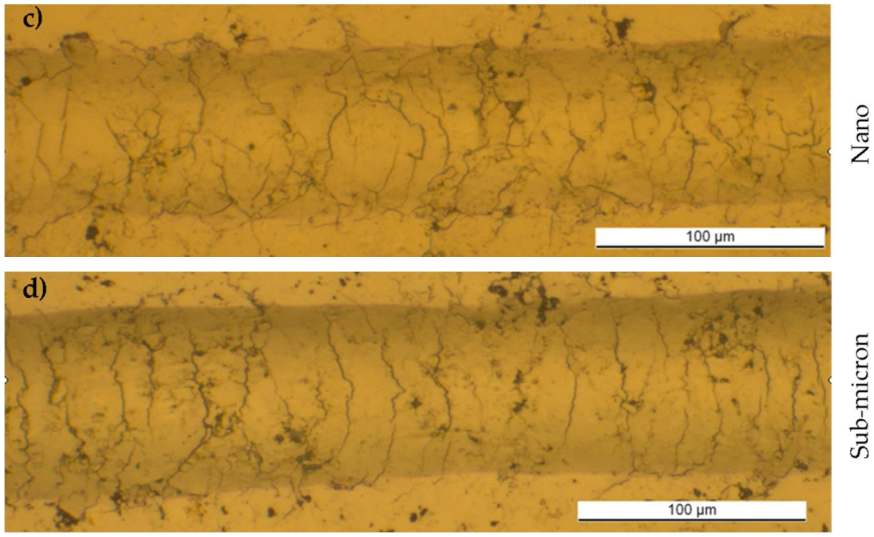

Figure 6.14. Middle of scratch on (c) nano coating and (d) sub-micron coating.

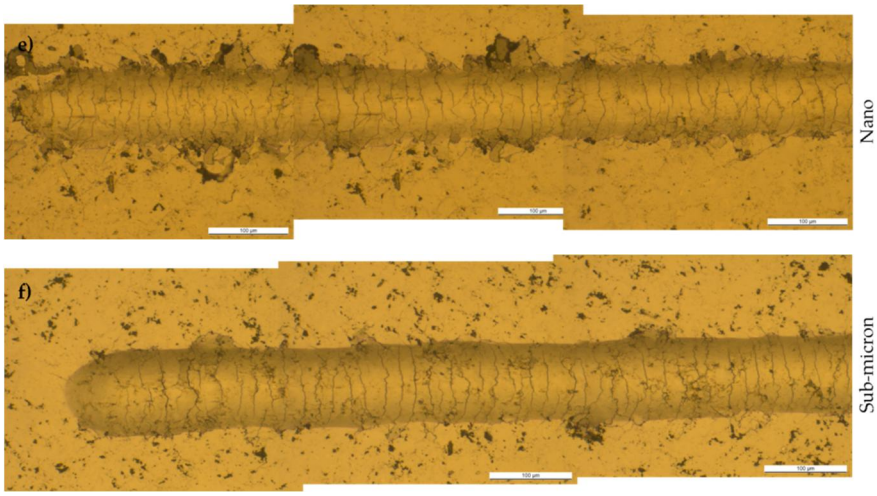

Figure 6.14. End of scratch on (e) nano coating and (f) sub-micron coating.

- Decreasing binder mean free path by decreasing carbide size causes accumulation of higher stresses in the binder and individual particles will interact with each other. This will limit the capability of binder to undergo further plastic deformation and cause the higher stresses within the carbides and at the carbide/binder interface. This mechanism is similar to the hardening of material.

The latter mechanism is defined by microstructural characteristics of material such as carbide grain size and binder fraction (these two define the binder mean free path). A combination of above mechanisms might yield a material with higher work hardening- like effect. However, this is true if the materials with different WC size have the same resistance to fracture. To further investigate the effect of carbide size without interfering W_2C that decreases fracture resistance significantly, producing the coating with different carbide size with no W_2C phase is necessary.

6.4.3 The effect of stresses on scratch test response of material

As explained in previous section it was proposed that intrinsic residual stresses affect the response of examined material to moving diamond stylus (scratch test). However, it was difficult so far to control the residual stresses of thermal sprayed coatings deliberately without affecting other microstructural and chemical characteristics of materials. Recently by developing the in-situ coating property measurement sensor the knowledge regarding to coating formation dynamics as well as developed stresses during the coating processing have been significantly improved. In this section an attempt has been made to address the correlation of damage mechanism and critical loads to residual stresses. Three WC-17Co coatings were deposited employing Jet kote torch. The level of residual stress was controlled by changing the substrate material (to have different CTE mismatch) and cooling the substrate. Coatings at three different residual stress levels as high tensile, low tensile and compressive were obtained. Table 6.4 shows the manipulated parameters to control the final residual stresses. However, during the controlling the residual stresses different evolving stresses were obtained as well.

Table 6.4. Manipulated parameters to control the residual stresses.

Residual stress level	Manipulated parameters	Residual stresses	Evolving stresses
High tension	Nitrogen cooling, steel substrate	502 MPa	630 MPa
Low tension	Nitrogen cooling, aluminium substrate	218 MPa	400 MPa
Compression	No cooling, aluminum substrate	-228 MPa	505 MPa

The XRD of three coatings were compared to make sure there are no differences in phase structures. However, a shift in location of peaks was observed that is well known and attributed to residual stresses. Mechanical properties (elastic modulus and hardness) of three coatings were measured by indentation technique. Figure 6.15 shows the measured elastic modulus and hardness values.

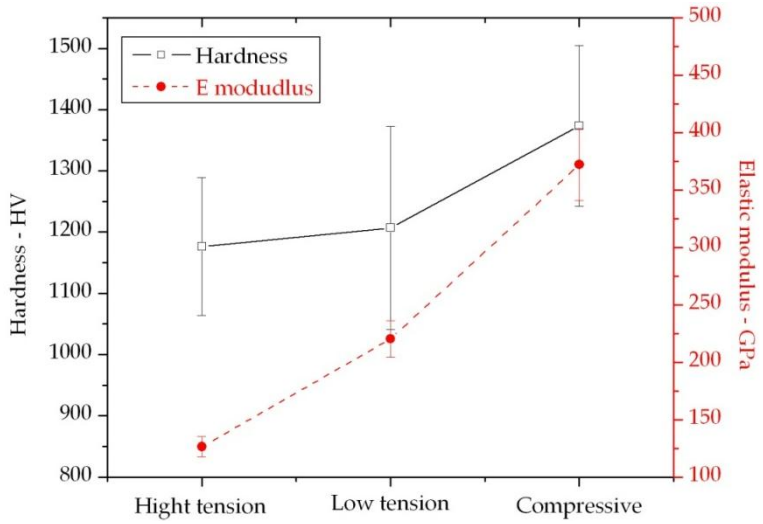

Figure 6.15. Indentation hardness and elastic modulus values for coatings with different residual stress levels.

In classic mechanics of material it has been noted that elastic modulus is not affected by level of residual stresses. However, as it is shown in Figure 6.15 coating with higher tensile residual stresses return lower elastic modulus. It is hypothesized that defective structure of thermal sprayed coating with tensile stresses is more prone to formation of micro-cracks or propagation of existing cracks under indentation loading. Similarly, formation or propagation of micro-cracks in coatings with compressive stresses will be more difficult.

Three scratches were made on each sample and analyzed by optical microscope to obtain the critical loads. Figure 6.16a to 6.16c show the critical load for angular crack formation, semi-circular crack formation and delamination. Both angular and semi-circular cracks formation load show the similar trend. In both cases necessary load for initiation of angular or semi-circular cracks is highest for the coating in compression stresses. However, for coatings in tension regardless of level of tensile stresses the difference is small. Unlike angular and semi-circular critical loads, delamination critical loads do not show any correlation with residual stresses. Nonetheless, delamination critical load shows direct correlation with evolving stress (Figure 6.16d). As it was explained in previous section it was hypothesized that critical load for delamination is an indication of splat/splat cohesion.

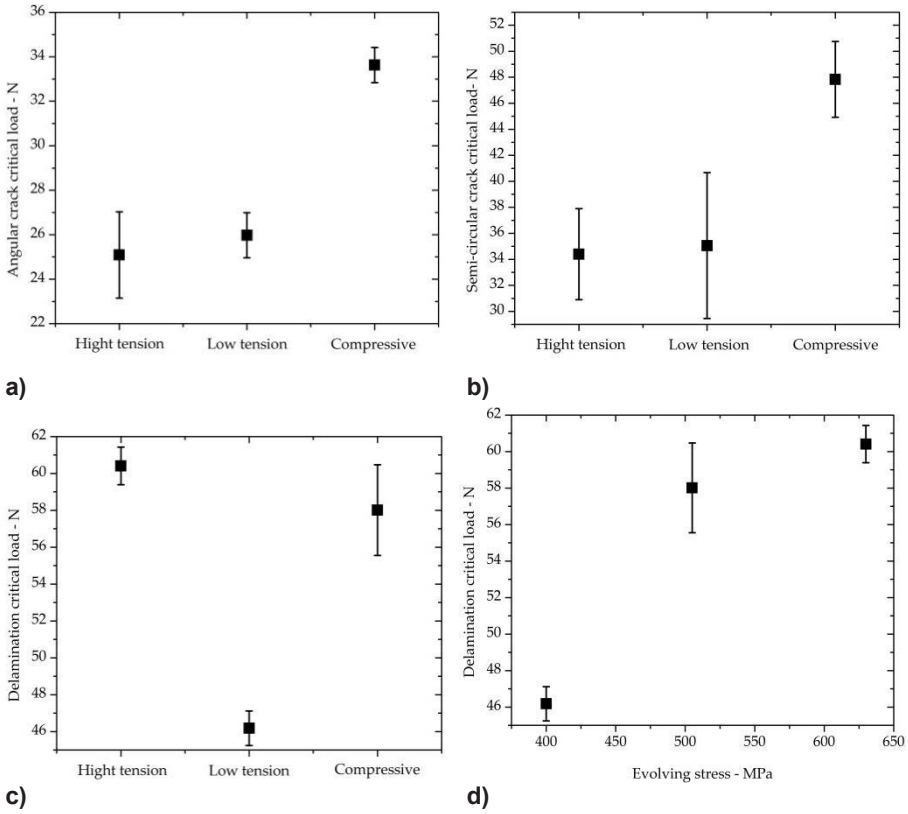

Figure 6.16. Angular critical load (a), semi circular critical load (b), delamination critical load (c) versus different residual stresses and delamination critical load versus different evolving stresses (d).

Better the splat/splat cohesion higher the load necessary to delaminate one splat from its underlying splat. As it was shown by Kuroda et al. [20] when a molten particle is solidifying upon impact, stress will be arisen due to solidification. If the particle is well bonded the level of developed stress will be higher. However, if the particle cohesion is loose, and it can slide on top of previous layer freely during the solidification, developed stress will be lower. Basically, the level of developed stress can be used to identify how well the splats bonded to each other. This developed stress at this level called evolving stress that is possible to estimate by ICP sensor. The correlation between delamination load and evolving stress is also valid for WC-CoCr coatings as it is shown in Figure 6.17 In fact, this correlation between delamination critical load and evolving stress (splat/splat cohesion) demonstrate the robustness of scratch testing in quantification of splat/splat cohesion.

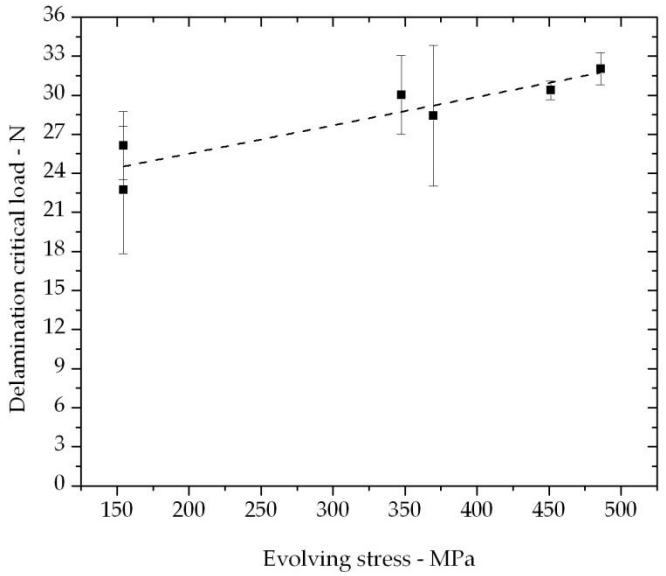

Figure 6.17. Correlation of delamination load and evolving stress for WC-CoCr coatings.

So far most of the studies were focused on surface appearance of scratch trace. However, it is of great interest to evaluate the cracking behavior beneath the moving diamond stylus. To study the sub-surface features of scratched sample, it is necessary to reveal the sub-surface cross section of scratched region. Nevertheless, conventional mechanical cutting and grinding techniques might introduce secondary defects or promote expansion of existing cracks. There are two possibilities to avoid such complexities; use the bonded specimen technique to prepare the sample before the scratch test or employ focused ion beam (FIB) technique to prepare subsurface cross section after scratch test is done. Previously examples of top surface and cross section images of samples prepared by bonded specimen technique were shown (Figures 6.4 and 6.8). To study the subsurface of WC-Co samples (stress effect) FIB technique was employed to prepare the cross section.

FIB systems operate in a similar fashion to a scanning electron microscope (SEM) except, rather than a beam of electrons a finely focused beam of ions (usually gallium) operating at high beam currents for site specific sputtering or milling.

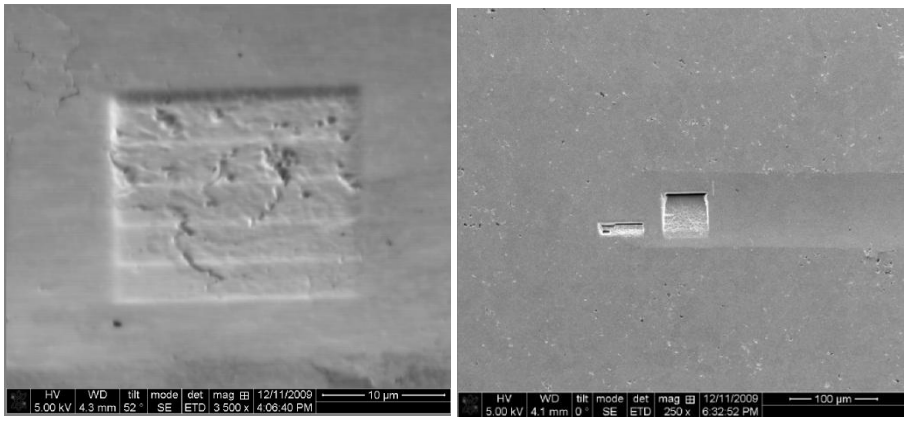

Figure 6.18. Top surface of coating after few minutes of milling (left) and top surface of coating after completed milling (end of scratch groove).

Figure 6.18 (left) shows the top surface of coating after few minutes of FIB milling. Figure 6.18 (right) shows the region (end of the scratch groove) that was milled for cross section studies. After finishing the milling process the sample was tilted 52° to be studied by SEM.

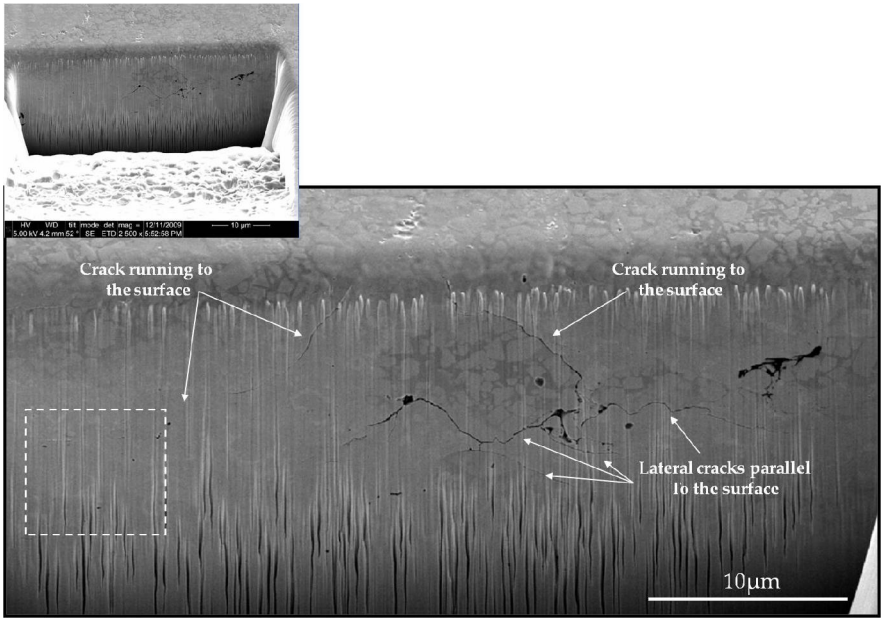

Figure 6.19. Sub-surface cross section of scratch groove on coating under tensile stress.

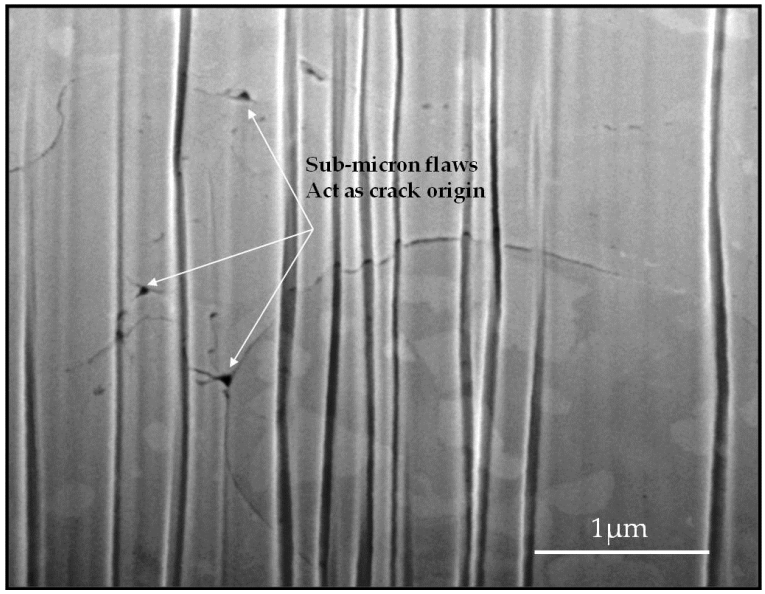

Figure 6.20. Sharp cornered pores act as stress concentration spots and promote cracking.

Figure 6.19 shows the SEM cross section of sample in high tensile stress milled by FIB. This figure reveals two sets of sub-surface cracks. One set of cracks are parallel to the surface that are called lateral cracks. It is hypothesized that lateral cracks originated due to loading and unloading of material beneath the moving diamond stylus. It can be considered that splat boundaries might be favorable path for lateral crack propagation as they exhibit higher level of brittleness and/or limited adhesion. Other set of identified cracks are oriented perpendicular to the surface. Presence of high tensile stresses parallel to the surface favors the propagation of vertical cracks. Another feature that was revealed during this study was the role of flaws in form of micron or submicron porosities in crack formation and propagation. Figure 6.20 is magnified image of region in Figure 6.19 highlighted by dotted rectangle. As it is shown in this figure cracks are formed from sharp corners of sub-micron flaws as the cracks and specifically their sharp corners act as stress concentration points in loaded structures. For comparison purposes similar cross section of coating in compression was prepared and Figure 6.21 shows the observed cross section. Similar to coating in tension lateral cracks were observed. However, there was no evidence of sub-surface vertical cracks. Presence of compressive stresses acting parallel to the surface reduces chance of the cracks to propagate in vertical directions. In this scenario higher stresses are necessary to propagate vertical cracks in the structure as it was verified by higher semi-circular crack critical load for coating in compression compared to coatings in tension.

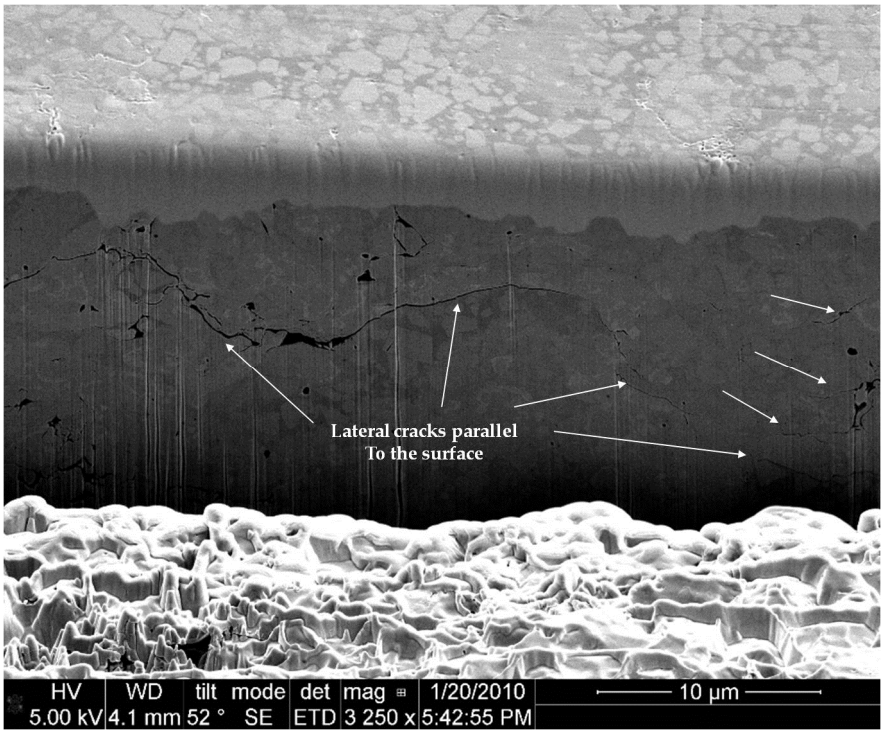

Figure 6.21. Sub-suface cross section of scratch groove on coating under compressive stress.

6.5 Conclusions

In this current work thermal sprayed WC-CoCr coatings with carbide sizes in the range of 0.2 µm to 3 µm were studied under increasing loading with a conical diamond tip. Similar study was done on WC-Co to comprehend the effects of stresses on the respond of coating to increasing lateral loading conditions. The scratch test turned out to be a suitable technique for assessment of thick thermal sprayed coatings giving both qualitative and quantitative information on their cracking and failure behavior. Five different cracking patterns were observed due to the surface scratch loading; i) Localized collapsing of material, ii) angular cracks, iii) semi-circular cracks, iv) developed semi-circular cracks and v) delamination. Crack types (i) and (v) are specifically observed in thick thermally sprayed composite coatings while crack types (ii), (iii) and (iv) are generic and similar to the ones observed for PVD and CVD thin coatings. The first cracks (angular crack) that were formed at lower loads at the groove edge are typically following a straight line path through the binder and carbides. On the other hand, the semi-circular cracks formed in the middle of the scratch groove mainly go through the binder and do not pass through the carbides. The possibility of extracting the coat-

ing fracture toughness based on obtained angular crack or semi-circular crack critical loads was discussed. Further, delamination critical load was correlated to evolving stress obtained by ICP sensor during spraying that is and indication of quality of splat/splat cohesion. The coating that was deposited with nano- size particles (0.2 μm) exhibits more brittle cracking behavior compared to sub-micron (0.4–1 μm) and conventional (1–3 μm) coatings.

References

1. Usmani, S., et al. Effect of Carbide Grain Size on the Sliding and Abrasive Wear Behavior of Thermally Sprayed WC-Co Coatings. Tribology Transactions, 1997. 40(3): p. 470–478.

2. Dent, A.H., S. DePalo, and S. Sampath. Examination of the wear properties of HVOF sprayed nanostructured and conventional WC-Co cermets with different binder phase contents. Journal of Thermal Spray Technology, 2002. 11(4): p. 551–558.

3. Wayne, S.F., J.G. Baldoni, and S.-T. Buljan. Abrasion and Erosion of WC-Co with Controlled Microstructures. Tribology Transactions, 1990. 33(4): p. 611–617.

4. Ghabchi, A., et al. Behavior of HVOF WC-10Co4Cr Coatings with Different Carbide Size in Fine and Coarse Particle Abrasion. Journal of Thermal Spray Technology, 2010. 19(1–2): p. 368–377.

5. Gouldstone, A., et al. Indentation across size scales and disciplines: Recent developments in experimentation and modeling. Acta Materialia, 2007. 55(12): p. 4015–4039.

6. Gahr, K.H.Z. Wear by hard particles. Tribology International, 1998. 31(10): p. 587–596.

7. Methods of tests for cermaic coatings: Part 3. Determination of adhesion and other mechanical failure modes by scratch test, in Advanced technical ceramics. 1999: European Standard. p. 44.

8. Perry, A.J. The adhesion of chemically vapour-deposited hard coatings to steel--the scratch test. Thin Solid Films, 1981. 78(1): p. 77–94.

9. Perry, A.J. Scratch adhesion testing of hard coatings. Thin Solid Films, 1983. 107(2): p. 167–180.

10. Mathia, T.G. and B. Lamy. Sclerometric characterization of nearly brittle materials. Wear, 1986. 108(4): p. 385–399.

11. Steinmann, P.A. and H.E. Hintermann. Adhesion of TiC and Ti(C,N) coatings on steel. Journal of Vacuum Science & Technology A: Vacuum, Surfaces, and Films, 1985. 3(6): p. 2394–2400.

12. Valli, J., et al. TiN coating adhesion studies using the scratch test method. Journal of Vacuum Science & Technology A: Vacuum, Surfaces, and Films, 1985. 3(6): p. 2411–2414.

13. Nledengvist, P. and S. Hogmark. Experiences from scratch testing of tribological PVD coatings. Tribology International, 1997. 30(7): p. 507–516.

14. von Stebut, J., et al. Major damage mechanisms during scratch and wear testing of hard coatings on hard substrates. Thin Solid Films, 1989. 181(1–2): p. 555–564.

15. Bromark, M., et al. Influence of substrate surface topography on the critical normal force in scratch adhesion testing of TiN-coated steels. Surface and Coatings Technology, 1992. 52(2): p. 195–203.

16. Bull, S.J. Failure mode maps in the thin film scratch adhesion test. Tribology International, 1997. 30: p. 491–498.

17. Laukkanen, A., et al. Tribological contact analysis of a rigid ball sliding on a hard coated surface, Part III: Fracture toughness calculation and influence of residual stresses. Surface and Coatings Technology, 2006. 200(12–13): p. 3824–3844.

18. Holmberg, K. and A. Matthews. Coating Tribology: Properties, Mechanisms, Techniques and Applications in Surface Engineering. second ed. Tribology and Interface Engineering, ed. B. Briscoe. 2009: Elsevier Science. 560.

19. Holmberg, K., et al. Tribological contact analysis of a rigid ball sliding on a hard coated surface: Part I: Modelling stresses and strains. Surface and Coatings Technology, 2006. 200(12–13): p. 3793–3809.

20. Kuroda, S., T. Fukushima, and S. Kitahara. Significance of quenching stress in the cohesion and adhesion of thermally sprayed coatings. Journal of Thermal Spray Technology, 1992. 1(4): p. 325–332.

21. Sampath, S. Method and apparatus for determining process- induced stresses and elastic modulus of coatings by in-situ measurement. 2002, The Research Foundation of State University of New York, Stony Brook, NY (US): United States. p. 6.

22. Matejicek, J. and S. Sampath. In situ measurement of residual stresses and elastic moduli in thermal sprayed coatings: Part 1: apparatus and analysis. Acta Materialia, 2003. 51(3): p. 863–872.

23. Alcalá, J., A.C. Barone, and M. Anglada. The influence of plastic hardening on surface deformation modes around Vickers and spherical indents. Acta Materialia, 2000. 48(13): p. 3451–3464.

Series title and number
VTT Science 29

Title	**Wear Resistant Carbide-Based Thermal Sprayed Coatings: Process, Properties, Mechanical Degradation and Wear**
Author(s)	Arash Ghabchi
Abstract	Thermally sprayed ceramic-metallic composite (CerMet) materials consist of ceramic particles mainly in form of carbides reinforced by metallic binder exhibit unique microstructural and mechanical characteristics. Such structure brings in a novel combination of hardness and toughness enabling application of this class of material in wear resistant surfaces. Final deposit microstructure that defines the mechanical properties and wear performance of material depends on process parameters and starting material characteristics. Complex interaction of in-flight particles with supersonic flame, formation of complex defective deposit structure comprising of pores, cracks and splat boundaries make comprehending of interrelation of process, microstructure, properties and performance a difficult task. Additional challenge is development of systematic understanding on mechanical degradation, damage and wear mechanisms of cermet coatings due to their complex structure. This dissertation attempts to address these issues first by taking a systematic step by step approach, process map, to establish a correlation between process, particle state, microstructure and properties. Different strategies were proposed and examined to control the high velocity thermal spray process. This strategy assessment enabled a better control over in-flight particles state in high velocity thermal spray process and provided better understanding on interaction of in-flight particles with the flame. Further, possible advantages of reducing the carbide particle size from micron to nano in terms of mechanical properties and different wear performance were explored. It was suggested that poor wear performance of nano-structured coating is due to presence of brittle phases and less available binder promotes the excessive stress detrimental to load carrying capability of material. Material damage and wear mechanisms of coating under different tribological conditions were examined. The results suggest a correlation between relative abrasive particle size/carbide particle size and observed wear mechanism. Additionally effect of surface open porosities was highlighted. A surface damage mechanisms map was developed for coatings under increasing tangential force. This work has significant implications in improved material and process design of composite wear resistant structures and systems as it provides comprehensive qualitative insight to the wear mechanism of complex composite thermally sprayed structures under different tribological contact conditions. Additionally, this wok provides an establishment between process, microstructure, properties and performance for this class of materials.
ISBN, ISSN	ISBN 978-951-38- 7960-0 (Soft back ed.) ISBN 978-951-38-7961-7 (URL: http://www.vtt.fi/publications/index.jsp) ISSN-L 2242-119X ISSN 2242-119X (Print) ISSN 2242-1203 (Online)
Date	February 2013
Language	English
Pages	136 p.
Name of the project	MOTRICOT, Nano-Vera
Commissioned by	TEKES, Metso Minerals Oy, Rautaruukki Oyj, OMG Kokkola Chemicals Oy, Millidyne Oy, Wärtsilä Finland Oy, SA-MO Oy, VTT
Keywords	Wear, thermal spray, coating
Publisher	VTT Technical Research Centre of Finland P.O. Box 1000, FI-02044 VTT, Finland, Tel. 020 722 111

VTT Technical Research Centre of Finland is a globally networked multitechnological contract research organization. VTT provides high-end technology solutions, research and innovation services. We enhance our customers' competitiveness, thereby creating prerequisites for society's sustainable development, employment, and wellbeing.

Turnover: EUR 300 million
Personnel: 3,200

VTT publications

VTT employees publish their research results in Finnish and foreign scientific journals, trade periodicals and publication series, in books, in conference papers, in patents and in VTT's own publication series. The VTT publication series are VTT Visions, VTT Science, VTT Technology and VTT Research Highlights. About 100 high-quality scientific and professional publications are released in these series each year. All the publications are released in electronic format and most of them also in print.

VTT Visions

This series contains future visions and foresights on technological, societal and business topics that VTT considers important. It is aimed primarily at decision-makers and experts in companies and in public administration.

VTT Science

This series showcases VTT's scientific expertise and features doctoral dissertations and other peer-reviewed publications. It is aimed primarily at researchers and the scientific community.

VTT Technology

This series features the outcomes of public research projects, technology and market reviews, literature reviews, manuals and papers from conferences organised by VTT. It is aimed at professionals, developers and practical users.

VTT Research Highlights

This series presents summaries of recent research results, solutions and impacts in selected VTT research areas. Its target group consists of customers, decision-makers and collaborators.

Wear Resistant Carbide-Based Thermal Sprayed Coatings: Process, Properties, Mechanical Degradation and Wear

Thermally sprayed ceramic-metallic composite (CerMet) materials consist of ceramic particles mainly in form of carbides reinforced by metallic binder exhibit unique microstructural and mechanical characteristics. Such structure brings in a novel combination of hardness and toughness enabling application of this class of material in wear resistant surfaces. Final deposit microstructure that defines the mechanical properties and wear performance of material depends on process parameters and starting material characteristics.

Complex interaction of in-flight particles with supersonic flame, formation of complex defective deposit structure comprising of pores, cracks and splat boundaries make comprehending of interrelation of process, microstructure, properties and performance a difficult task. Additional challenge is development of systematic understanding on mechanical degradation, damage and wear mechanisms of cermet coatings due to their complex structure.

This dissertation attempts to address these issues first by taking a systematic step by step approach, process map, to establish a correlation between process, particle state, microstructure and properties. Different strategies were proposed and examined to control the high velocity thermal spray process. This strategy assessment enabled a better control over in-flight particles state in high velocity thermal spray process and provided better understanding on interaction of in-flight particles with the flame.

ISBN 978-951-38-7960-0 (Soft back ed.)
ISBN 978-951-38-7961-7 (URL: http://www.vtt.fi/publications/index.jsp)
ISSN-L 2242-119X
ISSN 2242-119X (Print)
ISSN 2242-1203 (Online)